Aus dem Institut für Neuropathologie
(Zentrum für Neuropathologie und Prionforschung)
Institut der Ludwig-Maximilians-Universität München
Direktor: Prof. Dr. med. Jochen Herms

The role of TCF4 in cerebellum development and its influence on formation and growth of medulloblastoma

Dissertation
zum Erwerb des Doktorgrades der Medizin
an der Medizinischen Fakultät der
Ludwig-Maximilians-Universität zu München

vorgelegt von
Marlen Charlotte Lauffer
aus
Mannheim
2019

Mit Genehmigung der Medizinischen Fakultät
der Universität München

Berichterstatter:	Prof. Dr. Ulrich Schüller
Mitberichterstatter:	Prof. Dr. Rainer Glaß
	Prof. Dr. Florian Heinen
Dekan:	Prof. Dr. med. dent. Reinhard Hickel
Tag der mündlichen Prüfung:	25.07.2019

Major parts of this work have been published as:

TCF4 (E2-2) harbors tumor suppressive functions in SHH medulloblastoma

M. Hellwig, M.C. Lauffer, M. Bockmayr, M. Spohn, D.J. Merk, L. Harrison, J. Ahlfeld, A. Kitowski, J.E. Neumann, J. Ohli, D. Holdhof, J. Niesen, M. Schoof, M. Kool, C. Kraus, C. Zweier, D. Holmberg, U. Schüller

Acta Neuropathol (2019) 137: 657
(https://doi.org/10.1007/s00401-019-01982-5)

Eidesstattliche Versicherung

Ich erkläre hiermit an Eides statt, dass ich die vorliegende Dissertation mit dem Thema

The role of TCF4 in cerebellum development and its influence on formation and growth of medulloblastoma

selbständig verfasst, mich außer der angegebenen keiner weiteren Hilfsmittel bedient und alle Erkenntnisse, die aus dem Schrifttum ganz oder annähernd übernommen sind, als solche kenntlich gemacht und nach ihrer Herkunft unter Bezeichnung der Fundstelle einzeln nachgewiesen habe.

Ich erkläre des Weiteren, dass die hier vorgelegte Dissertation nicht in gleicher oder in ähnlicher Form bei einer anderen Stelle zur Erlangung eines akademischen Grades eingereicht wurde.

Rotterdam, den 17. August 2019

Marlen Lauffer

Acknowledgements

First and foremost, I would like to thank my supervisor, Prof. Ulrich Schüller, for his help, guidance, and constant support throughout this project. Thank you for giving me to opportunity to work on the TCF4 project, I very much enjoyed it.

I would also like to thank Daniel Merk, Julia Neumann, Julia Ahlfeld, and Jasmin Ohli, my former group members, for introducing me into the world of fascinating experiments and helping me to develop my practical skills. Thank you also to the rest of the Schüller group for support during this project and all the helpful ideas and feedback that I received.
Thank you to everyone who actively participated in the organisation and execution of the project and contributed to the experiments. Especially Malte Hellwig, thank you for helping me in the final stages; I hope all goes well with your part of the TCF4 project.

Thank you to all the diligent people at the ZNP. Thank you to everyone in the animal facility for helping with the mouse experiments. A big thank you goes to Michael Schmidt for helping with the immunohistochemistry. Thank you to our fabulous lab technicians, Silvia and Chrissi, for all the work you did!

Thank you to all my friends and family for sharing all my excitement and all my disappointment. A special thank you goes to Eliana and Matthias for help with experiments when I got stuck, for reading my thesis, and for listening to all my complaints. The biggest thank you is directed to Matus, who, by now, probably knows this thesis as well as I do; I have forgotten how many times you read it. Thank you for cheering me up when I needed it the most, thank you for always talking sense into me, thank you for all your help and support.

At last, I would like to thank the Kind-Philipp Stiftung for their financial support for this project. And also the Studienstiftung des deutschen Volkes for their support throughout my studies.

Disclaimer

The following thesis will use a variety of different gene names and protein symbols. According to the HGNC Guidelines for Human Gene Nomenclature and the MGI Guidelines for Nomenclature of Genes, Genetic Markers, Alleles, and Mutations in Mouse and Rat, gene names are italicised with all uppercase letters when referred to *Homo sapiens* and italicised with the first letter uppercase in *Mus musculus*. Protein names are generally all upper case and not italicised. For general rules on nomenclature please refer to page xix.

Zusammenfassung

Transkriptionsfaktor 4 (*TCF4*) ist unter anderem für die Entwicklung des zentralen Nervensystems (ZNS), speziell im Rahmen der Neurogenese, von großer Bedeutung. Seit 2007 ist bekannt, dass die Haploinsuffizienz von *TCF4* ursächlich für das sogenannte Pitt-Hopkins-Syndrom, eine schwerwiegende neurologische Entwicklungsstörung, ist. Das Pitt-Hopkins-Syndrom zeichnet sich durch eine erhebliche Intelligenzminderung sowie eine Tendenz zur Entwicklung von Epilepsien und Atmungsstörungen aus. Veränderungen im *TCF4*-Gen werden zusätzlich mit Schizophrenie und weiteren Erkrankungen aus dem Bereich der Autismus-Spektrum-Störungen in Verbindung gebracht.

Eine kürzlich veröffentliche Publikation identifizierte eine überraschend hohe Anzahl somatischer *TCF4*-Mutationen in adulten Sonic hedgehog assoziierten Medulloblastomen (SHH MBs). Medulloblastome sind hochmaligne, WHO Grad IV, Tumore der hinteren Schädelgrube, die hauptsächlich bei Kindern diagnostiziert werden.
Die vorliegende Arbeit beschäftigt sich nun erstmalig mit der Bedeutung von *TCF4* in der Kleinhirnentwicklung und seiner Rolle in der Entstehung von SHH-assoziierten Medulloblastomen.

Ein Teil dieser Arbeit konzentriert sich ausschließlich auf die Rolle von *TCF4* in der Kleinhirnentwicklung. Im Rahmen von *in vitro* und *in vivo* Versuchen konnte gezeigt werden, dass *TCF4* essentiell für die Entstehung des Kleinhirns ist und ein Verlust schwerwiegende Veränderungen in Struktur und Aufbau des Kleinhirns an sich, und der verschiedenen zellulären Schichten im Speziellen, nach sich zieht. Ein pränataler Knockout von *Tcf4* in Mäusen führt zu einer Mikrozephalie, hervorgerufen durch einen signifikanten Abfall der Proliferationsraten sowie einem signifikanten Anstieg in der Apopotoserate der Körnerzellen. Weiterhin zeigen die Ergebnisse dieser Arbeit, dass es durch den Verlust von *Tcf4* zu einer fehlerhaften bzw. nicht vollständigen Migration der Körnerzellen von der externen Körnerzellschicht in die interne Körnerzellschicht des Kleinhirns kommt. Das für diese Arbeit neu etablierte Mausmodell des Genotyps $hGFAP\text{-}cre::Tcf4^{fl/fl}$ zeichnet sich durch auffällige Übereinstimmung mit den phänotypischen Charakteristika des Pitt-Hopkins-Syndroms aus. Die vorliegende Arbeit stellt deshalb ein neues Mausmodell für das Pitt-Hopkins-Syndrom vor, das für ausführliche Untersuchungen des zentralnervösen Phänotyps dieser Erkrankung herangezogen werden kann. Eine Besonderheit dieses Tiermodells liegt in seinem homozygoten *Tcf4* Knockout, der normalerweise lethal ist.

Im Unterschied zu einem pränatalen Knockout konnte gezeigt werden, dass ein postnataler Knockout von *Tcf4 in vitro* zu einem Anstieg der Proliferation von Körnerzellvorläufern führt. Diese Ergebnisse sind ein erster Hinweis darauf, dass ein *TCF4* Verlust abhängig vom Zeitpunkt des Knockouts gegenteilige Effekte erzielt und *Tcf4* unterschiedliche Funktionen in unterschiedlichen Phasen der ZNS-Entwicklung übernimmt.

Ein zweiter Teil dieser Arbeit befasst sich mit der Bedeutung von *TCF4* im Rahmen der Entstehung von adulten SHH MBs. Die Ergebnisse einer ersten Analyse eines humanen Datensets zeigten auf, dass das Expressionsniveau von *TCF4* mRNA in SHH assoziierten Medulloblastomen gegenüber der normalen Expression im Cerebellum über alle Altersgruppen hinweg deutlich erhöht ist. Hohe Expressionslevel sind zudem mit einer besseren Progonse, d.h. einem längeren Gesamtüberleben, der Erkrankung assoziiert. Eine Untersuchung der Funktion von TCF4 innerhalb einer Medulloblastomzelllinie kam zu dem Ergebnis, dass die Überexpression von Wildtyp-TCF4 zu einer signifikanten Verringerung der Proliferationsrate der Zellen führt und dass unterschiedliche TCF4-Mutanten die Proliferationsrate abhängig von ihrer Restfunktion beeinflussen. Insgesamt zeigen die gewonnenen Ergebnisse, dass *TCF4* in der postnatalen Entwicklung tumorsuppressive Funktionen ausübt. *In vivo*-Versuche in Mäusen, die SHH MBs entwickeln, konnten zeigen, dass auch hier im Rahmen eines pränatalen *Tcf4*-Knockouts mit einem Anstieg der Apoptoserate zu rechnen ist.

Die Experimente, die im Zusammenhang der Untersuchungen von Medulloblastomen durchgeführt wurden, konnten demnach die zuvor aufgestellte Hypothese, dass die Funktion von *TCF4* zeitabhängig ist, bestätigen. Es zeigt sich, dass ein pränataler Knockout des *TCF4* Gens zu einer verringerten Profilferations- und erhöhrten Apoptoserate führt, wohingegen ein postnataler Knockout im Gegenteil einen Anstieg der Proliferation von Körnerzellen nach sich zieht.

Abstract

Transcription factor 4 (*TCF4*) plays an important role in development of the central nervous system (CNS), particularly in neurogenesis. In 2007, haploinsufficiency of TCF4 was found to be the underlying molecular cause of Pitt-Hopkins syndrome, a severe neurodevelopmental disorder that leads to intellectual disability and a tendency to develop epilepsy as well as breathing abnormalities. Furthermore, variants in *TCF4* have been associated with schizophrenia and other neurodevelopmental disorders causing autistic-like behaviour.

Very recently, a high number of somatic *TCF4* mutations were identified in adult Sonic hedgehog associated medulloblastoma (SHH MB), a malignant tumour of the posterior fossa, predominantly found in children.
This thesis, for the first time, investigates the role of *TCF4* in the formation and growth of medulloblastoma and the importance of *TCF4* in the development of the cerebellum.

One part of this thesis focuses on the role of *TCF4* during development of the cerebellum. Findings from *in vitro* and *in vivo* experiments show that *TCF4* is crucial for the development of the cerebellum and that its loss causes severe alterations to the anatomical structure of the cerebellum in general and the individual cellular layers in specific. Mice used for these experiments were of the genotype *hGFAP-cre::Tcf4*$^{fl/fl}$ whose phenotypical features were shown to match those of patients with Pitt-Hopkins syndrome. A prenatal knockout of *Tcf4* in mice leads to a significant decrease in proliferation and a significant increase in apoptosis of granule cells, leading to growth retardation and microcephaly. The results presented in the present work provide evidence for migratory deficits in granule cells caused by a knockout of *Tcf4*, as cells are no longer able to migrate from the external granular layer into the internal granular layer. Taken all these findings together, this work proposes a new mouse model for Pitt-Hopkins syndrome that can be used to investigate this disorder in more detail with specific focus on changes to the nervous system. Furthermore, this animal model is currently the only model that is viable as a homozygous knockout.

In contrast to a prenatal knockout, a postnatal knockout of *Tcf4* *in vitro* is shown to be responsible for an increase in proliferation in granule precursor cells, indicating that *TCF4* might have opposing effects depending on its time of knockout.

The second part of this thesis aimed at understanding the role of *TCF4* in development of adult SHH MBs. The analysis of a human dataset was able to show that mRNA levels of *TCF4* are highly increased in SHH MBs for all age groups and that high *TCF4* levels are associated with a favourable outcome. An investigation of the function of TCF4 in a medulloblastoma cell line showed that overexpression of wild-type TCF4 causes a significant decrease in proliferation and that different TCF4 mutants alter proliferation rates in accordance with their left-over functionality. These findings provide evidence that *TCF4* acts as a tumour suppressor in postnatal development. *In vivo* experiments in mice developing SHH-associated medulloblastoma showed that a loss of *Tcf4* results in an increase in apoptosis when the knockout occurs prenatally.

Finally, the experiments carried out in the tumorous environment confirmed the initial hypothesis that the function of *TCF4* is time-sensitive. A prenatal knockout of the *TCF4* gene therefore causes a decrease in proliferation and increase of apoptosis, whereas a postnatal knockout on the opposite leads to an increase in proliferation.

Contents

List of Figures

List of Tables

Abbreviations

AA	Amino Acid
AD	Activation Domain
ATCC	American Type Culture Collection
Atoh1	Atonal bHLH Transcription Factor 1
BCA	Bicinchoninic Acid
bHLH	Basix Helix-loop-helix
BrdU	Bromodeoxyuridine
C	Carnegie stage
CASP3	Caspase 3
CGH	Comparative Genomic Hybridisation
CGNP	Cerebellar Granular Neuron Precursor
CNS	Central Nervous System
CSF	Cerebrospinal Fluid
CRISPR	Clustered Regularly Interspaced Short Palindromic Repeats
DAPI	4',6-diamidino-2-phenylindole
DMEM	Dulbecco's Modified Eagle's Medium
DMSO	Dimethyl Sulfoxide
DNA	Deoxyribonucleic Acid
E	Embryonic day
EDTA	Ethylenediaminetetraacetic Acid
EGL	Extrenal Granular Layer
FCS	Fetal Calf Serum
FRT	Flippase Recognition Target
GCP	Granule cell progenitor
GFP	Green Fluorescent Protein
GI	Gastrointestinal
GLI	Glioma-associated oncogene
HBS	HEPES Buffered Saline
HBSS	Hanks' Balanced Salt Solution
HCl	Hydrogen Chloride
HDAC	Histone Deacetylase
H&E	Hematoxylin and Eosin
HEK	Human Embryonic Kidney cells
HEPES	4-(2-hydroxyethyl)-1-piperazineethanesulfonic acid
Het	Heterozygous
hGFAP	Human Glial Fibrillary Acidic Protein
Hom	Homozygous
ICH	Immunohistochemistry
ID	Intellectual Disability
IF	Immunofluorescence
IgG	Immunglobulin G
IGL	Internal Granular Layer

ITF	Immunoglobulin Transcription Factor
IRES	Internal Ribosome Entry Site
KO	Knockout
LB	Lysogeny Broth
LRL	Lower Rhombic Lip
MB	Medulloblastoma
ML	Molecular Layer
MRI	Magnetic Resonance Imaging
NLS	Nuclear Localisation Sequence
OMIM	Online Mendelian Inheritance in Man
P	Post partum (Post-natal day)
PAX6	Paired Box Protein 6
PBS	Phosphate-buffered Saline
PCL	Purkinje Cell Layer
PCR	Polymerase Chain Reaction
PFA	Paraformaldehyde
PGR	Postnatal Growth Retardation
PLO	Poly-L ornithine
PHH3	Phosphohistone H3
PTCH	Patched
PTHS	Pitt-Hopkins syndrome
RL	Rhombic Lip
RNA	Ribonucleic Acid
RT	Room Temperature
SD	Standard Deviation
SHH	Sonic hedgehog
shRNA	Short hairpin RNA
SMO	Smoothened
SNP	Single-nucleotide Polymorphism
SOC	Super Optimal broth with Catabolite repression
SUFU	Suppressor of fused homolog
TCF	Transcription factor
TCF4	Transcription factor 4
TCF7L2	Transcription factor 7 like 2
TE	Tris-EDTA
URL	Upper Rhombic Lip
VZ	Ventricular Zone
WT	Wild type
YFP	Yellow Fluorescent Protein

Gene names and symbols

Gene names and protein symbols are written according to the HGNC Guidelines for Human Gene Nomenclature (HGNC, 2018) and the MGI Guidelines for Nomenclature of Genes, Genetic Markers, Alleles, and Mutations in Mouse and Rat (MGI-Guidelines, 2018). Messenger RNA and complementary DNA in humans use the same format as the corresponding genomic DNA.

Table 1: Nomenclature for gene and protein symbols exemplified by TCF4.

Species	Gene symbol	Protein symbol
Homo sapiens	*TCF4*	TCF4
Mus musculus	*Tcf4*	TCF4
Danio rerio	*tcf4*	Tcf4

1 Introduction

1.1 Transcription factor 4 (*TCF4*)

Transcription factor 4 (*TCF4*) is a member of the superfamily of basic helix-loop-helix (bHLH) transcription factors. This family has a highly conserved role in the specification and differentiation of several cell types, such as neurons and cells of the immune system during development (Forrest et al., 2012). TCF4 is a member of the class A bHLH factors, also known as E-proteins, with the others being E2A (isoforms E12, E47) and HEB (Murre, 2005). E-proteins are widely expressed during nervous system development and they activate transcription through binding to so-called Ephrussi DNA box sequences (E-boxes) (Peippo and Ignatius, 2011). Binding to these E-boxes occurs as homo- or heterodimers, hence, the function of TCF4 is influenced by its dimerisation partner (Sepp et al., 2011).

Due to its role in the development of multiple cell types, *TCF4* was discovered in different contexts. *TCF4* is thus alternatively known by the names *SEF2, ITF2, E2-2, ME2*, and others (Sweatt, 2013). *TCF4* is not to be confused with the T cell factor 4, widely referred to as Tcf4, whose actual gene name is transcription factor 7-like 2 (*TCF7L2*) (Forrest et al., 2012). When talking about *TCF4*, it should be specified which *TCF4* is discussed, especially since a connection between T cell factor 4, a downstream effector of the β-catenin/WNT signalling pathway, and the actual *TCF4* has been made; with *TCF4* being a downstream target of the β-catenin/WNT/TCF pathway itself (de Pontual et al., 2009).

1.1.1 *TCF4* structure and function

TCF4 is located on chromosome 18q21.2; it spans a length of 414 kb (Homo sapiens Annotation Release 108, GRCh38.p7) and consists of 21 exons, with exon 21 not being translated (de Pontual et al., 2009).[1] 18 N-terminally distinct TCF4 isoforms (TCF4-A to -R) have been described to date (Sepp et al., 2011). The so-called full-length TCF4, that is isoform TCF4-B$^+$ and TCF4-B$^-$, consists of 671 and 667 amino acids (AA) respectively (Forrest et al., 2014). This full-length version of TCF4 exhibits, like other E-proteins, two activation domains - AD1 and AD2 - and a nuclear localisation signal (NLS) (Fig. 1). AD1 and AD2 are responsible for transcriptional activity, whereas the NLS mediates the import into the nucleus (Forrest et al., 2014). Regardless of their different N-terminal sequence, all TCF4 isoforms contain the AD2 (exons 14-16) and the bHLH domain (exon 19) (Sepp et al., 2011). For TCF4 to fully function, it needs to dimerise. The bHLH motif is necessary for dimerisation and is also required for DNA binding. TCF4 can operate as a homo- or heterodimer (Sepp et al., 2012), and depending on its dimerisation partner, TCF4 can function as a transcriptional activator or suppressor (Skerjanc et al., 1996; Flora et al., 2007).

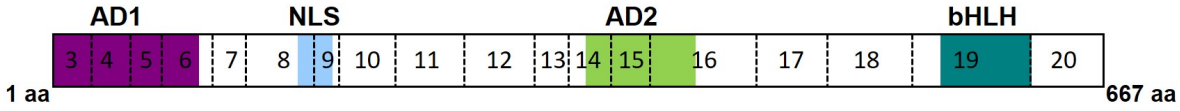

Figure 1: Simplified structure of the TCF4-B$^-$ protein sequence. 667 amino acids sequence of TCF4 isoform TCF4-B$^-$ (UniProtKB - P15884) which contains exons 3-20. The functional domains are highlighted in different colours. AD1 and AD2 are the activation domains (purple and green). NLS is the nuclear localization signal, responsible for the subcellular localization of TCF4 (light blue). The basic helix loop helix domain (bHLH) is necessary for dimerisation (turquoise). Exons 3 to 20 are marked and scaled according to their actual length.

The roles of the E-proteins in mammals overlap in many ways, so it can be difficult to decipher the exact function of the different E-proteins (Sepp et al., 2011). Nevertheless, TCF4 has been found to be involved in a variety of processes. For example, TCF4 is necessary for the regulation of neurogenesis (Flora et al., 2007), lymphogenesis (Cisse et al., 2008), myogenesis (Skerjanc et al., 1996), melanogenesis (Furumura et al., 2001), and epithelial to mesenchymal transition (Herbst et al., 2009a; Sobrado et al., 2009).

[1] Sepp et al. (2011) showed that *TCF4* consists of 41 exons in total, 21 of whom are 5′ initial exons that are interspersed with exons 1-9. These exons are followed by the constitutive exons 10-20. *TCF4* contains only one 3′ terminal exon, exon 21, which is non-coding. The different transcripts give rise to 18 N-terminally distinct isoforms, however, more transcripts exist due to alternate splicing. All transcripts contain the AD2 and the bHLH domain which is encoded by exon 19 (Kharbanda et al., 2016).

More precisely, in lymphogenesis TCF4 is responsible for the regulation of development of B-, T-, and plasmacytoid dendritic cells (Zhuang et al., 1996; Bergqvist et al., 2000; Cisse et al., 2008).
Mice lacking TCF4 do not survive postnatally (Flora et al., 2007), indicating how crucial this protein is. Its heterodimerisation with other bHLH transcription factors is essential for the development of the nervous system (Sepp et al., 2011). Activation or suppression of transcription by TCF4 is mediated through the regulation of histone acetyltransferases which remodel chromatin (Massari et al., 1999; Zhang et al., 2004). Just recently, the regulation of gene transcription in the CNS through TCF4 has been proposed as an *"underlying process in language comprehension, production, and recall"* (Kennedy et al., 2016). Jung et al. (2018) see the role of *TCF4* in *"the development and plasticity of cortical and hippocampal neurons"*.

A study carried out by Forrest et al. (2017), investigating TCF4 binding sites, furthermore concluded that TCF4 is involved in the regulation of a large number of genes, comprising risk loci for schizophrenia and neurodevelopmental disorders in general. Moreover, Moen et al. (2017) build a protein interaction network in neural stem cells, identifying interaction partners of TCF4 by mass spectrometry. Using this interaction network (Fig. 26, Appendix), the group was able to visualise that TCF4 interacts with several genes associated with and involved in intellectual disability, schizophrenia, and the autism-spectrum disorder.

Regarding the impact of *TCF4* on tumour growth and progression, opposing functions have been proposed by different research groups. *TCF4* has previously been described as a tumour suppressor (Herbst et al., 2009b; Brandl et al., 2015), other findings suggest TCF4 exhibits oncogenic potential (Kolligs et al., 2002; Mologni et al., 2010; Appaiah et al., 2014). Very recently, the loss of *TCF4* was shown to lead to chemoresistance in cancer (de Garibay et al., 2018).

1.1.2 *TCF4* during brain development

The importance of *TCF4* for neurodevelopment is highlighted by its wide expression during various prenatal and postnatal stages. Soosaar et al. (1994) were the first to map the expression of TCF4 during brain development in mice. In general, TCF4 expression was found to be at its maximum during embryonic development. On embryonic day (E) 12, TCF4 was detected in the cortex, the cerebellum, the pons, the medulla oblongata, and the spinal cord. From E18 onwards until adult stages, high TCF4 levels were found in pyramidal cells of the hippocampal layers CA1-CA4 and the granule cells of the dentate gyrus. As for the cerebellar granule and Purkinje cells, TCF4 was expressed during all stages. Overall, TCF4 expression was detected in proliferative zones during the development and in areas of neuroplasticity in the adult brain, i.e. hippocampus, cerebellum, neuroepithelium, and neocortex (Soosaar et al., 1994). Similar, de Pontual et al. (2009) collected embryos from terminated pregnancies and scanned them for TCF4 expression. The authors observed that from Carnegie stage (C) 13 (28-32 days post fertilisation) onward, TCF4 was highly expressed throughout the CNS.
In the adult CNS, TCF4 can be detected in the cerebral cortex, the Purkinje cell and granule cell layers of the cerebellum, the olfactory neuroepithelium, pyramidal cells of the hippocampal layers CA1-CA4, and the granule cells of the dentate gyrus (Soosaar et al., 1994).

1.1.3 *TCF4* animal models

Animal models are widely used to investigate the function of different genes, proteins, and pathways and are a useful tool to better understand the molecular basis of disease and to test new treatment strategies. A couple of animal models to study *TCF4* have been described so far. Apart from several mouse models, a *Danio rerio* (zebra fish) and *Drosophila melanogaster* model are also available.

One of the earliest genetically engineered *TCF4* mouse models exhibits a 'traditional' heterozygous *Tcf4* knockout ($Tcf4^{tm1Zhu}$, transcription factor 4; targeted mutation 1, Yuan Zhuang, MGI ID: MGI:2387399) and is available from the Jackson Laboratories (Zhuang et al., 1996). In this transgenic mouse model, the bHLH domain of *Tcf4* has been cut out by recombination (Zhuang et al., 1996). Mice homozygous for this knockout barely survive the first postnatal week, hence, a homozygous knockout is lethal (Zhuang et al., 1996; Flora et al., 2007). Furthermore, two conditional knockout mice have been published (Bergqvist et al., 2000; Skarnes et al., 2011).

One floxed *Tcf4* allele was generated by Skarnes et al. (2011). Its precise description is Tcf4$^{tm1a(EUCOMM)Wtsi}$ (MGI ID: MGI:4432303), which stands for 'transcription factor 4; targeted mutation 1a, Wellcome Trust Sanger Institute' and it is available through the EMMA mouse repository. The mouse is also referred to as *Tcf4*^{LacZ}, since the inserted cassette is composed of a flippase recognition target (*FRT*) flanked lacZ/neomycin sequence followed by a *loxP site*. This mouse model can therefore be used with the Cre-*lox* and the FLP-*FRT* system (Schnütgen et al., 2005). A second floxed allel of *Tcf4* was generated by Bergqvist et al. (2000) in the laboratory of Dan Holmberg. It is referred to as *Tcf4*^{tm1Hmb} (MGI ID: MGI:3036170), which stands for 'transcription factor 4; targeted mutation 1, Dan Holmberg'. Here, the exons encoding for the bHLH and the C-terminal domains have been flanked by *loxP sites* (Sweatt, 2013). These mice will be referred to as *Tcf4*$^{fl/fl}$ in this work. Furthermore, Rannals et al. (2016a) generated a *Tcf4* knockdown rat using short hairpin RNA (shRNA) as well as a *Tcf4* knockout rat using the CRISPR-Cas9 (Clustered Regularly Interspaced Short Palindromic Repeats-CRISPR associated protein 9) system.

In addition to these knockouts, Brzozka et al. (2010) generated a mouse model moderately overexpressing *Tcf4* postnatally (*Tcf4tg*), which has been used to investigate schizophrenia and the function of *Tcf4* in the adult brain.

Besides the described mammalian models, a *tcf4* zebra fish model has been published (Brockschmidt et al., 2011). *Tcf4* was knocked down through the injection of morpholino antisense oligonucleotides into zebra fish embryos. The model was created to study Pitt-Hopkins syndrome (see Section 1.2) in zebra fish and was able to show that reduction of *tcf4* delays the development of the brain. Tamberg et al. (2015) introduced another animal model using *Drosophila melanogaster*. They generated flies carrying Pitt-Hopkins syndrome-associated mutations in the TCF4 homolog *daughterless*.

1.1.4 *TCF4*-associated diseases

To date, *TCF4* has been associated with several distinct diseases. In 2007, mutations in *TCF4* were found to be the cause of the neurodevelopmental disorder Pitt-Hopkins syndrome (see Section 1.2) (Amiel et al., 2007; Zweier et al., 2007). *TCF4* has further been linked to other neurodevelopmental disorders: hemizygosity of *TCF4* has been found to increase the risk of autistic-like behaviour in patients with 18q deletions (O'Donnell et al., 2010; Hasi et al., 2011), and *TCF4* was identified as a significant schizophrenia susceptibility gene (Brzozka et al., 2010).

Single-nulceotide polymorphisms (SNPs) in *TCF4* are also associated with Fuchs corneal dystrophy, an autosomal dominant inherited disease that severely affects vision (Baratz et al., 2010; Li et al., 2011). Moreover, Kool et al. (2014) were the first to describe a series of somatic *TCF4* mutations in cancer (see Chapter 2, p. 20). *TCF4* has been suspected to increase the susceptibility to develop cancer before, but only rare cases have been reported (de Pontual et al., 2009).

1.2 Pitt-Hopkins syndrome

1.2.1 Cause of Pitt-Hopkins syndrome

De novo haploinsufficiency of *TCF4* causes Pitt-Hopkins syndrome (PTHS, OMIM ID # 610954), a rare neurodevelopmental disorder (Amiel et al., 2007; Zweier et al., 2007; Sweatt, 2013).
The syndrome was first reported by David Pitt and Ian Hopkins, a paediatrician and a paediatric neurologist, after following two unrelated cases of children with breathing abnormalities and unique facial features (Pitt and Hopkins, 1978). Main characteristics of the syndrome include severe intellectual disability (ID), typical facial gestalt, stereotypic movements, a tendency to develop epilepsy, and breathing abnormalities (Peippo and Ignatius, 2011).

The molecular basis of PTHS was described in 2007, when two separate groups identified microdeletions at chromosomal location 18q21.2 in PTHS patients which subsequently led to the finding that haploinsufficiency of *TCF4* is the underlying cause of the syndrome (Amiel et al., 2007; Zweier et al., 2007). PTHS is an autosomal dominant disorder. However, only a few cases have been published in which a child inherited the syndrome from a mosaic parent and there are no known cases of patients with PTHS having children themselves (de Pontual et al., 2009; Kousoulidou et al., 2013). The prevalence of children suffering from PTHS is hard to determine as there are only around 500 reported cases worldwide. Rosenfeld et al. (2009) estimated the frequency of *TCF4* deletions that cause PTHS to 1/34,000 - 1/41,000, not accounting for point mutations that also cause PTHS. The actual prevalence of PTHS amongst the population must therefore be higher. PTHS occurs in a 1:1 ratio in males and females and there is no indication for preference of ethnicities (Marangi et al., 2011).

1.2.2 Clinical features of PTHS

Patients with Pitt-Hopkins syndrome exhibit a set of unique symptoms. As seen in Fig. 2, facial features include *"the deep-set eyes, broad and beaked nasal bridge with down-turned, pointed nasal tip, and flaring nostrils; the wide mouth with widely spaced teeth, and Cupid-bowed and everted lower lip; the mildly cup-shaped, fleshy ears; as well as increased coarsening of the facial features with age"* (Peippo and Ignatius, 2011).

Figure 2: Facial features of patients with PTHS. Figure taken from the original publication by Zweier et al. (2007)[2]. The pictures illustrate the typical facial gestalt of PTHS patients with their deep-set eyes, as well as the distinct nasal features. Other characteristics include a broad and beaked bride, flaring nostrils, and a pointed nasal tip. The mouth is wide and the teeth are widely spaced (Peippo and Ignatius, 2011).

[2]Reprinted from The American Journal of Human Genetics, 80(5), Christiane Zweier, Maarit M. Peippo, Juliane Hoyer, Sérgio Sousa, Armand Bottani, Jill Clayton-Smith, William Reardon, Jorge Saraiva, Alexandra Cabral, Ina Göhring, Koen Devriendt, Thomy de Ravel, Emilia K. Bijlsma, Raoul C.M. Hennekam, Alfredo Orrico et al., Haploinsufficiency of TCF4 Causes Syndromal Mental Retardation with Intermittent Hyperventilation (Pitt-Hopkins Syndrome), 994-1001, Copyright (2007), with permission from Elsevier.

The distinct facial gestalt normally becomes recognisable around three years of age. Postnatal growth retardation is common, and about 60 % of the patients show postnatal microcephaly (Peippo and Ignatius, 2011; Marangi and Zollino, 2015). One of the main clinical features is the intellectual disability; illustrated by the fact that patients fail to reach developmental milestones beyond the age of 12 months (Hasi et al., 2011). These children exhibit a severe impairment of speech; with most patients being limited to a few words only (Peippo and Ignatius, 2011). Children may also present with a happy disposition or autistic behaviour (Rosenfeld et al., 2009; O'Donnell et al., 2010). Furthermore, the majority of patients do not learn how to walk independently and if, walking is atactic and unsteady (Peippo and Ignatius, 2011). Generally, patients suffer from hypotonia (Sweatt, 2013).

Children with PTHS present with stereotypical movements of the hands and sometimes of their head. Over 40 % of cases develop epilepsy with an usual onset before school age and more than half of patients show breathing abnormalities such as breath-holding cyanosis and paroxysms of hyperventilation (Peippo and Ignatius, 2011). Moreover, patients often present with symptoms in other systems, e.g. gastrointestinal disorders (mostly constipation) or myopia (Peippo and Ignatius, 2011; Grubišić et al., 2015).

1.2.3 Diagnosis, treatment, and prognosis of PTHS

Diagnosis of PTHS is based on the stereotypic clinical features and the molecular confirmation, typically done using array-comparative genomic hybridisation (CGH) to detect deletions that often cause PTHS, i.e. encompass *TCF4*. Whalen et al. (2012) proposed a 'Clinical Diagnostic Score' to help decide when a *TCF4* screening is indicated. However, international diagnosis criteria have not yet been established (de Winter et al., 2016).

Treatment for patients with PTHS has mainly been focused on the treatment of symptoms such as the epilepsy and breathing abnormalities. Several single-case studies have been published making suggestions regarding the therapeutic options for treating these complications (Gaffney and McNally, 2015; Aquino et al., 2017; Casey et al., 2017). Presently, several research groups are looking into new treatment strategies to tackle the whole syndrome. For example, Kennedy et al. (2016) recently proposed histone deacetylase 2 (HDAC2) inhibitors as a potential treatment after showing that HDAC inhibition is able to rescue learning and memory deficits in PTHS mice (Kennedy et al., 2016). Furthermore, Rannals et al. (2016b) suggested the ion channel SCN10a as a potential therapeutic target for PTHS, since haploinsufficiency of TCF4 leads to its ectopic expression.

Although Hasi et al. (2011) have suggested PTHS patients have an increased risk of death, the actual life expectancy of patients suffering from Pitt-Hopkins syndrome is still unknown and the cause of death remains questionable. Several cases have been reported in which PTHS patients died due to their breathing problems (Zweier et al., 2007; Peippo and Ignatius, 2011).

1.2.4 Mutational spectrum of PTHS

Over a hundred different *TCF4* mutations causing PTHS have been described so far, with the mutational spectrum including a variety of mutations, e.g. chromosomal deletions, partial gene deletions, frame-shift mutations, splice site mutations, missense mutations, and nonsense mutations. *TCF4* abnormalities seen in PTHS patients are intragenic or perigenic and deletions range from <100 kb to 12 Mb in size (Peippo and Ignatius, 2011). Most intragenic mutations create stop codons or alter the conserved bHLH domain of the protein (Rosenfeld et al., 2009). The identified mutations are mostly private mutations and only a few have been found in more than one patient (Sepp et al., 2012; Whalen et al., 2012). *TCF4* mutations can generally be found throughout the gene (Sepp et al., 2012), however, at least one mutational hotspots was identified (Whalen et al., 2012). de Pontual et al. (2009) initially declared a mutational hotspot in the bHLH domain, which was later verified by Whalen et al. (2012), who came to the conclusion that mutations cluster in exon 19, where 25 % (28/110) of total mutations in their cohort were located.
Moreover, Sepp et al. (2012) proposed that symptoms present in PTHS patients vary depending on the site and the kind of mutation. Interestingly, apart from haploinsufficiency of *TCF4* caused by deletions, some of the known mutations will still lead to the expression of a mutant TCF4 protein, which can cause dominant-negative effects, thus generating the PTHS phenotype in these cases (Sepp et al., 2012). There are also deletions encompassing the 18q locus and mutations within *TCF4* that are reported to not cause Pitt-Hopkins syndrome (Kalscheuer et al., 2008; Soileau et al., 2015; Kharbanda et al., 2016; Mary et al., 2018).

1.2.5 Pitt-Hopkins animal models

To better understand Pitt-Hopkins syndrome, its symptoms, clinical appearance and their molecular causes, the establishment of a suitable animal models to study the disease is essential. Kennedy et al. (2016) proposed the $Tcf4^{+/-}$ mouse, originally published by Zhuang et al. (1996), as a suitable mouse system to model Pitt-Hopkins syndrome (see Section 1.1.3).

Kennedy et al. (2016) used these mice to asses behavioural and learning disabilities and concluded, that the mice mimic PTHS in this respect. In a separate effort, Grubišić et al. (2015) investigated the $Tcf4^{+/-}$ mouse in relation to the common gastrointestinal disorders (GI disorders) and found that the mice indeed exhibit GI abnormalities seen in PTHS patients.

As mentioned before, another PTHS model has recently been published by Rannals et al. (2016b) who knocked down *Tcf4* with two different shRNA molecules in rat prefrontal neurons. They also created a *Tcf4* knockout rat using the CRISPR/Cas9-system (Rannals et al., 2016a).
In early 2018, five more mouse models to research Pitt-Hopkins syndrome were published (Jung et al., 2018; Thaxton et al., 2018). Jung et al. (2018) assessed the previously published $Tcf4^{LacZ}$ mouse, originally generated by Skarnes et al. (2011), for its use to model PTHS. They examined a solely heterozygous knockout of *Tcf4*, describing that these mice show a CNS phenotype similar to PTHS as well as a microcephaly. Thaxton et al. (2018) used the $Tcf4^{fl/fl}$ mouse and created two different conditional knockouts expressing the Cre recombinase under the *Actin* promoter and the *Nestin* promoter respectively. Additionally, Thaxton et al. (2018) generated two more mice introducing mutations that had previously been described in PTHS, the $Tcf4^{R579W}$ mouse and $Tcf4^{\Delta 574-579}$ mouse which both exhibited characteristic features of PTHS (see Section 4.2 on p. 54 for comparison of PTHS mouse models).

Apart from these mammalian animal models, another model was generated using *Drosophila melanogaster* producing different fly strains that exhibit several of the known TCF4 mutations (Tamberg et al., 2015).

1.3 Cerebellum

1.3.1 Structure and function of the cerebellum

The cerebellum, colloquially known as the 'little brain', resides in the posterior cranial fossa and is part of the hindbrain of all vertebrates (Trepel, 2009). It is located inferior to the occipital and temporal lobes, separated from these lobes by the tentorium cerebelli. The cerebellum lies posterior to the pons, separated from it through the fourth ventricle (Aumüller and Wurzinger, 2010). From a superficial point of view, the cerebellum is divided into horizontal folia. It consists of a left and right hemisphere and a medial expansion called vermis.

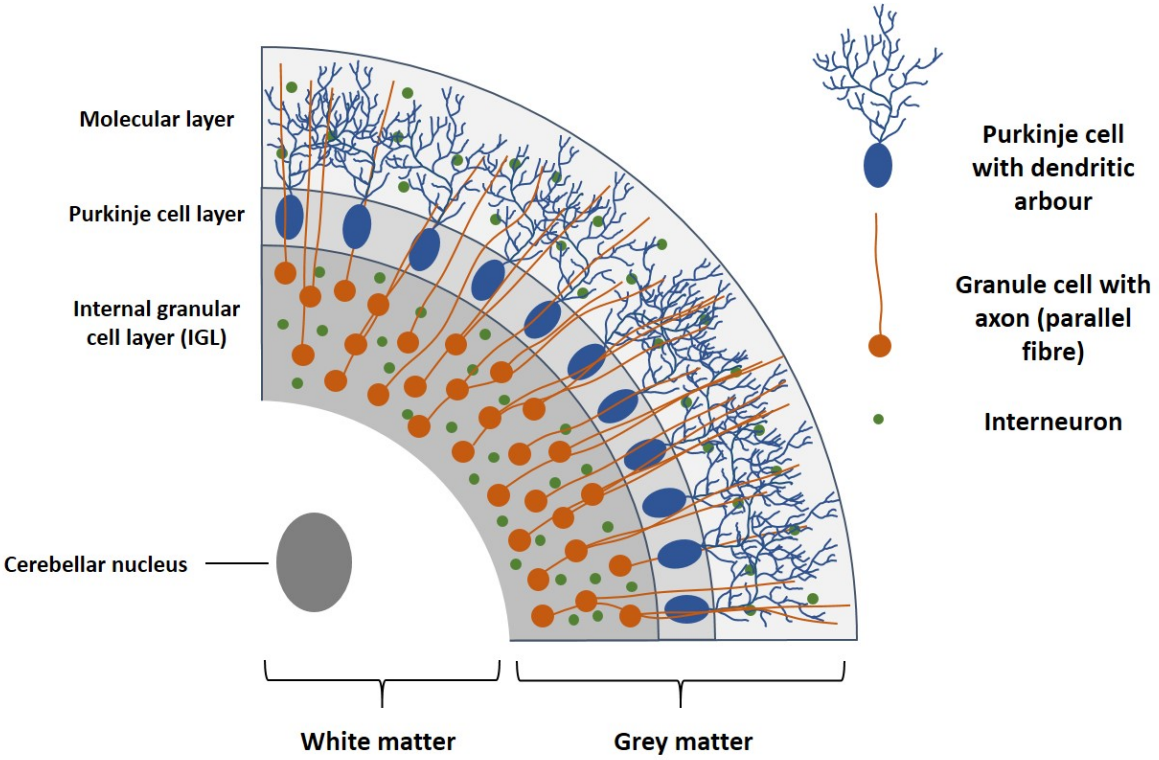

Figure 3: Overview of the cerebellar layers in a sagittal section. Sagittal section through the cerebellum showing the different structures of the white and grey matter. The grey matter consists of three layers, the molecular layer, the Purkinje cell layer, and the granule cell layer (internal granule layer, IGL). The layers also contain different interneurons. The axons of granule cells form parallel fibres that are orthogonally to the dendritic arbours of the Purkinje cells (not shown here) (Butts et al., 2014).

The cerebellum is essential for motor control; and although it does not initiate movement, it is responsible for coordination. Recent work has shown that the cerebellum additionally plays a big role in cognitive function, e.g. feed-forward sensory-motor learning, speech, and spatial memory (Schmahmann and Caplan, 2006; Hatten and Roussel, 2011; Zakrzewska et al., 2013). Its importance is also highlighted by the fact that the majority of the mature neurons in the adult brain are in the cerebellum (Butts et al., 2014), most of them being cerebellar granule neurons (Hatten and Roussel, 2011). The adult cerebellum exhibits a rather simple histological composition, consisting of the white matter and three outer layers forming the cortex (Fig. 3). The white matter, containing the cerebellar nuclei, is surrounded by the internal granular layer (IGL), followed by the Purkinje cell layer (PCL), and the sub-pial molecular layer (ML), comprised of the Purkinje cell dendritic trees and the axons of the granule cells (Butts et al., 2014).
Input from outside the cerebellum is received by the granule cells which then project to the Purkinje cells that forward information to the different cerebellar nuclei. Additionally, a network of interneurons is able to modulate this output (Trepel, 2009).

1.3.2 Development of the cerebellum

During the early embryonic stages of development, the brain can be divided into three segments: the prosencephalon (forebrain), the mesencephalon (midbrain), and the rhombencephalon (hindbrain) (Smeyne and Goldowitz, 1989; Müller and O'Rahilly, 1990). The cerebellum develops from the rhombencephalon, the most caudal of these segments. This part of the developing CNS can itself be divided into two sections, the metencephalon and the myelencephalon. The metencephalon has been shown to build eight swellings (structural units) on its posterior part, so-called rhombomeres. Rhombomere 1 later forms the cerebellum (Wingate and Hatten, 1999). This whole posterior section of the developing metencephalon is called the rhombic lip (RL) (Gilthorpe et al., 2002). The upper rohmbic lip (URL, rhombomere 1) is responsible for the development of the cerebellum; the lower part of the RL (LRL, lower rhombic lip) gives rise to cells that later form parts of the precerebellar system and cochlear nucleus (Landsberg et al., 2005).

Investigations in mice have shown that the cerebellar 'anlage' is allocated to the boundary between the hindbrain and the midbrain as early as E8.5 (Butts et al., 2014). Two days later, around E10.25, the cerebellar nuclei and cerebellar cortex begin to be generated by a complex pattern of cell movement and neurogenesis (Hatten and Heintz, 1995; Hatten and Roussel, 2011). The Purkinje cells of the cerebellum and the deep cerebellar nuclear neurons are thought to arise from the ventricular zone (VZ) which lies in the roof of the fourth ventricle. During days E11 to E14, Purkinje progenitors migrate from the VZ into the cerebellar 'anlage' (Morales and Hatten, 2006). Proliferating cells that later form the external granular layer (EGL), birthplace of the granule neuron, emigrate from the rhombic lip around E12.

The EGL can still be found in newborns as the outermost layer of the cerebellum. During the early post-natal phase, granule cells from the EGL migrate into inner parts of the cerebellum underneath the Purkinje cell layer to form the internal granular layer (Müller and O'Rahilly, 1990). For granule cells to exit the cell cycle and migrate into the IGL, several processes need to be completed. On postnatal days two to four (P2-4), granule cell progenitor (GCP) proliferation within the EGL is influenced by various signalling pathways. At P5-8, a peak period of proliferation can be observed, hence, precursor cells are mostly isolated around this age for further studies (Roussel and Hatten, 2011). Starting from birth up until P14, the progenitor cells exit the cell cycle and can be found in the inner section of the EGL.

From there, they migrate into the inner cerebellar parts underneath the Purkinje cell layer along the radial fibres of the Bergman glia (Edmondson and Hatten, 1987). This new formed layer is called internal granular layer. Migration is thought to be completed around P20 (Hatten and Heintz, 1995). Only the IGL - not the EGL - can be found in the mature brain.

1.4 Medulloblastoma

Medulloblastoma (MB) is the most common malignant tumour of the central nervous system in children (Kool et al., 2008; Taylor et al., 2012). MBs can also be found in other age groups, such as infants and adults, however, it accounts for only 1 % of adult CNS tumours (Giordana et al., 1999). Medulloblastomas are a heterogenous class of embryonal tumours and are divided into several subgroups depending on their histological and genetical characteristics (Louis et al., 2016b). These genetical characteristics include anomalies in pathways that are essential to the development of the hindbrain, e.g. the WNT and SHH pathway (Roussel and Hatten, 2011). Due to the differences in the MB subgroups, treatment has shown to be difficult and new strategies try to design subgroup-specific therapies. Survival of patients with MB is also dependent on the group and reaches from very good prognosis with over 90 % 5-year survival rates, to very poor prognosis with about 30 % 5-year survival rates (Northcott et al., 2011). Medulloblastomas are rapidly growing, but non-invasive. Interestingly, unlike other brain tumours, MBs metastasize frequently within the CNS, however, extraneural metastases are rarely found (Dufour et al., 2012).

1.4.1 Medulloblastoma subgroups

The latest version of the *'WHO classification of tumours of the central nervous system'* was published in 2016. Here, for the first time, the WHO defines different classifications of medulloblastoma: one being histologically defined subgroups; the other genetically defined ones (Louis et al., 2016a).

For this project, the genetically defined subgroups are of special interest. There are four distinct genetically defined subgroups to date. The WHO differentiates between MB with activation of the WNT signalling pathway, MB with activation of the SHH signalling pathway, with distinguished groups of TP53-mutants and TP53-wildtype, and non-WNT/non-SHH MBs called groups 3 and 4 (Louis et al., 2016b,a). An overview of the genetically defined groups and their histological counterparts is given in Fig. 4.

Taylor et al. (2012) published the first consensus of MB subgroups outlining that *"there were four principal transcriptional subgroups of medulloblastoma, with many of these subgroups showing a subsequent level of hierarchical structure that will be designated the subtypes of the subgroups"*. The first two subgroups were named due to the pathway that is thought to play an important role in the pathogenesis of the respective group. Following, a short outline of the different groups and their characteristics is given.

WNT The WNT subgroup is best known for its very good long-term prognosis, with a 5-year survival rate of over 90 % (Ellison et al., 2011). Most of the tumours in this group have classic histology. Interestingly, although males are usually more likely to develop medulloblastoma, WNT-activated MB show a 1:1 ratio for male to female patients. The tumour does normally not occur in infants (Fig. 4) (Taylor et al., 2012).

	Genetic profile	Histology	Prognosis	Demographics
WNT	WNT-activated	Classic	low-risk tumour; classic morphology found in almost all WNT-activated tumours	♂ : ♀ = 1 : 1
		Large cell / anaplastic (very rare)	tumour of uncertain clinicopathological significance	I : C : A = 0 : 2 : 1
SHH	SHH-activated, *TP53*-mutant	Classic	uncommon high-risk tumour	
		Large cell /anaplastic	high-risk tumour; prevalent in children aged 7-17 years	
		Desmoplastic / nodular (very rare)	tumour of uncertain clinicopathological significance	♂ : ♀ = 1 : 1
	SHH-activated, *TP53*-wildtype	Classic	standard-risk tumour	I : C : A = 2 : 1 : 3
		Large cell /anaplastic	tumour of uncertain clinicopathological significance	
		Desmoplastic / nodular	low-risk tumour in infants; prevalent in infants and adults	
		Extensive nodularity	low-risk tumour of infancy	
Group 3	non-WNT/non-SHH, group 3	Classic	standard-risk tumour	♂ : ♀ = 2 : 1
		Large cell / anaplastic	high-risk tumour	I : C : A = 1 : 2 : 0
Group 4	non-WNT/non-SHH, group 4	Classic	standard-risk tumour	♂ : ♀ = 2 : 1
		Large cell / anaplastic (rare)	tumour of uncertain clinicopathological significance	I : C : A = 1 : 3 : 1

Figure 4: Overview of medulloblastoma subgroups. Table gives an overview of the four MB subgroups and their main characteristics, i.e. genetic profile, histology, prognosis, and demographics. Male to female ratios are shown using the standard sex symbols. Ratios of age groups are shown in comparison of infant (I) to child (C) to adult (A) patients. Table adapted from Louis et al. (2016a), original content reprinted with kind permission from Dr. David W. Ellison, St. Jude Children's Research Hospital in Memphis, TN US.

SHH The Sonic hedgehog (SHH) signalling pathway is thought to be the cause for development of MBs in group 2. Germline mutations in *PTCH* and *SUFU* as well as somatic mutations in *GLI1, GLI2, PTCH, SMO,* and *SUFU*, all of which belong to the SHH pathway, have been found in SHH MBs (Taylor et al., 2002; Slade et al., 2011; Taylor et al., 2012).

The location of SHH MB is distinct, depending on the age group: in adults, SHH MBs are located in the cerebellar hemispheres, however, infant SHH MBs are often seen in the vermis (Wefers et al., 2014). SHH-associated tumours can be found in both infants and adults with no preference for sex (ratio 1:1). Prognosis for this subgroup can be described as 'intermediate' as it is worse than that of the WNT subgroup, but better than the poor outcome for patients of group 3 (Taylor et al., 2012).

Group 3 Medulloblastomas in group 3 mostly show 'classic' histological features. To classify a tumour as a member of group 3, its transcriptional profile has to match others from the same group (Kool et al., 2008). There is no defined marker for this subgroup, although a few have been proposed (Northcott et al., 2011; Hatten and Roussel, 2011). Tumours in group 3 are more often found in males and almost never occur in adults (Taylor et al., 2012). MBs in this group have a very poor prognosis.

Group 4 MBs in group 4 are described as the 'prototypical medulloblastoma' (Taylor et al., 2012). As with group 3, MBs from group 4 are identified through matching transcriptional profiles. An isochromosome 17q is often found in these tumours (Kool et al., 2012). Similar to group 3, tumours in group 4 show a high male-to-female ratio; prognosis is comparable to group 2.

For this thesis, focus was on Sonic hedgehog associated medulloblastoma of the adult brain (group 2), as this group was found to have additional somatic mutations in *TCF4* in 14 % of cases (Kool et al., 2014).

1.4.2 SHH signalling pathway

The Sonic hedgehog signalling pathway is essential for human development, especially for the organisation of the brain. And even after successful development, SHH remains important; for example, for the cell division of adult stem cells (Choudhry et al., 2014). Its constitutive activation in the postnatal cerebellum has been shown to be sufficient to initiate MB development in mice (Schüller et al., 2008; Rimkus et al., 2016). The SHH pathway is thought to be defective in more than 25 % of medulloblastomas (Gilbertson and Ellison, 2008). Consequently, the SHH/PTCH (Patched) signalling pathway is the best studied pathway in MBs (Rosenfeld et al., 2009).

Sonic hedgehog belongs to a family of three proteins named the Hedgehog family, with the other two being Desert hedgehog and Indian hedgehog (Echelard et al., 1993; Marigo et al., 1995). The main responsibility of SHH is the upregulation of transcription of numerous target genes (Ingham et al., 2011). This protein acts as a morphogen, i.e. its various concentrations determine the cell's fate in different ways. Hence, exposure to the different levels of SHH will result in several distinct cells. Low concentrations of SHH lead to ventral neurons, high concentrations induce motor neurons, whereas very high concentrations produce so-called floor plate cells (Ericson et al., 1997; Jessell, 2000).

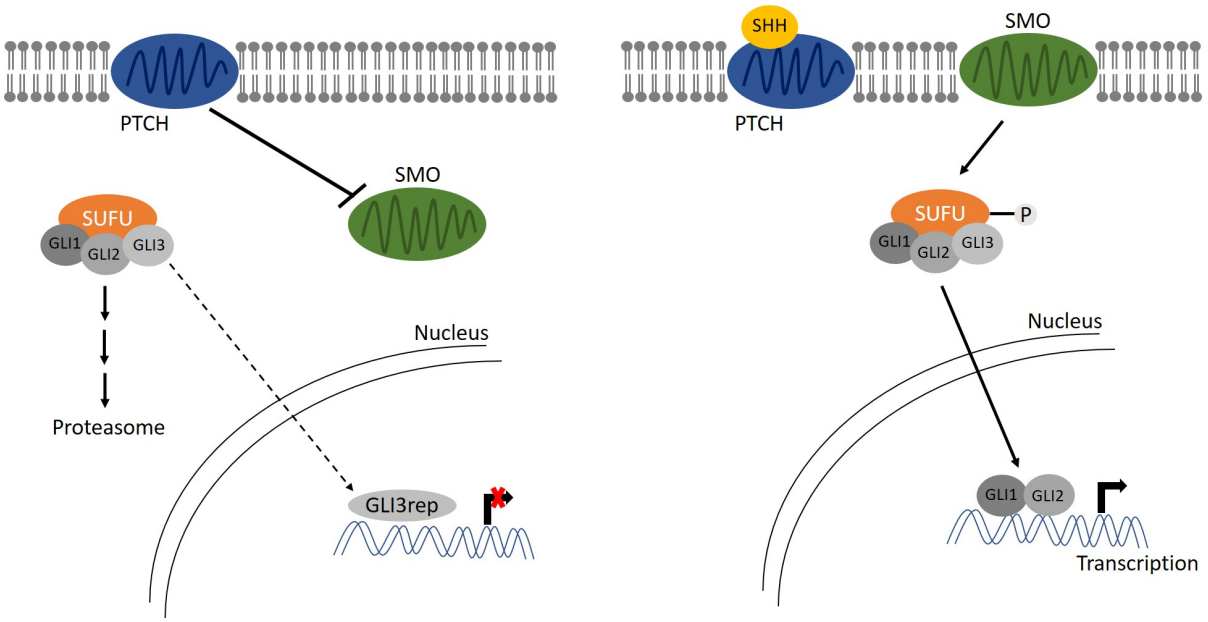

Figure 5: Sonic hedgehog (SHH) signalling pathway. Left: In absence of SHH, Patched (PTCH) represses the function of Smoothened (SMO). This causes SUFU to retain the GLI proteins in the cytosol and GLI is either ubiquitylated and degraded by the proteasome or cleaved and turned into a transcriptional repressor. Only the transcriptional repressor forms of GLI are able to enter the nucleus and inhibit transcription. **Right:** In the presence of SHH, PTCH cannot repress SMO which translocates into the cell membrane. SMO mediates downstream signal transduction which leads to the phosphorylation of SUFU and subsequent dissociation of GLI1 and GLI2 which can now enter the nucleus to activate transcription.

Although interactions within the SHH pathway are complex and not yet fully understood, the main features can be described as follows (Fig. 5): SHH is able to drive proliferation of granule cell precursors by binding to the transmembrane receptor Patched (PTCH). In the absence of SHH, PTCH represses the function of Smoothened (SMO), another transmembrane receptor normally located in intracellular vesicles (Choudhry et al., 2014). SMO is a seven-transmembrane receptor responsible for the activation of the transcription factors GLI1 and GLI2 and the inhibition of the trancriptional repressor GLI3.

These transcription factors serve as regulators of the transcriptional programme in the cell nucleus (Rosenfeld et al., 2009).
As long as SHH is absent, GLI is cleaved and following a series of chemical reactions the C-terminus is ubiquitylated which leads to its degradation by the proteasome (Ingham et al., 2011). This process also yields transcriptional repressor forms of GLI, preventing activation of SHH target genes (Rubin and de Sauvage, 2006). Furthermore, SUFU, another negative regulator of the SHH pathway interacts with the three uncleaved GLI proteins in order to retain them in the cytosol (Jia et al., 2009). In the presence of SHH, PTCH becomes inactive allowing SMO to translocate to the membrane and therefore become activated. The activation of SMO triggers a cascade of reactions allowing the phosphorylation of SUFU which thus dislocates from GLI. GLI can now find its way into the nucleus to initiate transcription (Ingham et al., 2011).

Due to its role in the SHH signalling pathway, SMO has been found to exhibit oncogenic potential and activating mutations will give rise to neoplasia, i.e. SHH-associated medulloblastoma (Choudhry et al., 2014). SMO is therefore not only a popular target for new treatment strategies but also widely used in animal models to mimic SHH-associated MB (see Section 1.4.5).

1.4.3 Origins of medulloblastoma

Knowing the origins of a tumour, the cells it arises from and their exact location, is a prerequisite for generating matching animal models and targeted treatment strategies. As mentioned before, medulloblastoma is a heterogeneous group of tumours that can be divided into several subgroups due to their genetic background. Consequently, different cell populations of the rhombic lip give rise to different MB subgroups (Gibson et al., 2010; Grammel et al., 2012).

Gibson et al. (2010) were the first to demonstrate that the WNT MB subtype originates from cells of the dorsal brainstem outside of the cerebellum; these cells are precursor cells of the precerebellar rhombic lip (rhombomere 6-8) that migrate and later form nuclei throughout the developing hindbrain. As for the SHH-associated MB, Grammel et al. (2012) were able to show that two distinct cell populations give rise to this particular tumour entity. It was already known that activation of the SHH pathway in cerebellar granule neuron precursors (CGNP), a progenitor population of the URL (rhombomere 1, see Section 1.3.2) and in precursors of the EGL is able to give rise to SHH MBs (Schüller et al., 2008; Behesti and Marino, 2009).

Grammel et al. (2012) then demonstrated that SHH MBs can also arise from granule neuron precursors of the cochlear nuclei, a cell population from the auditory lower rhombic lip (rhombomere 2-5). The cellular origins for groups 3 and 4 have yet to be identified.

Besides the identification of different cell populations giving rise to the different MB subgroups, investigations on the exact localization of the tumours have been carried out and shown to be age-dependent as well as dependent on the age of initiation (Wefers et al., 2014; Ohli et al., 2015). Wefers et al. (2014) were able to show that localisation of SHH MBs differed between infant SHH MB and adult SHH MB, while Ohli et al. (2015) could demonstrate that the age of initiation determines the localization of the tumours.

1.4.4 Symptoms, diagnosis, and current treatment strategies of MB

Symptoms associated with MB are mostly non-specific in the beginning and mainly caused by increased cranial pressure, leading to headache and vomiting. Patients can further become listless. With time, patients will develop ataxia and more cognitive problems as well as dizziness. Especially infants can also develop a hydrocephalus (Polkinghorn and Tarbell, 2007). Symptoms of increased cranial pressure usually start a few months before diagnosis and worsen with tumour growth. Depending on the metastatic state of the tumour, other symptoms are possible. Different magnetic resonance (MR) imaging techniques are normally used for diagnosis and in case of MB reveal a mass in the posterior fossa (Polkinghorn and Tarbell, 2007).

Current treatment strategies for medulloblastomas encompass surgical resection, radiation, and chemotherapy independent of the MB subgroup. Over the past 20 years, progress has been made regarding treatment for MB patients; currently around 60 % of patients show a 5-year survival (Rutkowski et al., 2005). Nevertheless, many of the therapies still come with adverse secondary effects and significant morbidity (Gajjar et al., 2006). Especially the long-term effects of radiation on the immature brains of infants are of great concern (MacDonald, 2008).

With a better understanding of the disease on a molecular level, new therapeutic approaches are becoming available, trying to optimise treatment in respect to the specific subgroup and their characteristics (Roussel and Hatten, 2011). Some of these new drugs have already been developed and tested in mouse models (Romer and Curran, 2005; Beauchamp et al., 2011; Lee et al., 2012).

Further research on the molecular basis of development and progression of medulloblastoma will give rise to new therapeutic targets and therefore treatment strategies.

1.4.5 Medulloblastoma mouse models

For a better understanding and the possibility to investigate medulloblastoma in more detail, mouse models for the different subgroups of MB have been generated. There are over 20 different mouse models for MB published to date; most of which model SHH MBs (Wu et al., 2011; Pöschl et al., 2014; Neumann et al., 2017). Pöschl et al. (2014) were able to show that the majority of the known SHH MB mouse models match adult SHH MB in humans. They further showed that especially medulloblastoma driven by a *SMO* mutation, constitutively activating the SHH pathway, match adult SHH MB best. These mouse models were thus used for this project.

Schüller et al. (2008) published the *hGFAP-cre::SmoM2-YFP*$^{fl/+}$ mouse model in which the Cre recombinase is expressed under the Human glial fibrillary acidic protein (*hGFAP*) promoter (Zhuo et al., 2001). In these mice, CRE expression begins on E13.5 in the forbrain and from then on, SMO will be constantly activated (Zhuo et al., 2001). HGFAP is mainly expressed in astrocytes in the adult brain. However, cells that express the Cre recombinase under the *hGFAP* promoter were found to be radial glia that generate most cerebellar cell types, also including (cerebellar) granule neuron precursors, interneurons, forebrain stem cells, and astrocytes (Spassky et al., 2008; Schüller et al., 2008). Schüller et al. (2008) further published the *Math1-cre::SmoM2-YFP*$^{fl/+}$ mouse model, which also leads to the development of adult SHH MB (Pöschl et al., 2014). Expression of *Math1* can be detected as early as E12.5 in granule cells of mice; by E17, all granule precursors express *Math1* (Machold and Fishell, 2005). Thus, the *Math1-cre* system can be used for specific knockouts in granule precursors.

2 Aims

The aim of this study was to investigate the importance of *TCF4* in the development of the cerebellum and its influence on growth and progression of Sonic hedgehog associated medulloblastoma.
A recent study, published in collaboration with Stefan Pfister's group (German Cancer Research Center, Heidelberg), found that in a group of 50 adult patients with SHH MB, 14 % (7 adult patients) carried a somatic mutation in *TCF4*, making it one of the most frequently mutated genes in SHH MB (Kool et al., 2014). Since the growth of medulloblastoma, especially in adults, has not been fully understood and a successful therapy has yet to be developed, *TCF4* is an interesting target to study; not only in terms of its role in the growth of MB but also for screening of useful therapeutics later on. Interestingly, mutations in *TCF4* have also been identified as the cause of Pitt-Hopkins syndrome. How the haploinsufficiency of *TCF4* causes this disorder, the accompanying brain abnormalities, and intellectual disability however, remains to be understood. Hence, investigating the influence of *TCF4* on cerebellar development will further increase the understanding of PTHS and its molecular mechanisms. At the start of this project, no PTHS mouse model was published and this study therefore aimed at testing whether the *TCF4* mouse model, generated for the present study, is suitable to also serve as a model for PTHS.

In the context of this thesis, different sets of experiments were performed to gain more insight into the function of *TCF4*. Mouse models to mimic Pitt-Hopkins syndrome as well as SHH MB carrying a *Tcf4* knockout were established with the intention to investigate prenatal and postnatal knockouts of *Tcf4 in vivo*. For a better understanding, the mouse models were analysed using different histological techniques. Granule precursor cells were used to establish primary cell lines with the aim to understand cell growth and proliferation following a TCF4 loss *in vitro*. Of further interest was the function of *TCF4* in medulloblastomas with an impaired SHH signalling pathway, which was examined using a human SHH MB cell line transfected with wild-type (WT) TCF4 and different known mutant TCF4 proteins that were recently found in MBs.

3 Results

3.1 Human data

In a series of 130 patients with medulloblastoma and a secured pathological activation of the SHH signalling pathway, 14 % of adult patients (7 out of 50 patients >18 years) were found to have somatic mutations in the *TCF4* gene (Kool et al., 2014). This intriguingly high number of SHH MB patients carrying a somatic *TCF4* mutation was the reason to investigate the influence of *TCF4* on growth and progression of medulloblastoma.

3.1.1 *TCF4* expression levels in medulloblastoma

To gain more insight into the importance of *TCF4* in growth of medulloblastoma, mRNA expression profiles of medulloblastomas were screened. Therefore, a sample of 464 medulloblastoma expression profiles, available through the open access database R2 (R2: microarray analysis and visualization platform, http://r2.amc.nl), with 122 being SHH-associated medulloblastoma, were analysed. The 464 available patient data sets consisted of several sets produced by different research groups and had to be normalised to allow for direct comparison (see Section 7.2.5).
The mRNA expression of *TCF4* in medulloblastoma was compared to mRNA expression of *TCF4* in healthy brain tissue, in specific, foetal cerebellum and adult cerebellum to examine whether the base line level of *TCF4* was altered. The results showed that the mRNA levels of the whole SHH MB subgroup (112 patients) are significantly higher in comparison to the levels found in foetal and adult cerebellum respectively ($p=0.0002$ and $p<0.0001$). Although the expression levels of the SHH subgroup are relatively scattered (Fig. 6A), the mean expression level is clearly raised compared to the normal tissue and lies more than one standard deviation (SD) above the base line. Apart from the elevated mRNA levels in medulloblastoma, it was identified that during development of the brain, i.e. foetal cerebellum, *TCF4* levels are significantly higher compared to the adult cerebellum ($p=0.0068$). This is in accordance with the knowledge that *TCF4* regulates neurogenesis (Sepp et al., 2011).

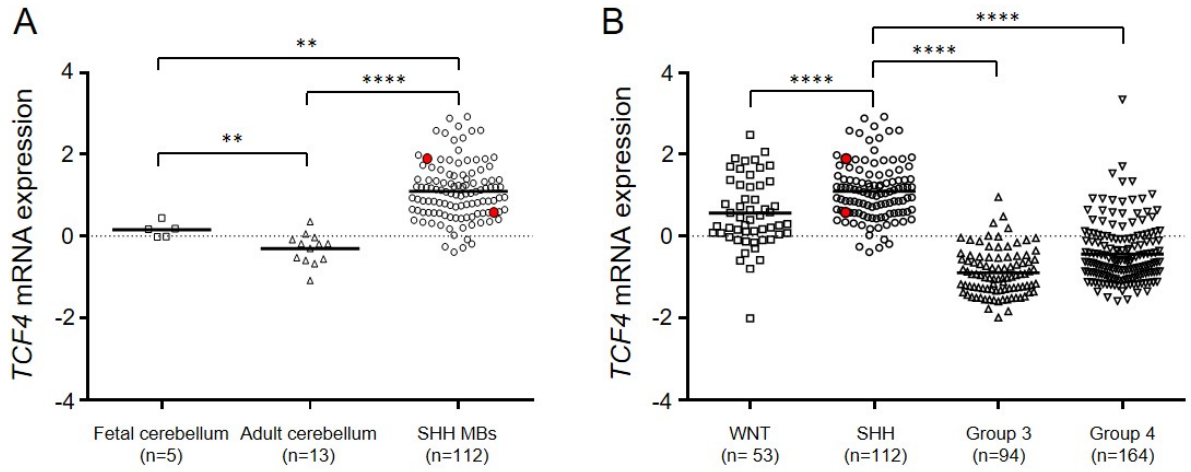

Figure 6: *TCF4* mRNA expression in MB is significantly increased.
(A) *TCF4* mRNA expression in the cerebellum (foetal and adult) and SHH MB. Results showed significantly higher levels for SHH MB. **(B)** *TCF4* expression in distinct molecular subgroups of MB. SHH MB *TCF4* mRNA expression levels were significantly higher compared to all other groups. Red dots indicate cases with known somatic *TCF4* mutations. Relative gene expression values were calculated using z-scores. Scale on y-axis indicate the number of standard deviations by which the value of the expression level is different from the overall mean. Bars indicate the mean of each group. Groups were compared using two-tailed t-tests and Mann-Whitney-U tests respectively. ** = $p < 0.01$, **** = $p < 0.0001$.

Moreover, mRNA expression levels of *TCF4* were compared between the different MB subgroups to examine if the elevation of *TCF4* expression is unique to subgroup 2. Fig. 6B illustrates that mRNA expression was significantly elevated in the SHH subgroup compared to all other analysed groups ($p<0.0001$). In addition to the SHH subgroup, also the WNT subgroup showed elevated expression levels, whereas group 3 and 4 showed a mean *TCF4* expression level below the overall mean. A comparison between the different age groups within the SHH subgroup (infant MB, childhood MB, adult MB) resulted in no significant difference in *TCF4* expression (Fig. 27, Appendix).
These results highlight that the *TCF4* expression in SHH-associated medulloblastoma is highly elevated not only compared to healthy tissue but also compared to the other subgroups. This raises the question whether elevated *TCF4* levels influence the patient's outcome, i.e. the overall survival.

3.1.2 Analysis of long-term survival of MB patients

The data sets available on R2 did not only contain the mRNA expression levels of the 464 patients but also the survival data for the majority of patients. It was therefore possible to link the expression levels of *TCF4* with the overall survival.

Interestingly, the generated Kaplan-Meier plots in Fig. 7 demonstrate that a high level of *TCF4* is correlated with a better overall survival. A high level of *TCF4* was defined as a z-score of 1.5 and above.[3] Comparing all SHH MBs, the results revealed a significantly better survival for patients with high *TCF4* levels (p=0.045). A 5-year survival rate of over 90 % for patients with high *TCF4* levels was calculated compared to 70 % for low *TCF4* mRNA levels.

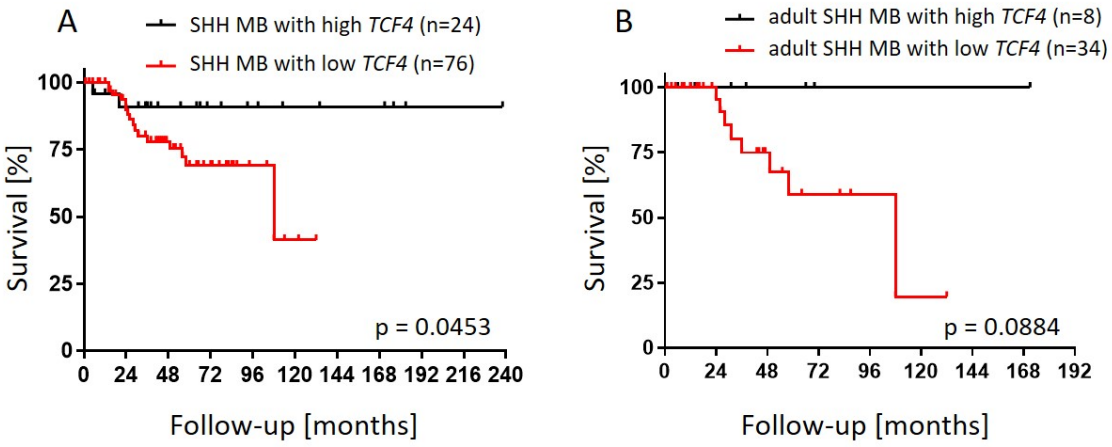

Figure 7: Kaplan-Meier plots for SHH MB reveal overall better survival for patients with high *TCF4* levels. (A) Kaplan-Meier analysis reveals a significantly better survival for SHH MB patients with high expression of *TCF4*. **(B)** A similar result was observed regarding only adult patients with SHH MBs. Analysis was performed using a logrank test. A high mRNA level was defined as a z-score of 1.5 and above. Bars mark events of death.

These results suggest that the expression of *TCF4* is advantageous for patients with SHH-associated medulloblastoma, strengthening the hypothesis that *TCF4* functions as a tumour suppressor (Herbst et al., 2009a). However, the data available do not allow to draw a definite conclusion as only mRNA expression was measured and a direct correlation between RNA and protein levels cannot be assumed (Vogel et al., 2010). This is highlighted by the fact that the two patients with known *TCF4* mutations (shown as red dots in Fig. 6) are expressing *TCF4* mRNA at different levels although their mutations - R157X and R174X - are both nonsense mutations and no functioning protein is produced (Fig. 9, Section 3.2.2).

[3]The z-score defines how many standard deviations a data point is below or above the (population) mean, and is often used when several different data sets are combined to one. I.e. a deviation of 1.5 SD from the mean was defined as high level of *TCF4* expression.

Evaluating the data from patients with adult SHH MBs only, it is evident that adult patients with a high expression level of *TCF4* have a better overall survival (Fig. 7B), though not with a significant difference (p = 0.088). It should be noted however, that there were only eight patients in the 'high *TCF4* level' group and a larger cohort might show a more significant result.

3.2 Investigation of known TCF4 mutations

3.2.1 TCF4 mutations in MB

A series of 133 SHH MBs was previously sequenced in collaboration with the German Cancer Research Center (Kool et al., 2014), with 50 patients being 3 years and younger (infant SHH MB), 33 patients aged 4-17 years (childhood SHH MB), and 50 cases being over 18 years (adult SHH MB). Somatic mutations in the *TCF4* gene were found in eight cases (Fig. 2), which accounts for a total of 6 % of patients. However, seven of these patients were adults, i.e. over 18 years old, and the eighth patient was already 17 years of age at diagnosis, so that 14 % of patients with adult SHH MB exhibited *TCF4* mutations (7 out of 50).

Table 2: Mutations found in TCF4 in SHH MBs. All except one patient, 17 years of age, were adults. Mutations were found throughout the gene and were of different kind, i.e. frame-shift (fs), deletion (del), nonsense (X), missense, and splice site. Mutations R157X and R174X belong to patients shown as red dots in Fig. 6 and the same mutations were also found in patients with PTHS. The mutations are denoted according to the TCF4-B$^-$ protein sequence.

Mutation	Age of patient in years
Q619X	17
216_219del	25
D304fs	25
R157X	28
R174X	32
451_453del	38.5
V613F	46
splice site	46

No cluster of somatic mutations was found in *TCF4*. Instead, the mutations were scattered throughout the gene, affecting different domains of the protein (Fig. 8). Furthermore, the different kinds of mutations were rather versatile.

Deletions, frame shift mutations, nonsense mutations as well as missense mutations and one splice site mutation were identified. Two of the mutations found during sequencing - R157X and R174X - have been described before as germline mutations in patients with Pitt-Hopkins syndrome (Sepp et al., 2012). To determine the functionality of these mutants and investigate their influence on growth and progression of medulloblastoma, five of the above listed mutations were designed using site directed mutagenesis and transfected into the MB cell line DAOY.

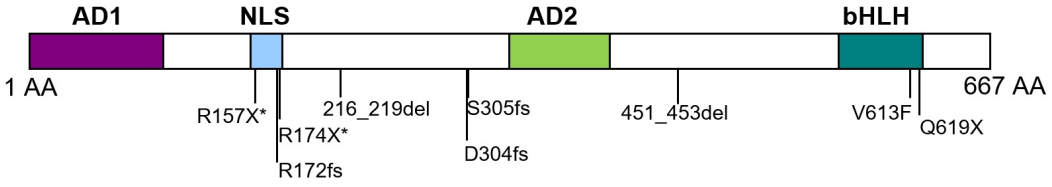

Figure 8: Structure of TCF4 protein sequence highlighting known TCF4 mutations. Positions of TCF4 mutations identified in SHH MB shown on a scheme of TCF4-B$^-$. Note that except Q619X, which was found in an 17-year-old patient, all mutations were detected in adult SHH MB patients (>18 years). Asterisks mark mutations that had previously been identified in the germline of patients with Pitt-Hopkins syndrome. Different domains are shown in different colours. Activation domains AD1 and AD2 (purple and green), nuclear localisation sequence (NLS, light blue), and the basic helix-loop-helix domain (bHLH, turquoise). Mutations are given in Table 2.

3.2.2 Influence of WT TCF4 and TCF4 mutants on proliferation in a MB cell line

Five out of the eight discovered mutations (R157X, R174X, 216_216del, 451_453del, V613F) as well as WT TCF4 were cloned into the *MSCV-IRES-GFP* vector and subsequently transfected into the MB cell line DAOY to study the functionality of the (mutated) proteins and determine their influence on cell growth. The DAOY cell line is an adherent cell line derived from a desmoplastic cerebellar medulloblastoma from a Caucasian male at the age of four (Jacobsen et al., 1985), that has been identified to belong to the SHH subgroup of MB (Liang et al., 2015).

First, the MB cell line was tested for its expression of TCF4 and found not to express the protein, i.e. cells could not be stained for TCF4 (Fig. 9A, no red fluorescent cells). The experiment was then carried out in eight different settings. A control with no plasmid was performed to determine the base line cell proliferation rate. The DAOY cells were furthermore transfected with the *MSCV-IRES-GFP* backbone alone to determine if the

transfection of the plasmid itself influences cell growth, assuming that it does not. DAOY cells were then transfected with WT TCF4 to study the effect on cell proliferation rates of introducing TCF4 to a TCF4-deficient MB cell line. Finally, the DAOY cell cultures were transfected with the TCF4 mutants R157X, R174X, 216_219del, 451_453del, and V613F to investigate their functionality and influence on cell growth in MB.

The transfected and fixated cells were initially stained for a combination of TCF4, GFP (green fluorescent protein), and DAPI (4',6-diamidino-2-phenylindole). Staining of GFP (green) was used to determine cells that were transfected, and the TCF4 staining (red) gave information whether a functioning TCF4 protein was produced (Fig. 9A-H, orange fluorescent cells are positive for GFP and TCF4). However, the TCF4 antibody only binds to a specific domain (AAs 468-525), and the staining therefore only verifies if this specific domain is present and functioning (Fig. 32, Appendix). Truncated proteins that are missing domains other than AA 468-525 will be detected by the antibody. The transfected cells were additionally stained with antibodies against BrdU (Bromodeoxyuridine), GFP, and DAPI; with GFP (green) again visualizing cells that were transfected and BrdU (red) marking the cells that were actively proliferating. For the evaluation of proliferation rates, only double positive cells (orange) were counted (Fig. 9J-Q and R).

Staining of TCF4 showed that besides the WT TCF4, the mutants 216_219del, 451_453del and V613F were able to express a TCF4 protein, which can be recognised by the anti-TCF4 antibody. In particular, Fig. 9I (a magnification of 9H) shows that the V613F mutant precipitates in the cell. This phenomenon of TCF4 mutants forming protein aggregates has been described before, with mutations found in patients with Pitt-Hopkins syndrome (Forrest et al., 2012; Sepp et al., 2012). Namely, Sepp et al. (2012) proposed that *"PTHS-associated mutations in the second helix of the bHLH domain and C-terminal part of TCF4 induce protein destabilization and aggregation"*.
The analysis of the proliferation rates clearly showed that the introduction of WT TCF4 into the DAOY cells decreases the proliferation significantly, from around 50 % (49±2 %) to less than 15 % (14±3 %) (Fig. 9R). As expected, the transfection of DAOY cells with the sole plasmid backbone did not alter cell growth and all the effects found can be accredited to the respective version of TCF4. The results illustrate that the mutants R157X and R174X are non-functioning (no staining of TCF4) and the proliferation rates are not altered compared to the base line proliferation. Due to the early nonsense mutation of these mutants (Fig. 8), this was to be expected. The mutants 216_219del and 451_453del resulted in some function, as seen by the staining for TCF4, and also a decreased cell proliferation. However, the count of $BrdU^+$ cells is still significantly higher than that for

the WT TCF4. For the V613F mutant, proliferation rates were not altered which shows that this TCF4 mutant is non-functioning. This comes as no surprise, since the mutation occurs in the bHLH domain and, as described above, the mutant protein forms aggregates in the cell.

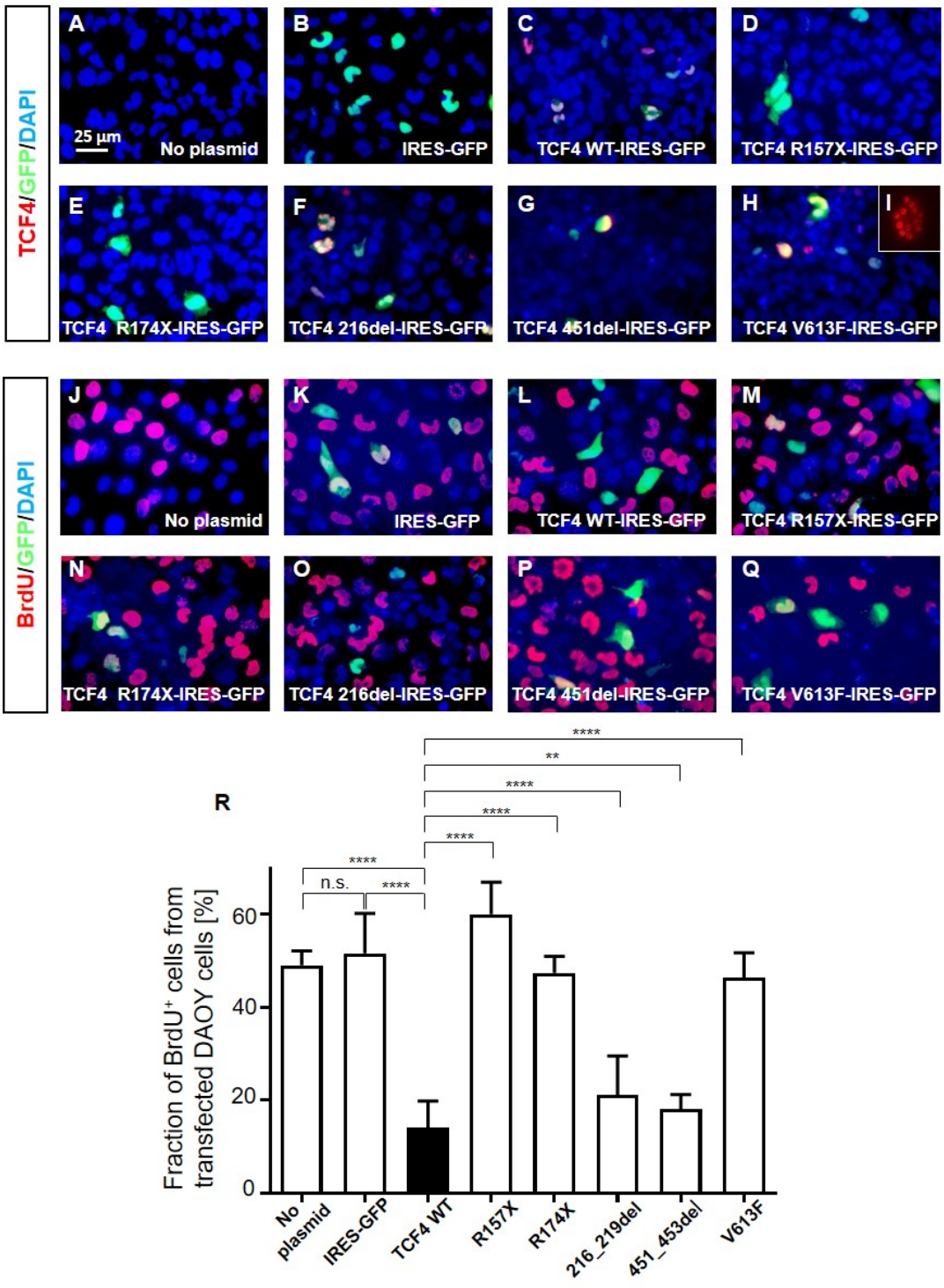

Figure 9: See the following page for description.

Figure 9: WT TCF4 is able to decrease proliferation of DAOY cells significantly. (A-H) DAOY cells were stained with antibodies against TCF4 (red), GFP (green), and DAPI (blue). **(A)** DAOY cells do not express TCF4. **(B–H)** Transfection of DAOY cells with *IRES-GFP* plasmids containing either no TCF4, TCF4 WT or the TCF4 mutants shown in Fig. 8. **(I)** Magnification of **(H)** where precipitation of TCF4 in the nucleus can be observed. **(J-P)** DAOY cells stained with antibodies against BrdU (red), GFP (green), and DAPI (blue). **(K-P)** Transfection of DAOY cells with *IRES-GFP* plasmids containing either no TCF4, TCF4 WT or the TCF4 mutants. **(R)** Analysis of proliferation of transfected DAOY cells. Plotted were the fraction of $BrdU^+$ cells from transduced cells (GFP^+) and the baseline proliferation rate respectively. WT TCF4 reduced proliferation significantly in comparison to unaffected DAOY cells and all tested mutants. Mutants 216del and 451del showed partial functionality and also reduced proliferation. Analysis was done comparing cell counts using chi-squared tests. Each transfection was carried out three times (n=3). Error bars show mean+SD. **** = $p<0.0001$, ** = $p<0.01$, n.s. = $p>0.05$.

It can be concluded that WT TCF4 reduces cell proliferation in a SHH MB cell line indicating that TCF4 functions as a tumour suppressor, which had already been seen in the previous experiment (Section 3.1.1).

3.3 Establishing the mouse models

There are several known and well-described mouse models for SHH MB and some proposed mouse models for PTHS (Sections 1.2.5 and 1.4.5). For the experimental part of this thesis, several SHH MB mouse models and a *Tcf4* mouse model were adjusted to the project's needs so that a variety of different transgenic mice with conditional and inducible knockouts were generated.

Starting from the two basic models, in which the Cre recombinase is expressed under the control of the *hGFAP* or the *Math1* promoter (Zhuo et al., 2001; Matei et al., 2005; Schüller et al., 2007), the different mouse models for this project were generated. Therefore, the already described SHH MB mouse models *hGFAP-cre::SmoM2-YFP*$^{fl/+}$ and *Math1-creER*^{T2}*::SmoM2-YFP*$^{fl/+}$ were bred with *Tcf4*$^{fl/fl}$ mice to create an additional *Tcf4* knockout in the tumourous environment and thus having a tool to investigate the influence of *Tcf4* on growth of medulloblastoma. By using the different conditional and inducible systems, knockouts of *Tcf4* could be controlled easily in a time- and tissue-specific manner.

To investigate the influence of *Tcf4* in cerebellar development, a new mouse model was established, knocking out *Tcf4* solely in a subset of neuronal cells.

Mice expressing the Cre recombinase under the *hGFAP* and *Math1* promoter were bred with $Tcf4^{fl/fl}$ mice to generate *hGFAP-cre::*$Tcf4^{fl/fl}$ and *Math1-cre::*$Tcf4^{fl/fl}$ mice. The former mice, following a closer observation, exhibited impressive similarities to the features found in Pitt-Hopkins syndrome and were proposed as a new model to study the disease, differing from the models already published (Kennedy et al., 2016; Jung et al., 2018; Thaxton et al., 2018). This model can be distinguished from other known PTHS models by the fact that it is the only model that is viable following a homozygous knockout of *Tcf4* giving it the advantage to study a full loss of the gene in the CNS. As the generated mice loose *Tcf4* only in a defined subset of cell lines, it fails to mimic other PTHS features outside the CNS such as the gastrointestinal changes.

3.4 *In vitro* loss of *Tcf4*

A cerebellar granule neuron precursor (CGNP) cell culture carrying a homozygous *Tcf4* knockout was established to receive a first impression of the effect of *Tcf4* on cell growth and its function in cerebellar development. Proliferation rates of the CGNP cells were compared to a wild type CGNP culture. Granule cerebellar progenitors are said to be the origin of SHH medulloblastoma and the experiment was therefore also of interest in respect to the influence of *Tcf4* on progression and development of medulloblastoma (Gilbertson and Ellison, 2008; Behesti and Marino, 2009).

Primary cell cultures of CGNP cells were established using $Tcf4^{fl/fl}$ mice aged five to seven days. CGNPs show a peak period of proliferation around P5-8, so this age was ideal for generating the cell cultures (Roussel and Hatten, 2011). The granule precursors were isolated and cultured as described in Section 7.2.2.1. Cells were then transduced with a virus either carrying the plasmid *MSCV-IRES-GFP* or *MSCV-Cre-IRES-GFP* with the latter causing a knockout of *Tcf4*. This transduction corresponded to a post natal knockout of *Tcf4* around P6-8. The cells were pulsed with BrdU and subsequently fixed and stained for BrdU and GFP 24 h post transduction. GFP^+ and $BrdU^+$ double positive cells from both experimental settings were counted and the numbers compared using a chi-squared test. The cultures were prepared a total of five times (n=5). The results are given in Fig. 10, where the fraction of $BrdU^+$ cells from all transduced cells is plotted. It was identified that a total loss of *Tcf4* in granule neuron precursors increased cell proliferation significantly ($p<0.0001$). The findings from this experiment further strengthen the assumption that *Tcf4* functions as a tumour suppressor.

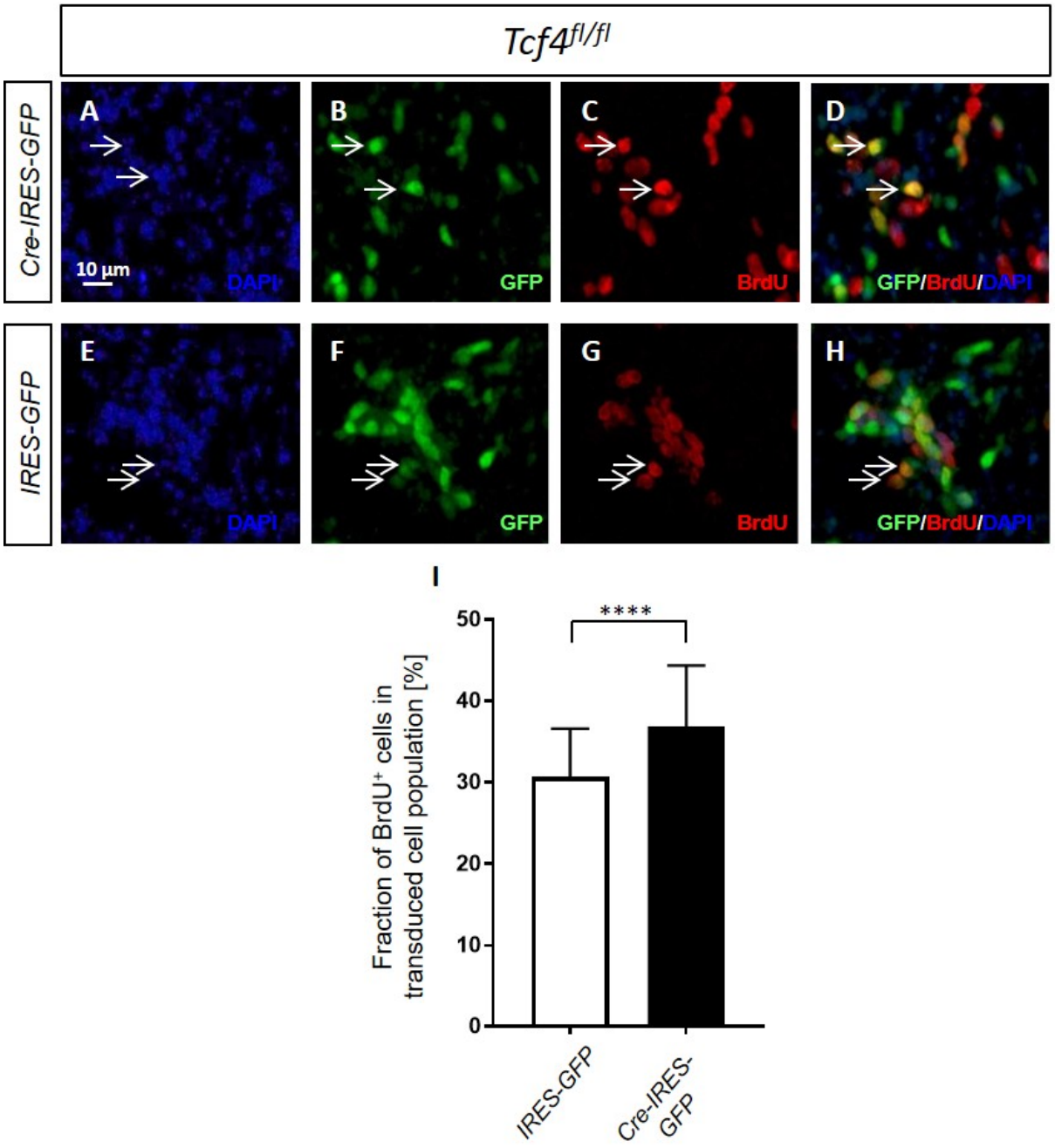

Figure 10: Knockout of *Tcf4* increases proliferation of CGNP cells. (A-D) Granule precursor cells of $Tcf4^{fl/fl}$ mice, after transduction with *Cre-IRES-GFP* to knockout *Tcf4*. Stained for DAPI (blue), GFP (green), and BrdU (red). **(D)** is an overlay of pictures A-C. **(E-H)** Control group. Granule precursor cells of $Tcf4^{fl/fl}$ mice after transduction with *IRES-GFP*. Cells were stained as above. **(H)** is an overlay of pictures E-G. **(I)** Analysis of proliferation of granule precursor cells after knockout of *Tcf4*. Results showed that proliferation increases significantly following the loss of *Tcf4*. Cell counts were compared using a chi-squared test. Fraction of $BrdU^+$ cells from transduced cells were plotted. Error bars show mean+SD. **** = $p < 0.0001$, n=5. Arrows mark the same cells in pictures A-D and E-H.

A similar, correlating experiment was conducted *in vivo* by one of the group's members (Malte Hellwig). *Math1-creER*^{T2} *Tcf4*$^{fl/fl}$ mice were used for this experiment. The mice were treated with tamoxifen on P5 and pulsed with BrdU on P7, P12 or P15. Mice were sacrificed two hours after pulsation and the fraction of BrdU^{+} cells in the EGL was determined. The experiments revealed that there was a significantly higher proliferation for mice carrying a homozygous *Tcf4* knockout compared to the controls (data not shown). These *in vivo* results were thus in accordance with the findings illustrated in Fig. 10 for the *in vitro* experiment.

3.5 *In vivo* loss of *Tcf4*

To investigate the effect of a loss of *Tcf4* on growth in mice, brain development - with the main focus on cerebellar development -, and formation of granular layers, several *in vivo* experiments were conducted. For a more comprehensive understanding of the function of *Tcf4*, knockouts using different promoters - *hGFAP* and *Math1* - were compared and the knockouts were induced prenatally as well as postnatally (see Section 7.2.3.1).
First, macro-anatomical features were compared. Namely, mouse whole body and brain weights, including cerebrum and cerebellum weights in specific, were determined. Mouse brains were then investigated closer, regarding the general organisation of the brain, with focus on the cerebellum. Further observations were carried out focussing on the formation of the granular layers, migration of granule cells as well as proliferation and apoptosis rates.

3.5.1 Macro-anatomical aspects

Mice carrying homozygous *Tcf4* knockouts were generally lighter in weight and smaller in size than wild type mice and mice with heterozygous knockouts (Fig. 11). Observations of anatomical structures under the microscope (Fig. 14 and 16), as well as macro-anatomical examinations of mouse brains (Fig. 12), suggested a significant difference in brain sizes between the examined genotypes. To quantify this effect, whole mice and their brains were systematically weighed. *HGFAP-cre::Tcf4*$^{+/+}$, *hGFAP-cre::Tcf4*$^{fl/+}$, and *hGFAP-cre::Tcf4*$^{fl/fl}$ were weighed every second day starting from birth. Brain weights as well as cerebrum and cerebellum weights were measured on day 7, 14, and 21 post partum.

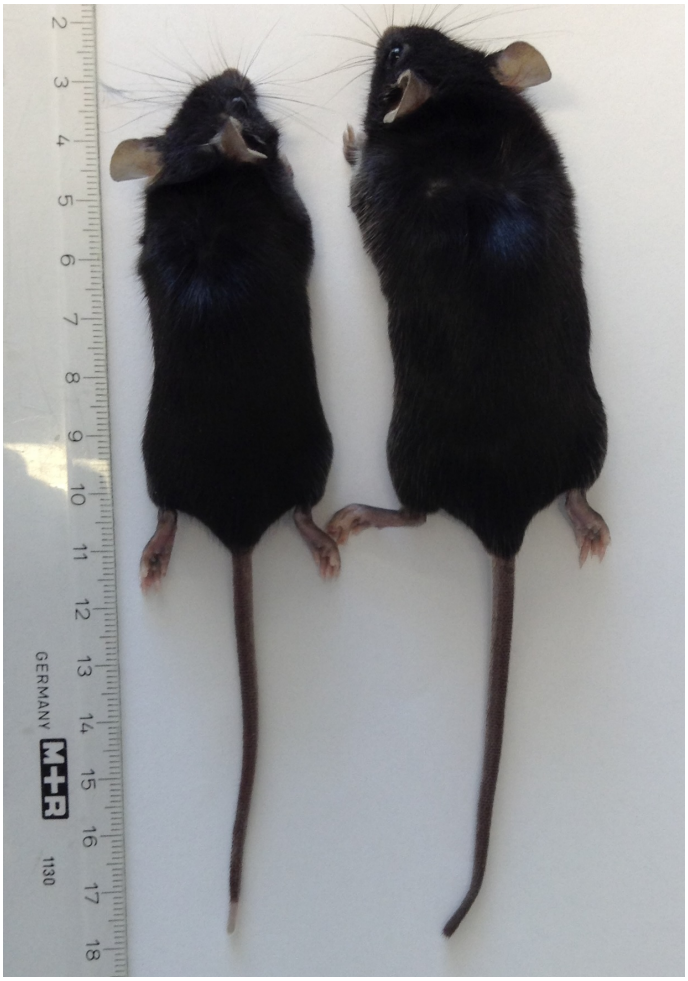

Figure 11: Loss of *Tcf4* *in vivo* causes growth retardation in mice. Shown are a *hGFAP-cre::Tcf4*$^{fl/fl}$ mouse on the left and a *hGFAP-cre::Tcf4*$^{fl/+}$ mouse on the right. A homozygous *Tcf4* knockout leads to a thinner and shorter body in comparison the heterozygous littermate. The left mouse measures 8.2 cm in length (excluding tail) and weighs 16.65 g. The right mouse is 9.2 cm long and weighs 28.30 g. Mice were siblings and at time of death 60 days old.

The measurements were visualized by plotting the weight of the investigated body part against the time of measurement (Fig. 13). Growth curves were not calculated since not all of the necessary variables could be determined with the data available. Instead, the parameter 'weight' was compared using t-tests for the different time points separately. For whole body weights, t-tests were only carried out for day P21. For all other measurements, t-tests were carried out for days 7, 14, and 21 post partum (see Tab. 10, Appendix).

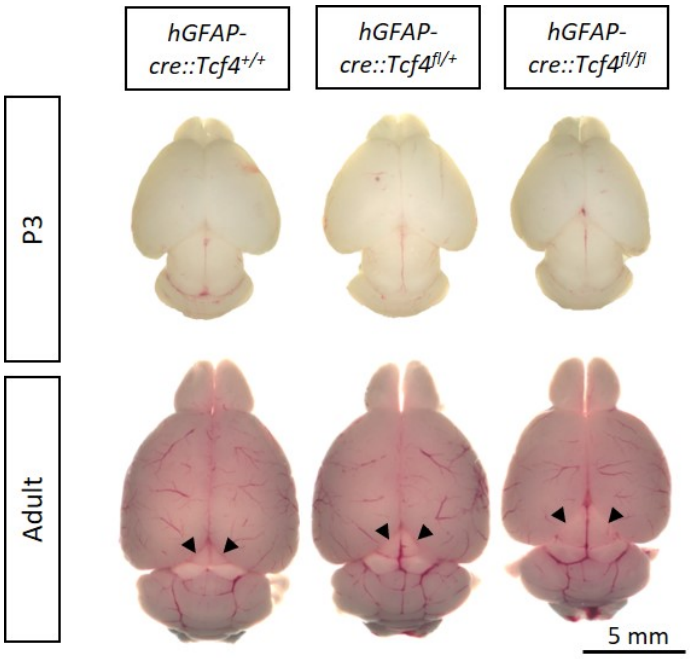

Figure 12: *Tcf4* knockout in mice leads to microcephaly. Mouse brains of *hGFAP-cre::Tcf4*$^{+/+}$, *hGFAP-cre::Tcf4*$^{fl/+}$, and *hGFAP-cre::Tcf4*$^{fl/fl}$ are shown at age P3 and adult stage. Mice with homogzygous knockouts of *Tcf4* show marginal differences at P3, however, are different in length and width at adult stage. Arrows mark view of superior and inferior colliculus. Depending on the genotype, the colliculus can be partially or almost fully seen.

The results demonstrate that mice carrying homozygous *Tcf4* knockouts were lighter on P21 compared to their wild type littermates as were their brains (p-values for whole body weight = 0.0656).[4] The separate analysis of cerebrum and cerebellar weights demonstrated that both parts were affected by the *Tcf4* knockout. Especially the cerebrum showed a significantly lower weight on all days tested, i.e. P7, 14, and 21 (Fig. 13, see also Table 10 in the Appendix). Interestingly, not only did the homozygous knockout mice show a lower brain weight but also the brains of the heterozygous knockouts were significantly lighter on P21, hinting at the fact that a heterozygous knockout alone can cause a microcephaly as seen in Pitt-Hopkins syndrome.
Even more astonishing is the comparison of brain weights of days P14 and P21 in cerebrum and cerebellum of homozygous KO mice, where a decrease in weight was observed (Fig. 13B). It was later confirmed, that this weight loss is due to a decrease in proliferation and an increase in apoptosis (see Section 3.5.2).

[4]For whole body weights, a one-tailed t-test would be justified regarding the fact that patients with PTHS are known to be smaller and exhibit growth retardation. In case of a one-tailed t-test, p = 0.0328 and is therefore significant.

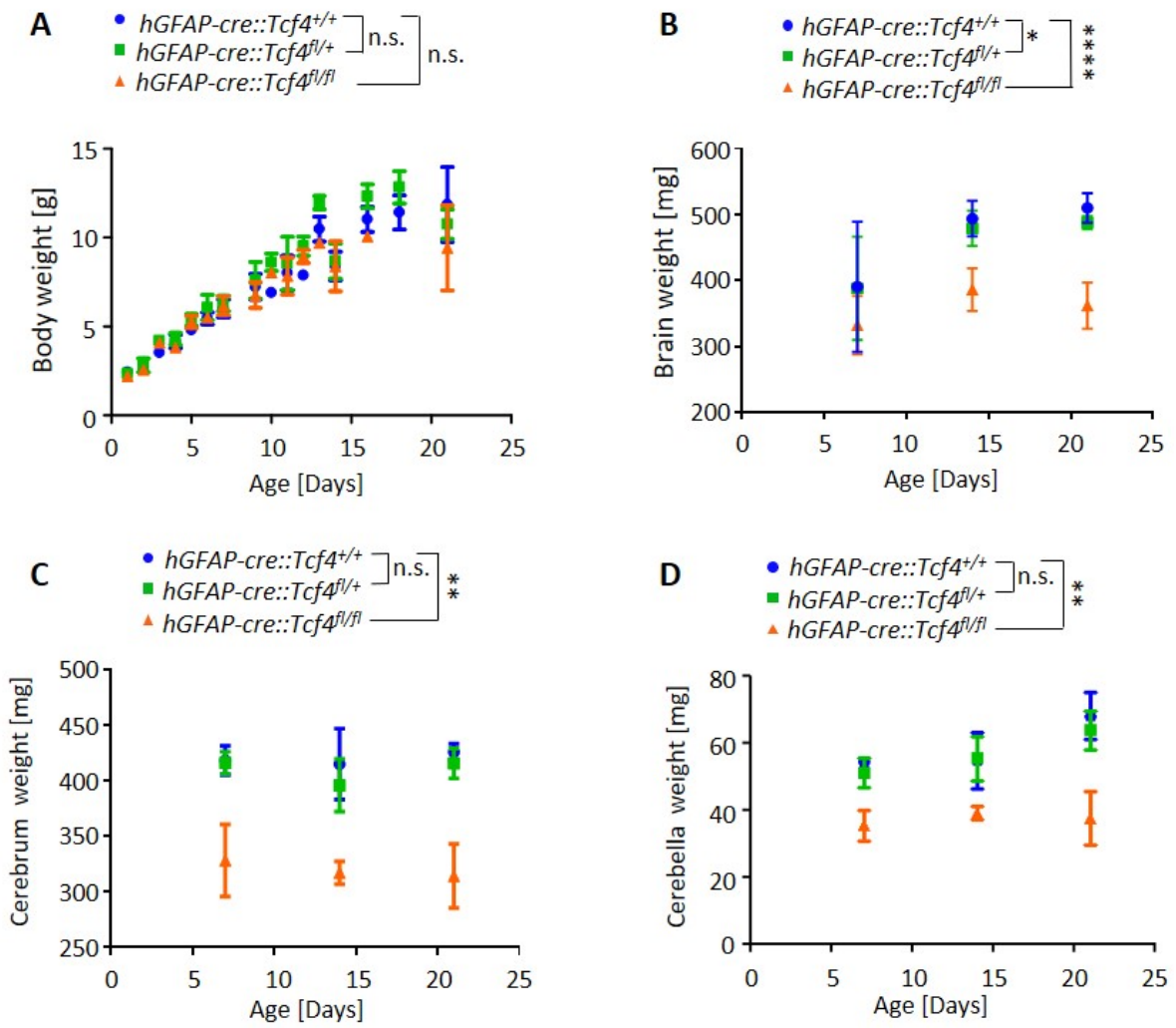

Figure 13: Loss of *Tcf4* causes a decrease in whole body and brain weights. **(A)** Mice with the genotypes *hGFAP-cre::Tcf4*$^{+/+}$, *hGFAP-cre::Tcf4*$^{fl/+}$, and *hGFAP-cre::Tcf4*$^{fl/fl}$ were weighed every second day starting at birth. **(B-D)** Brain, cerebrum, and cerebellum weights were determined on P7, 14, and 21. At least three mice were measured for any given point in time. Results showed that whole brain, cerebrum, and cerebellum weights are significantly lower for mice carrying a homozygous *Tcf4* knockout. The entire weight in grams for whole body weights and milligrams for brain, cerebrum, and cerebellum weights were plotted against time in days. Groups were compared using t-tests for P21 only. Error bars show mean ± SD. **** = $p<0.0001$, ** = $p< 0.01$, * = $p< 0.05$, n.s. = $p> 0.05$.

3.5.2 Micro-anatomical aspects

3.5.2.1 Cerebrum

In addition to the macro-anatomical aspects of a prenatal *Tcf4* knockout, a micro-anatomical investigation of the mouse brains was performed. H&E stainings of the brains of mice aged 7, 14, and 21 days were observed under the microscope. The general anatomical structure and formation of specific brain parts, such as the hippocampus and the cerebellar layers, were compared. These are the regions where granule cells can predominantly be found (Shepherd, 2004), and were therefore of special interest for this project.

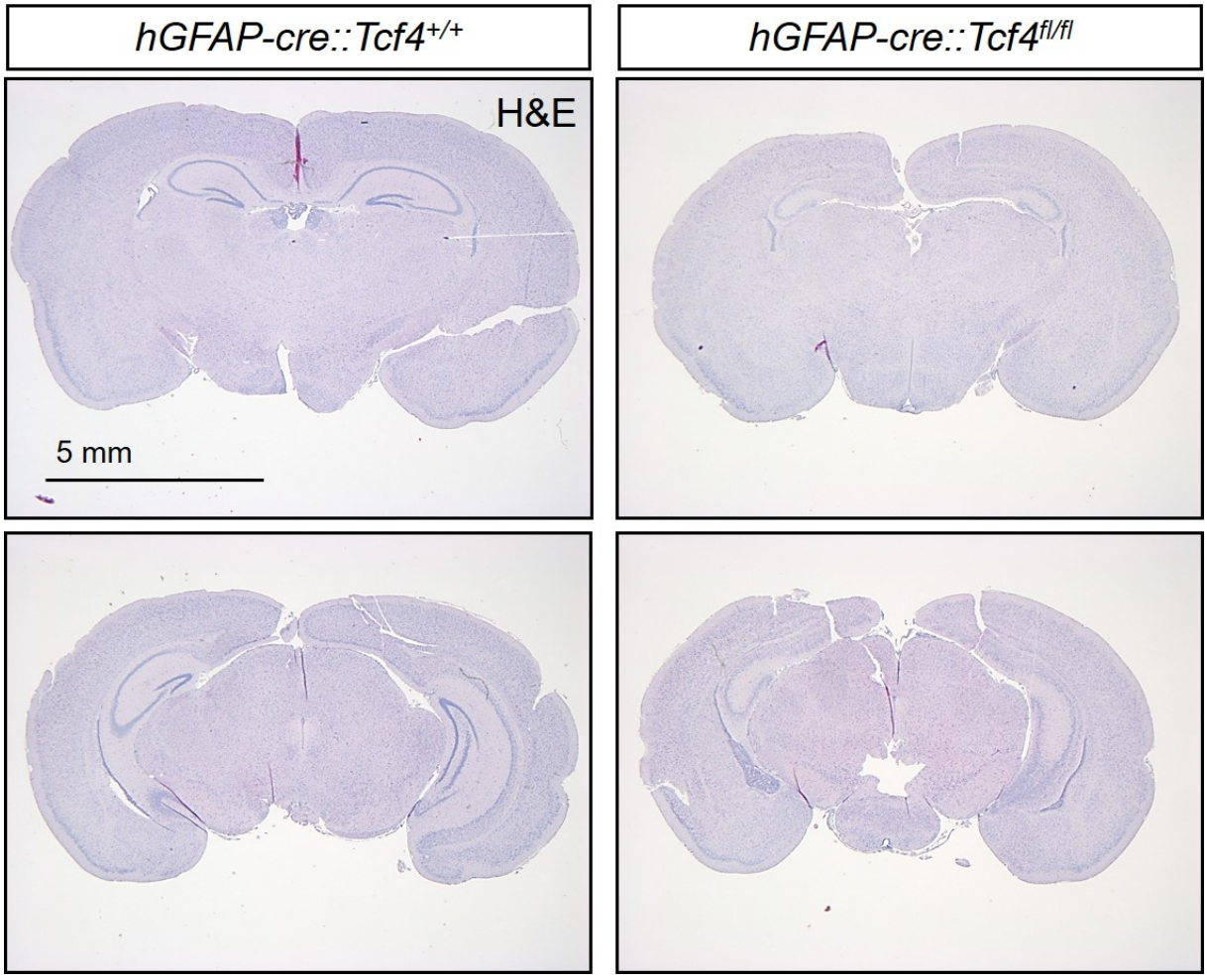

Figure 14: Hippocampus of adult mice is altered due to *Tcf4* knockout. H&E stain of coronal sections through the hippocampus of mice aged 21 days. Formation of hippocampus of mice carrying a *Tcf4* knockout was observed to be altered and cells forming the hippocampus appeared more scattered (bottom right).

Firstly, the cerebrum of *hGFAP-cre::Tcf4*$^{+/+}$ and *hGFAP-cre::Tcf4*$^{fl/fl}$ mice was compared using H&E stainings from different sections. It was found that the formation of the hippocampus was altered in mice carrying a homozygous *Tcf4* knockout. For illustration, a coronal section of mice aged 21 days is shown in Fig. 14. It can be seen that the loss of *Tcf4* led to a less differentiated structure of the hippocampus; the formation itself is altered with important parts missing and the overall number of cells forming the hippocampus seems to be decreased. Furthermore, a closer observation of the hippocampus revealed that the cells are more scattered in mice carrying the knockout compared to wild type mice. The weight measurements of the cerebrum performed in this project already indicated that the structure of the brain and or the total cell number must be altered for the cerebrum to weigh significantly less. In accordance with these findings, Jung et al. (2018) described that the arrangement of TCF4-expressing cells in the hippocampus of the *Tcf4*^{LacZ} mouse was less organised.
Further investigation on the formation of the hippocampus and migration of granule cells as well as their quantification following a *Tcf4* knockout was carried out by one of the group members leading to a separate project and was therefore not pursued for this work.

3.5.2.2 Cerebellum

One of the main aims of this project was the investigation of the formation of cerebellar structures following the loss of *Tcf4*. Therefore, several experiments were conducted to not only observe cell formation but also measure proliferation and apoptosis rates and track the migration of granule cells.

TCF4 expression in the cerebellum To investigate the consequences of a *Tcf4* knockout in mice, the expression of TCF4 in the cerebellum was analysed. Stainings for TCF4 in the cerebella of mice aged one week and 2.5 months were prepared as well as in a SHH-associated MB from a two months old *Math1-creERT2::Smo*$^{fl/+}$ mouse that had received tamoxifen on P5. None of the mice were carrying a *Tcf4* mutation. As pictured in Fig. 15, TCF4 is highly expressed in the granule cells of the cerebellum, shown by the staining of the EGL at P7 and the IGL in the adult mouse. TCF4 was also highly expressed in tumour tissue as highlighted in Fig. 15C and F. These findings stand in contrast with the expression analysis published by Jung et al. (2018), who found the most prominent TCF4 expression in the Purkinje cell layer, which did not show any TCF4 expression in this study (Fig. 15).

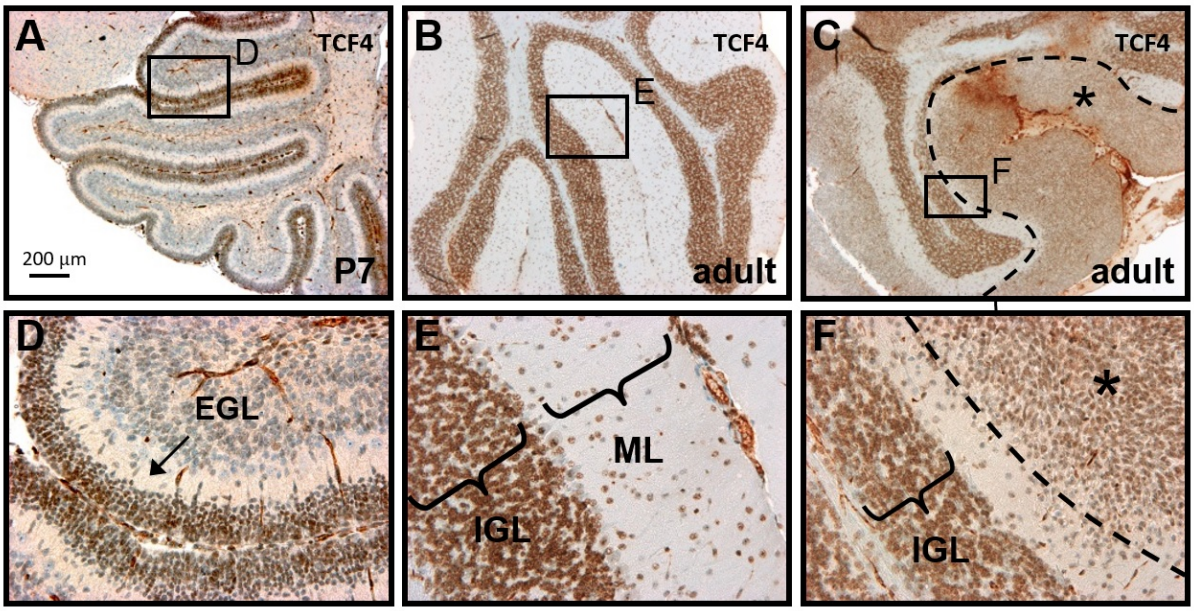

Figure 15: TCF4 expression in the cerebellum of mice at different ages. Staining for TCF4 in a **(A)** WT mouse at P7, **(B)** adult mouse aged 2.5 months, and **(C)** a *Math1-creERT2::Smo*$^{fl/+}$ mouse aged 2 months which had received tamoxifen on P5. Asterisk marks the SHH MB, tumour and healthy tissue are separated by a dotted line. **(D-F)** show a higher magnification of **(A-C)**. Stainings show that TCF4 is highly expressed in granule cells. EGL = external granular layer, ML = molecular layer, IGL = internal granular layer.

Anatomical structure H&E stainings of cerebella of mice aged 7 and 21 days with the genotypes *hGFAP-cre::Tcf4*$^{+/+}$, *hGFAP-cre::Tcf4*$^{fl/+}$, and *hGFAP-cre::Tcf4*$^{fl/fl}$ were observed under the microscope. Fig. 16 visualises clearly that at the age of 7 days, cerebellar structure and formation in the three different groups were approximately the same, with all of them showing a distinct EGL, ML, and forming IGL. However, the cerebellum of the *hGFAP-cre::Tcf4*$^{fl/fl}$ mice already seemed to be smaller and the cortex - seen in the magnification - seemed to be thinner. This impression was confirmed by the comparison of cerebellar weights between WT and homozygous knockout mice for P7 which showed a significantly lower weight (p=0.0023). Two scenarios for the decreased size had to be considered: (1) either proliferation rates following a *Tcf4* knockout were lower, or (2) apoptosis rates were increased. To distinguish between these two scenarios, further experiments were conducted, with special attention paid to the migration of the granule cells.

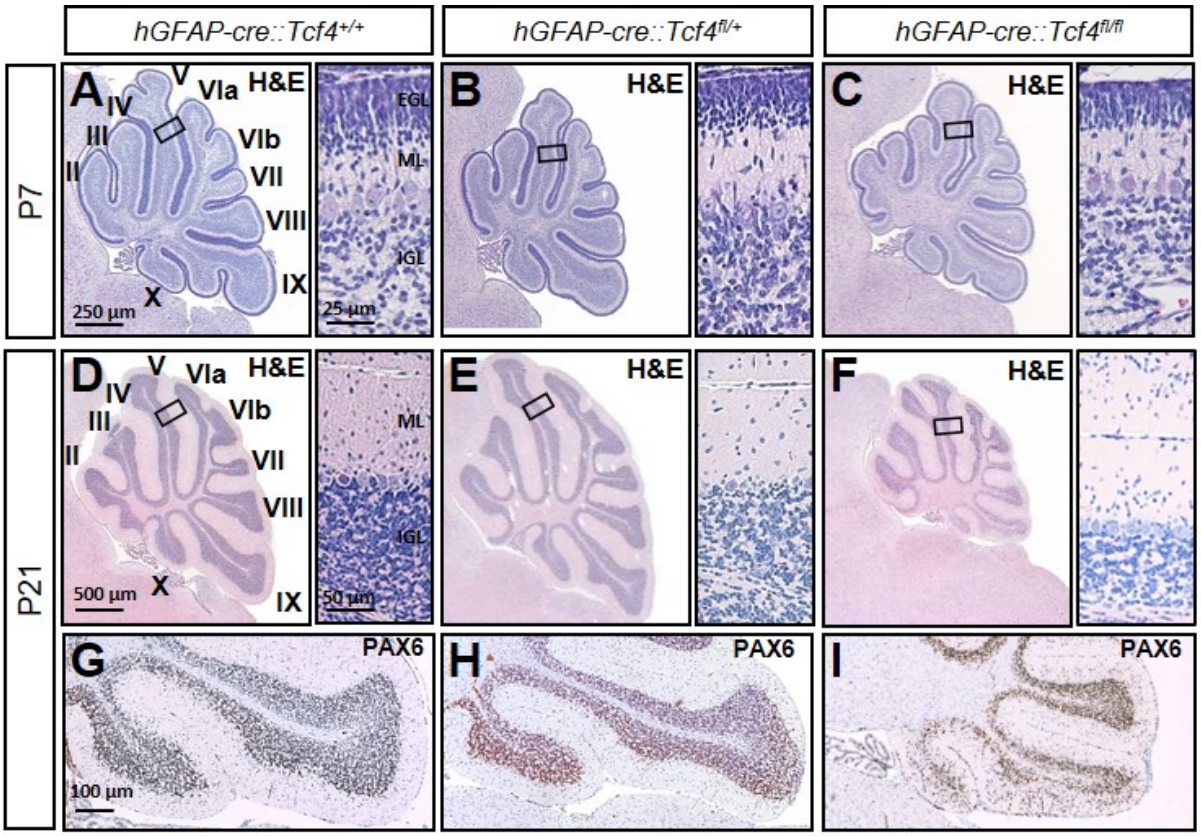

Figure 16: Anatomical structure of the cerebellum is distinctly altered due to loss of *Tcf4*. H&E stains of mouse brains of mice with genotypes *hGFAP-cre::Tcf4*$^{+/+}$, *hGFAP-cre::Tcf4*$^{fl/+}$ and *hGFAP-cre::Tcf4*$^{fl/fl}$ at P7 **(A-C)** and P21 **(D-F)**. Lobules are marked and named in (A) and (D). Magnifications show cortex of cerebellum of lobulus V. **(G-H)** magnification of lobules IX and X stained for PAX6. On P7, mice with a homozygous *Tcf4* knockout exhibit a slightly smaller cerebrum and thinner cortex. More extinct effects can be seen on P21 where the cerebellum is exceedingly smaller. The formation of lobules IX and X is clearly altered and granule cells are scattered. EGL = external granular layer, ML = molecular layer, IGL = internal granular layer.

Regarding the histology of the cerebella, distinct alterations in the structure of the cerebellum in mice carrying a homozygous loss of *Tcf4* was observed for mice at P21. Not only was the cerebellum smaller in size, which was confirmed in measuring cerebellar weights (Fig. 13) but also the formation of granule cells, especially in lobules IX and X, was different from that seen in wild type mice (Fig. 16D-F and G-I).

For a better investigation of lobules IX and X, brains were stained using Paired box protein 6 (PAX6), a marker for granule cells (Chung et al., 2010). Staining of PAX6 highlights clearly that granular cells in lobules IX and especially X in mice carrying a homozygous *Tcf4* knockout were scattered heavily and the formation of the internal granular layer was altered. It seemed that migration of granule cells failed and the cells 'got stuck' in the molecular layer.

Experiments carried out using the *hGFAP* promoter were later repeated using the *Math1* promoter with very similar results. The size of the cerebellum of mice with a homozygous loss of *Tcf4* was smaller compared to WT mice (Fig. 29, Appendix). However, the effects seen here were not as distinct as seen with the *hGFAP* promoter which might be due to the fact that more cell lines are affected in *hGFAP-cre* mice (Machold and Fishell, 2005; Spassky et al., 2008).

Proliferation and apoptosis rates To unravel the cause of the observed microcephaly, the proliferation rate in the EGL of mice aged 7 days was determined. Mice were pulsed with BrdU 2 h before decapitation and sagittal sections were prepared. Embedded tissues were then stained for BrdU; the $BrdU^+$ fraction in the EGL was calculated and values were compared. Proliferation rates in lobules IV/V and lobules IX/X were significantly reduced in homozygous knockout mice compared to the wild-type (Fig. 17G).

Apopotosis rates were compared by staining the embedded tissues for Caspase-3 (CASP3). Caspase-3 is a protein that plays an essential role in cell apoptosis (Harrington et al., 2008). For mice aged 7 days, the fraction of $CASP3^+$ cells in the EGL in lobules V and X was determined. There were no significant differences in the apoptosis rates (Fig. 17H). However, for mice at P14, a significantly increased number of $CASP3^+$ cells in mice carrying a homozygous knockout in lobules IV/V was calculated ($p<0.001$, Fig. 30, Appendix). Apoptosis rates on day 21 were determined for lobules IV/V and lobules IX/X and total numbers of $CASP3^+$ cells per section were counted. Interestingly, although significantly higher on P14, apoptosis rates were non-significant in lobules IV/V on P21. Nevertheless, a tendency of increased apoptosis following a *Tcf4* knockout was observed at P21. For lobules IX/X, a significant higher number of $CASP3^+$ cells in the mutant mice was determined (Fig. 17I).

This suggests that the difference in brain size due to a homozygous loss of *Tcf4* is caused by a decrease in proliferation and an increase in apoptosis in granule cells. These findings would also explain the decrease in brain weights from P14 to P21 seen in Fig. 13, as increased apoptosis starts around two weeks post partum.

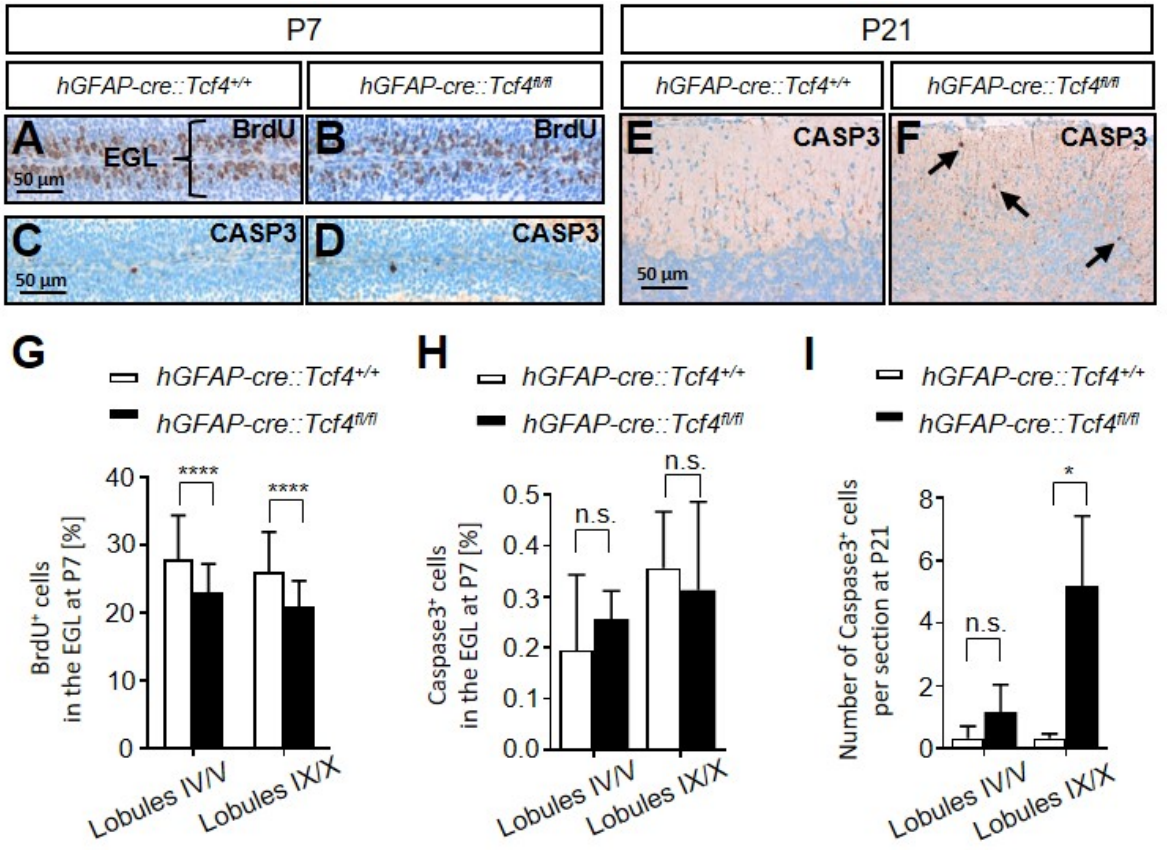

Figure 17: *Tcf4* knockout influences proliferation and apoptosis rates of granule cells significantly. **(A-B)** BrdU staining of the EGL at P7 in lobulus V. Compared were the proliferation rates of mice at P7 using the fraction of $BrdU^+$ cells in the EGL. **(C-D)** Caspase-3 staining of the EGL at P7 in lobulus V. Fractions of $CASP3^+$ cells in the EGL were used to compare apoptosis in mice. **(E-F)** $CASP3^+$ staining of lobulus V in **(E)** and lobulus X in **(F)**. Cell counts of $CASP3^+$ cells were determined by section at P21. Arrows mark $CASP3^+$ cells. **(G-H)** Results show that a knockout of *Tcf4* causes a significant difference in proliferation rates at P7. No significant difference could be determined for $CASP3^+$ counts. **(I)** For mice at P21, a significant difference in apoptosis rate was found, when comparing lobules IX/X. Analysis was done using chi-squared tests **(G-H)** and t-tests **(I)** respectively. Error bars show mean + SD. n.s. = $p>0.05$, * = $p<0.05$, **** = $p<0.0001$.

Migration of granule cells To elucidate the structural alterations seen in mice carrying a homozygous *Tcf4* knockout, the migration of granule cells from the external granular layer into the internal layer throughout early postnatal development was inspected more closely. Two different experiments were performed.

Firstly, to receive an estimate on the migratory deficits, the number of granule cells - made visible through staining of PAX6 - in the molecular layer of lobulus IV/V on P21 was determined. The migration of granule cells should usually be completed by P20 and thus the number of granule cells in the ML very low (Edmondson and Hatten, 1987).

The results revealed that there was a significant higher number of PAX6$^+$ cells per mm^2 in the ML of *hGFAP-cre::Tcf4*$^{fl/fl}$ mice on P21 compared to *hGFAP-cre* WT mice (Fig. 18G), suggesting that either migration is slowed down or not completed.

A second experiment was performed aiming to confirm that the granule cells from the EGL do not migrate properly into the IGL. For this experiment, mice were pulsed with BrdU on P7 and either decapitated two hours later that same day or sacrificed seven days after the initial BrdU pulse on P14. The number of BrdU$^+$ cells per mm in the EGL for day 7 and 14 were counted as well as the BrdU$^+$ cells in the ML. This was to show that the granule cells, resting in the EGL on day 7, where they actively proliferate, as suggested by the uptake of BrdU, later migrate into the IGL. Since BrdU stays in the DNA of the cell for several days, it can still be made visible a week later.

The number of BrdU$^+$ cells on P7 in the EGL and ML were not significant different between the two genotypes (Fig. 18L). This result was unexpected, as Fig. 17 showed a significant decrease in proliferation on P7 for the homozygous knockout mice in the EGL. However, a decreased absolute number of BrdU$^+$ was calculated for the homozygous knockouts (Mean $\pm$ SD = 285.7 $\pm$ 44.1) and WT mice (Mean $\pm$ SD = 383.9 $\pm$ 83.6), yet not significant. The differences in the statistical outcome might also be explained by the different use of absolute and relative cells counts.
Cell counts of BrdU$^+$ cells on day 7 were furthermore higher in the EGL compared to the ML which was to be expected since granule cells exhibit mitotic activity with a peak at P5-8 and start migration 24-48 h later (Roussel and Hatten, 2011; Komuro et al., 2013). On day 14, the number of BrdU$^+$ cells in the EGL was decreased as cells had migrated to the IGL; migration is thought to be completed around P20 (Galas et al., 2017). Cell counts comparing the BrdU$^+$ cells between the two genotypes showed no significant difference for the EGL (Fig. 18M). However, looking at the numbers for BrdU$^+$ in the ML, there was a highly significant difference between mice carrying a homozygous *Tcf4* knockout compared to wild type mice (Fig. 18M).

These two experiments confirm that a loss of *Tcf4* changes the migrating behaviour of granule cells, causing them to leave the EGL but not to migrate properly into the IGL and therefore stay in the ML. This explains the alterations observed in the formation of the IGL and the rather scattered look of lobules IX and X in the homozygous knockouts respectively.

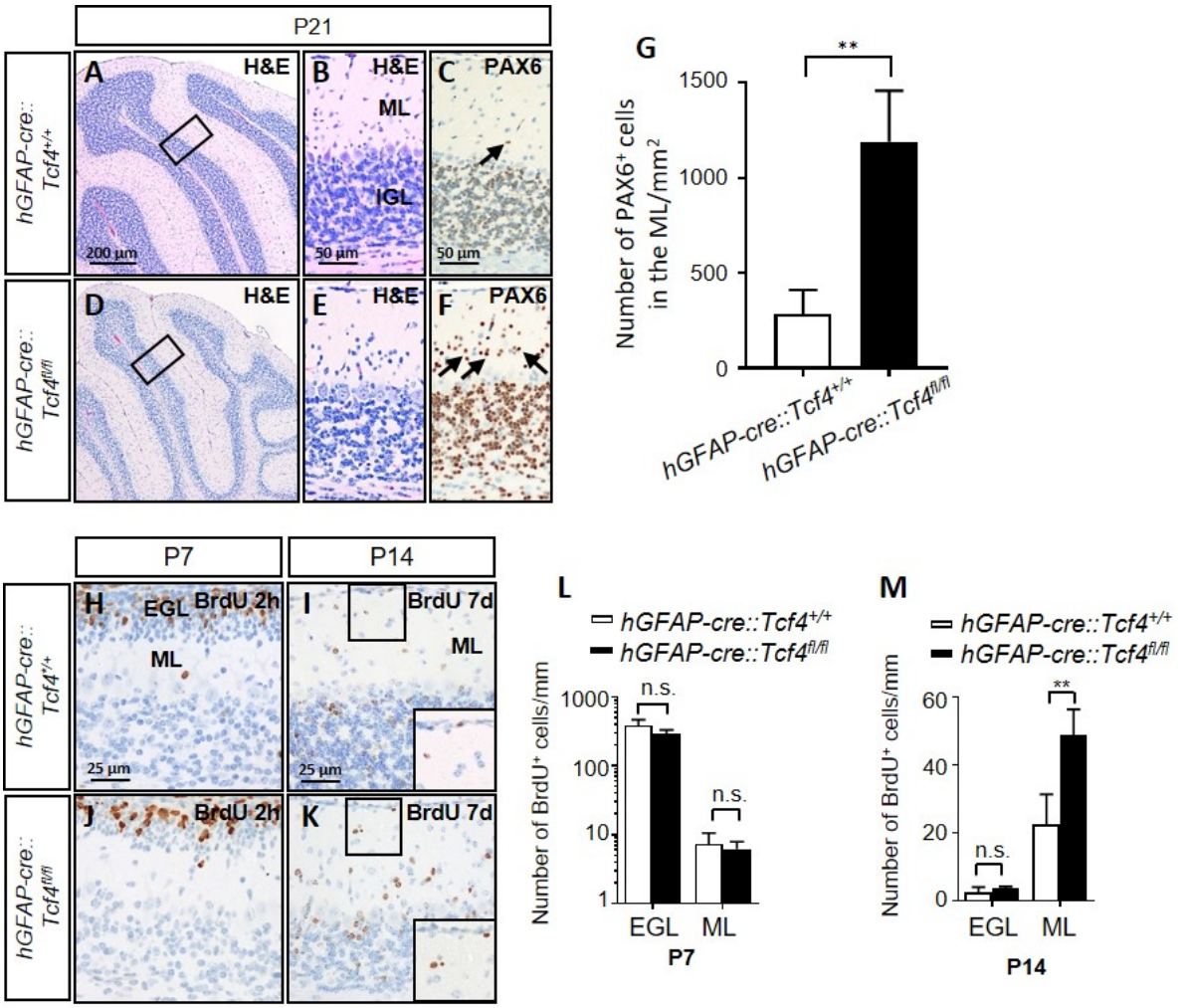

Figure 18: Loss of *Tcf4* causes migratory deficits in granule cells. **(A-F)** Granule cells are shown in the ML on day P21 in lobulus V. **(C+F)** Staining for PAX6, arrows mark granule cells ($PAX6^+$ cells) in the ML. **(G)** Analysis of number of $PAX6^+$ cells in the ML/mm^2 for *hGFAP-cre::Tcf4*$^{fl/fl}$ mice compared to *hGFAP-cre* WT mice on P21. There was a significant higher number of cells in the ML in mice with a homozygous *Tcf4* knockout. **(H-K)** Mice pulsed with BrdU on P7 and killed of either on P7 or P14. Staining for BrdU shows proliferating granule cells and their migration on P7 and P14. **(L+M)** Analysis of number of $BrdU^+$ cells per mm on P7 and P14 in the EGL and ML. There was no significant difference on P7; for P14 a, significant difference in $BrdU^+$ cells in the ML of *hGFAP-cre::Tcf4*$^{fl/fl}$ mice was found. EGL = external granular layer, ML = molecular layer. Analysis was done using t-tests. Error bars show mean + SD. n.s. = $p>0.05$, ** = $p<0.01$.

3.5.3 Mouse model and Pitt-Hopkins syndrome

Haploinsufficiency of *TCF4* causes Pitt-Hopkins Syndrome (Amiel et al., 2007). Children with this form of developmental disorder show distinct features in the structure of their brains, features that can also be found in the herein described mouse models.

To compare the *hGFAP-cre::Tcf4*$^{fl/fl}$ mouse model with PTHS, magnetic resonance brain images (MRI) of a 19-months old patient with Pitt-Hopkins syndrome and from an aged-matched control were analysed.[5]
Fig. 19 shows a widening of the outer and inner cerebrospinal fluid (CSF) spaces, a reduced volume of the parenchyma of the subtentorial brain (see also Fig. 31, Appendix) as well as hypoplasia of the cerebellar hemispheres and vermis in the PTHS patient. Furthermore, a slight disorganisation of the cerebellar folia is present. There are also increased signal intensities in the deep cerebellar hemispheres (adjacent to the 4th ventricle) and the posterior pons. Compared to an age-matched control, the entire corpus callosum is profoundly thinner. The cisterna magna is widened and a slight increase of the caudal opening of the 4th ventricle can be seen (Fig. 19).

Very similar MRI findings in PTHS were reported by Amiel et al. (2007). The authors described a thin corpus callosum with moderate hypoplasia, a marked white matter hyperintensity in the temporal poles, and small hippocampi in PTHS. Furthermore, Peippo and Ignatius (2011) mention 67 reports from MRI scans of PTHS patients, of which 64 % were abnormal (43 out of 67). *"Most common abnormal findings reported are hypoplastic/thin corpus callosum, often more pronounced in the rostral parts, and enlarged ventricles. Bulging caudate nuclei have been described in 4 individuals [...]. Additional findings reported include small hippocampi, frontal lobe hypoplasia, thin hindbrain, and delayed myelination."*(Peippo and Ignatius, 2011).

Several of these features were also observed in the mouse models presented in the this work, especially the *hGFAP-cre::Tcf4*$^{fl/fl}$ mice. The reduced volume of the cerebellar hemispheres and vermis can be seen in the mouse model and have been addressed above (Fig. 12 and Fig. 13). Furthermore, the described disorganisation of the cerebellar folia can be compared to the structural changes identified in the lobules of mice carrying a homozygous *Tcf4* knockout (Fig. 16). Finally, alterations in the hippocampi have been described in Fig. 14.

[5]The images and the radiology report were kindly provided by Prof. Dr. Ertl-Wagner, LMU Munich.

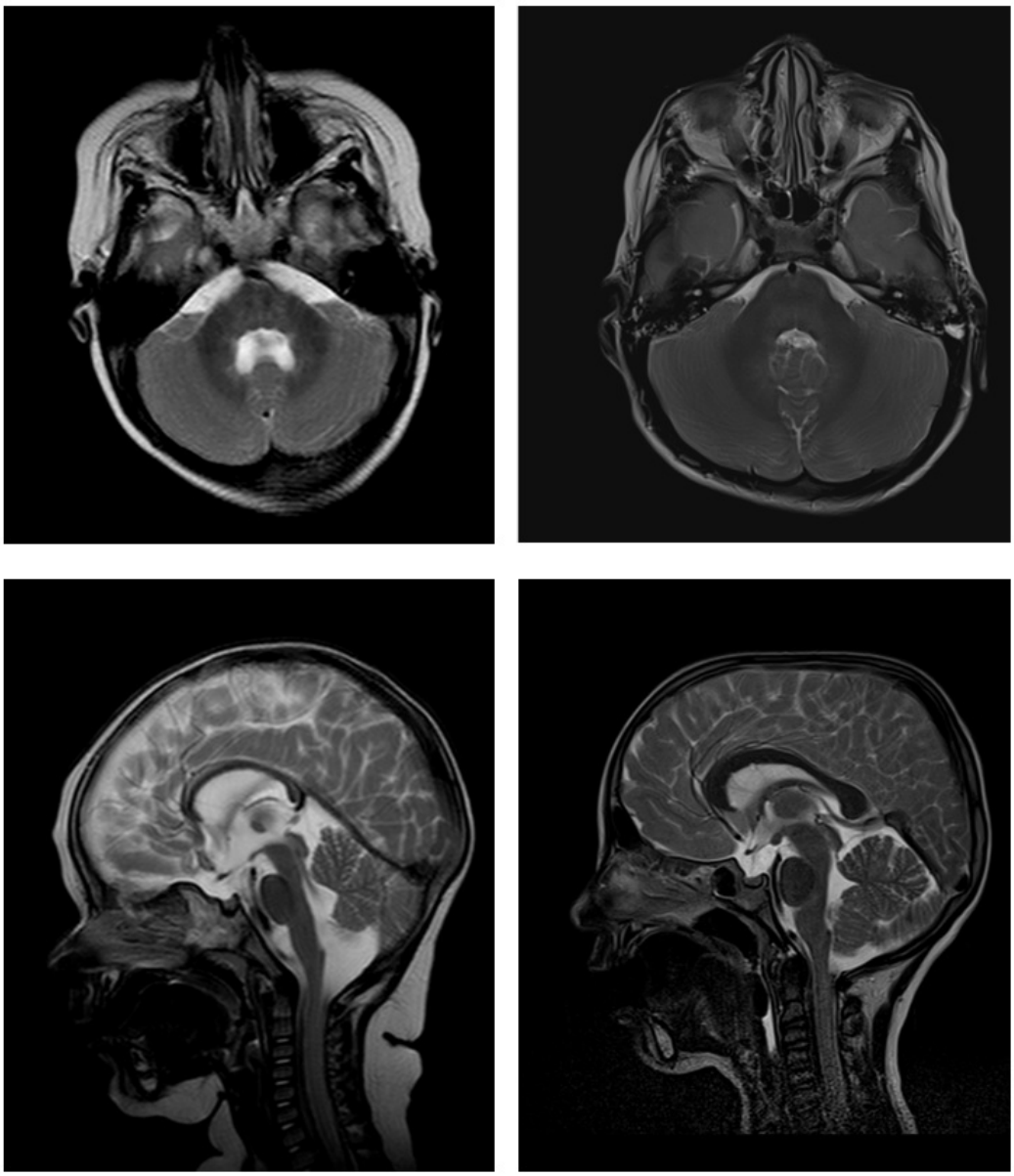

Figure 19: MRI brain of a patient with PTHS and aged-matched control. MR images of a 19-months old patient with Pitt-Hopkins syndrome (left) and aged matched control (right). **Top:** Transverse plane of the cerebellum (T2). **Bottom:** sagittal plane of the head (T2). Images for the PTHS patient show hypoplasia of the cerebellum, the corpus callosum is profoundly thinner, and the outer and inner CSF spaces are widened. Pictures were received with kind permission from Prof. Dr. Ertl-Wagner (LMU Munich).

Overall, the mouse model established in this work features many of the key characteristics that have been described in children suffering from Pitt-Hopkins syndrome. Although the learning difficulties that go along with this neurodevelopmental disorder have not yet been investigated in the *hGFAP-cre::Tcf4*$^{fl/fl}$ mouse model, alterations and structural differences in the hippocampus of these mice suggest that learning difficulties might be

present and further research in this direction needs to be conducted. Moreover, patients with Pitt-Hopkins syndrome also exhibit motor deficits which have been observed in some of the *hGFAP-cre::Tcf4*$^{fl/fl}$ mice (video footage available). These mice showed an atactic style of walking, seemed to be rather insecure when moving, and were even smaller than their littermates, weighing only around 3 to 5 g at adult stage. Due to the limitations of this project, it was not possible to follow up on these rather 'special' mice.

3.6 *In vivo* loss of *Tcf4* in SHH MB

Since *Tcf4* was found to be mutated in 14 % of adult SHH-associated MB (Kool et al., 2014), it was of great interest to investigate a loss of *Tcf4* in a medulloblastoma mouse model. Two different mouse models were used for this part of the project. First, loss of *Tcf4* in SHH MBs was examined using *hGFAP-cre::Tcf4*$^{fl/fl}$*SmoM2-YFP*$^{fl/+}$ mice in comparison to *hGFAP-cre::Tcf4*$^{+/+}$*SmoM2-YFP*$^{fl/+}$ mice, creating a prenatal knockout of *Tcf4* and a constitutively active SMO. Survival rates of the different genotypes were determined as well as proliferation and apoptosis rates. Second, the inducible system *Math1-creER*^{T2} was used to create a postnatal knockout of *Tcf4* on day five, together with an activation of the SHH signalling pathway by introducing a *Smo* mutation. Again, survival rates were measured.

3.6.1 Prenatal loss of *Tcf4*

To improve the understanding of the impact of *Tcf4* in the development and progression of medulloblastoma, the *hGFAP-cre::Tcf4*$^{fl/fl}$*SmoM2-YFP*$^{fl/+}$ mouse line was established. Survival rates of mice carrying a *Smo* mutation and a *Tcf4* mutation simultaneously were compared to those mice solely carrying a *Smo* mutation to determine whether a prenatal loss of *Tcf4* influences the survival of mice. Mice were examined on a day-to-day basis by the staff of the animal facility and notice was given as soon as mice showed symptoms (e.g. hyperplasia of the skull, refusal to eat, general illness). The mice were sacrificed as soon as they were in a bad physical stage. Analysis of survival rates was carried out using a Kaplan-Meier plot and tested for significance using a logrank test. As Fig. 20 illustrates, no difference in survival was found, suggesting that an additional loss of *Tcf4* in SHH MB does not affect the overall survival. All mice died between the ages of 13 and 21 days.

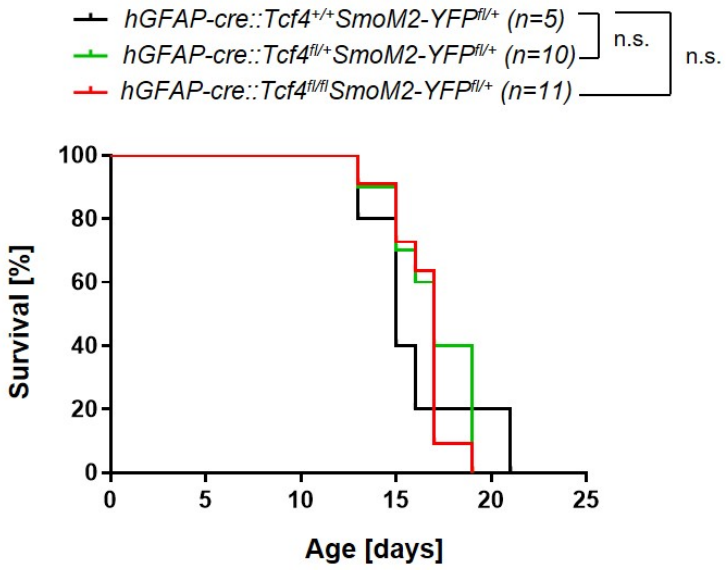

Figure 20: Prenatal loss of *Tcf4* does not alter survival rates in SHH MB. Kaplan-Meier plot for SHH MB with prenatal knockout of *Tcf4*. Survival rates for the three different genotypes observed showed now significant difference. Mice died between two and three weeks of age. Statistical analysis was carried out using a logrank test.

Cell proliferation and apoptosis rates were determined in the same fashion as described before (see Section 3.5.2.2, p. 36ff). Embedded tissues were stained for CASP3 to measure apoptosis and the mitosis-specific marker phospho-histone H3 (PHH3) for determination of proliferation. Due to the anatomical structure of the medulloblastomas, the cerebellar layers were non-existent and observation was done throughout the tumour tissue.
The investigation of cell proliferation did not show any significant difference for the two time points observed, i.e. P13 and P17 (Fig. 21). This stands in contrast to the results determined with a sole homozygous *Tcf4* knockout as pictured in Fig. 17, where the loss of *Tcf4* in *hGFAP-cre::Tcf4*$^{fl/fl}$ mice led to a decrease in proliferation. As for the apoptosis rates on P17, but not on P13, the number of CASP3^{+} cells was significantly higher in the population carrying a homozygous *Tcf4* mutation. This was observed likewise in mice not carrying a *Smo* mutation (Fig. 17).

These findings indicate that a prenatal loss of *Tcf4* has a strong effect on apoptosis, independently of the constitutive activation of the SHH signalling pathway, and therefore the development of MB. The prenatal loss of *Tcf4* does not interfere with the overall survival of the mice and does not alter cell growth. These results, however, are in contrast to the hypothesis that *Tcf4* functions as a tumour suppressor (Herbst et al., 2009b), providing evidence that the function of *Tcf4* might be time-sensitive, i.e. there are differences in a prenatal versus a postnatal knockout.

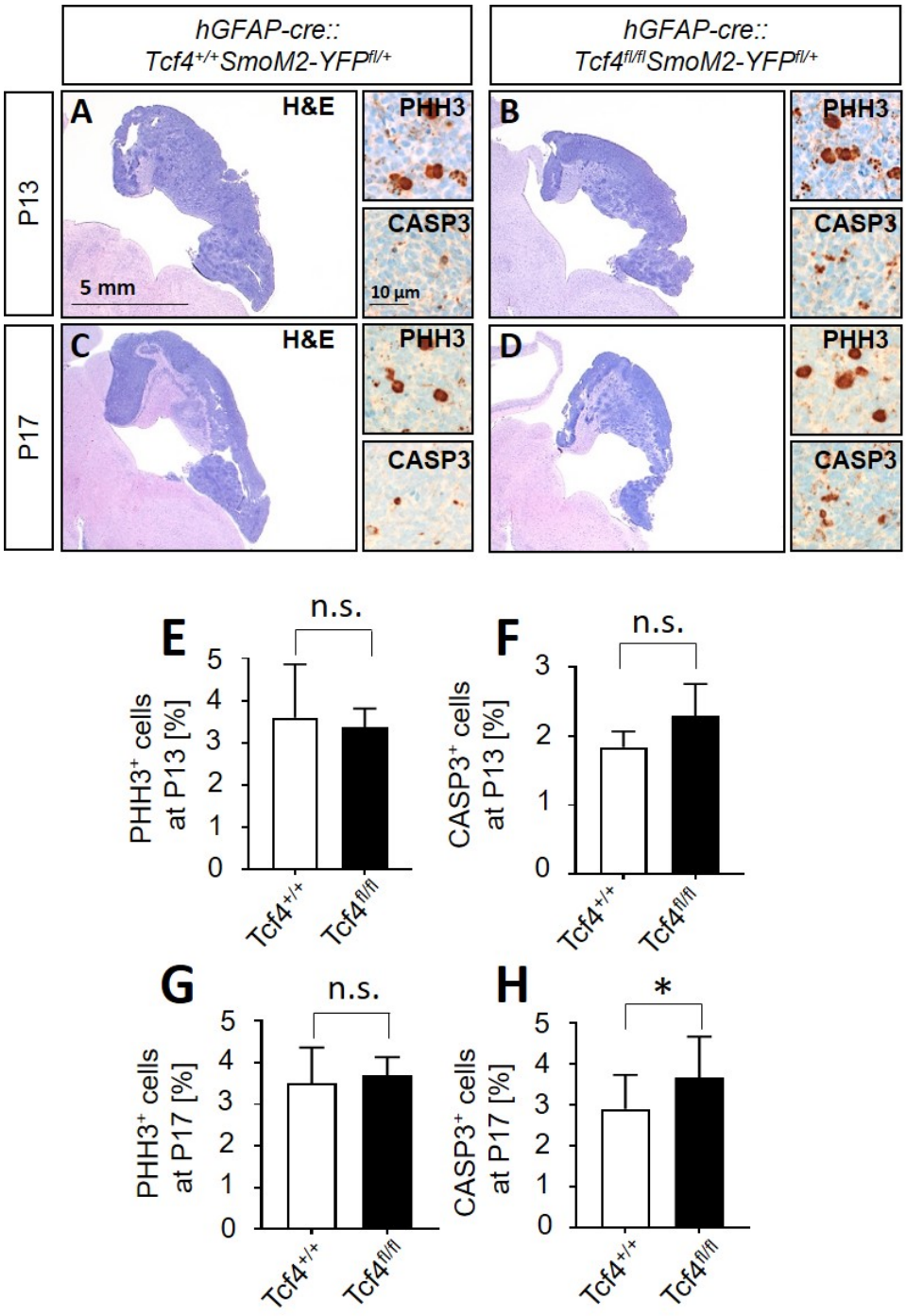

Figure 21: Prenatal knockout of *Tcf4* in SHH MB increases apoptosis rates but does not influence proliferation. (A-D) H&E stains of cerebella with SHH MB in mice with WT and homozygous knockout of *Tcf4* and activation of SMO. Additional stainings for PHH3 and CASP3 are shown. **(E-H)** Statistical analysis of fraction of $PHH3^+$ and $CASP3^+$ cells for P13 and P17. No significant difference in $PHH3^+$ cells at P13 and P17 was found. No increase in apoptosis was determined for P13, however, on P17 a homozygous knockout of *Tcf4* caused a significant increase in $CASP3^+$ cells. Total numbers of stained cells were compared using a chi-squared test. Error bars show mean+SD. n.s. = $p>0.05$, * = $p<0.05$. Genotypes in the statistical analysis are simplified to $Tcf4^{+/+}$ (*hGFAP-cre::*$Tcf4^{+/+}$*SmoM2-YFP*$^{fl/+}$) and $Tcf4^{fl/fl}$ (*hGFAP-cre::*$Tcf4^{fl/fl}$*SmoM2-YFP*$^{fl/+}$) for better illustration.

3.6.2 Postnatal loss of *Tcf4*

Besides looking into a prenatal knockout of *Tcf4* in respect to the development of medulloblastoma, a postnatal knockout of *Tcf4* with a constitutive activation of the SHH signalling pathway was also examined.

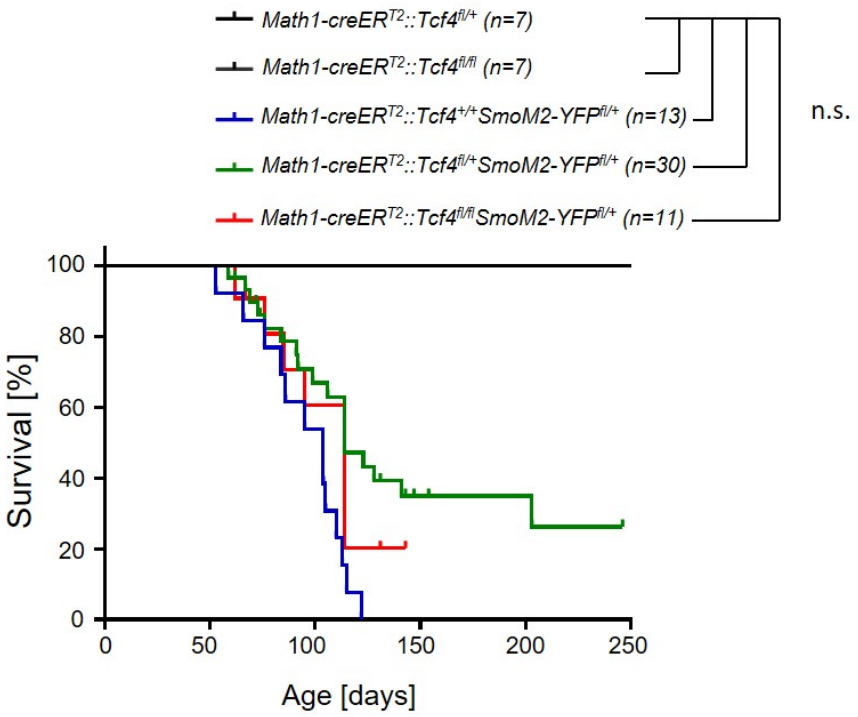

Figure 22: Postnatal *Tcf4* knockout does not alter survival in SHH MB. Survival rates of mice of different genotypes expressing the Cre recombinase under the *Math1* promoter, using the inducible *Math1-creER^{T2}* system, were plotted in a Kaplan-Meier plot. The *Tcf4* knockout and activation of the SHH signalling were induced on day 5 through a tamoxifen injection. No significant differences were found when comparing the different genotypes with *Tcf4* and *Smo* mutations. Analysis was carried out using a logrank test.

Therefore, the survival rates of mice of different genotypes using the inducible *Math1-creER^{T2}* system were determined (Fig. 22). These mice express the Cre recombinase under the *Math1* promoter and a *Tcf4* loss and activation of SMO were induced through tamoxifen injection on P5. Mice carrying sole *Tcf4* knockouts were not affected in their survival and lived as long as the wild-type controls; the experiment was stopped after 250 days. Mice that were additionally carrying a *Smo* mutation developed MB within the first 100 days of life and mostly died between P80 and P150 (with median survival of 104 days for *Math1-creER^{T2}::Tcf4$^{+/+}$SmoM2-YFP$^{fl/+}$*, 114 days for *Math1-creER^{T2}::Tcf4$^{fl/+}$SmoM2-YFP$^{fl/+}$*, and 114 days for *Math1-creER^{T2}::Tcf4$^{fl/fl}$SmoM2-YFP$^{fl/+}$*).

There was no significant difference in survival for mice carrying a sole *Smo* mutation and mice carrying an additional homozygous *Tcf4* knockout. Interestingly, mice with a heterozygous loss of *Tcf4* seemed to survive for a longer period of time as seen in Fig. 22, although median survival was equal to that of mice with a homozygous knockout of *Tcf4*.

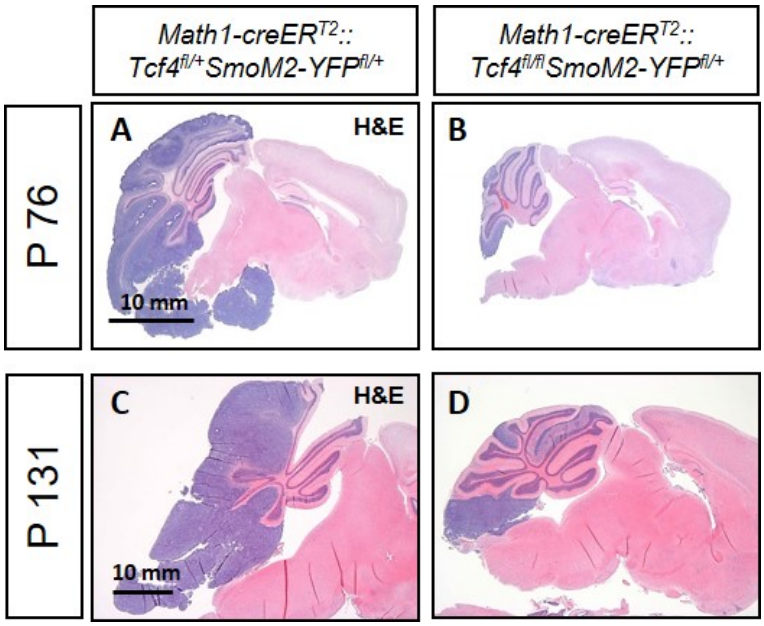

Figure 23: Postnatal knockout of *Tcf4* in SHH MB. H&E stain of SHH MB of siblings at P76 **(A-B)** and P131 **(C-D)**. Comparison of heterozygous and homozygous knockout of *Tcf4*. The *Tcf4* and *Smo* mutations were induced on P5 through tamoxifen injection. Mice carrying a heterozygous knockout are shown to grow larger tumours.

Surprisingly, mice carrying a heterozygous *Tcf4* knockout were growing bigger tumours compared to mice with a homozygous loss (Fig. 23). A different experiment, performed by another group member (Jasmin Ohli), measured the relative tumour area in the vermis and the hemispheres and found that mice with a heterozygous loss of *Tcf4* exhibited the biggest tumours (data not shown). This independent effort found that a postnatal loss of *Tcf4* induced through a tamoxifen injection on day 5, either heterozygous or homozygous, causes significantly bigger tumours compared to a *Smo* mutation alone (data not shown). These results are yet another indication that *Tcf4* functions as a tumour suppressor and inhibits proliferation and tumour growth postnatally.

Currently, proliferation rates of granule cells in *Math1-creER*^{T2}*::Tcf4*$^{+/+}$*SmoM2-YFP*$^{fl/+}$, *Math1-creER*^{T2}*::Tcf4*$^{fl/+}$*SmoM2-YFP*$^{fl/+}$ and *Math1-creER*^{T2}*::Tcf4*$^{fl/fl}$*SmoM2-YFP*$^{fl/+}$ are examined by another group member (Malte Hellwig) for further investigation and comparison to the prenatal *Tcf4* knockouts in SHH MB.

4 Discussion

The aim of this project was the investigation of the role of transcription factor 4 in cerebellar development and its influence on initiation and growth of Sonic hedgehog associated medulloblastoma. The function of *TCF4* has been subject to different research projects in the recent years, mainly focusing on the different diseases associated with *TCF4*, understanding their molecular backgrounds and finding new treatment strategies (see Section 1.1, p. 1). This thesis, for the first time, addresses the role of *TCF4* in medulloblastoma and describes in more detail its importance for cerebellar development. The obtained results provide evidence that *TCF4* exhibits different functionality at different developmental stages and its loss affects cells in opposite ways, depending on the time of knockout, i.e. prenatal versus postnatal knockout.

One of the main obstacles that had to be faced throughout the project was the absence of a suitable anti-TCF4 antibody to confirm the correct recombination in the knockout mice used. Even though several antibodies were tested, only one was available that was proven to work. This anti-TCF4 antibody unfortunately binds to the AA sequence 468-525 which lies before the *loxP sites* (Fig. 32, Appendix, Anti-TCF4 Sigma). This antibody could be used for *in vitro* experiments to visualize the presence of the TCF4 protein in cells and tissues. However, it could not be used to verify the absence of TCF4 in granule cells after recombination, as the translated TCF4 protein from the knockout mice is only missing its functional domain and still expresses the domain detected by this specific anti-TCF4 (AA 468-525). Unfortunately, other approaches to test for recombination, such as quantitative PCR or western blot analysis, also failed to work. Although it was not possible to show the correct recombination for the duration of the project, the distinct features exhibited by the mice and the obtained results are evidence that recombination was successful and the findings indeed do result from a loss of *TCF4*. To avoid this problem in the future, other mouse models, such as the one generated by Skarnes et al. (2011) could be used; here, recombination is visualized by the expression of LacZ. Another approach would be to generate a new antibody targeting an epitope within the *loxP sites*.

4.1 Importance of *TCF4* in cerebellum development

The present work highlights the importance of *TCF4* for correct formation and structure of the cerebellum during brain development; illustrating that the loss of *TCF4* causes severe alterations in the cerebellum (Fig. 16). The findings described in regard to the *in vivo* experiments in *hGFAP-cre::Tcf4*$^{fl/fl}$ mice (Section 3.5), demonstrate that a prenatal homozygous loss of *Tcf4* in mice leads to a significant decrease in cerebellar volume, caused by a decrease in proliferation and an increase in apoptosis (Fig. 13 and 17). The obtained results furthermore provide evidence that the observed structural alterations are caused by the failed migration of granular cells from the EGL to the IGL (Fig. 18).

4.1.1 Anatomical alterations and correlations to PTHS in *Tcf4*-deficient mice

Through the investigation of the newly generated *hGFAP-cre::Tcf4*$^{fl/fl}$ transgenic mice, it was possible to gain a good insight into the pathologies caused by a prenatal loss of *Tcf4*, i.e. the anatomy of the whole mouse body in general and the micro-anatomy of the cerebellum in specific. The decrease in body and brain weights and the structural alterations detected under the microscope became more distinct with time and could properly be observed starting from P14 (Fig. 13). Evidence was provided that an increase in apoptosis and a decrease proliferation led to the significant differences in the measured weights (Fig. 17). In a similar approach, Flora et al. (2007) demonstrated that *Tcf4*$^{-/-}$ mice have a substantially reduced number of neurons in the pontine nucleus on P0.
Moreover, the onset of postnatal microcephaly in mice at P14 correlates with findings from PTHS patients, where half of the patients develop a microcephaly during the first twelve months of life and mostly before 1.5 years of age (Peippo and Ignatius, 2011). According to Dutta and Sengupta (2016), one human year corresponds to roughly nine mice days, so that 1.5 human years correspond to two weeks in the life of a mouse. Apart from the microcephaly, case reports of PTHS patients have shown that similar to the herein described mouse model, PTHS patients are smaller in size and height in comparison to their peers (Taddeucci et al., 2010). In total, postnatal growth retardation is seen in 25 % of PTHS patients (Peippo and Ignatius, 2011).

Measuring mice and brain weights was a useful first step to obtain an estimate on the influence of *Tcf4* on the development and growth of the whole body in general and the cerebellum in particular. Interestingly, although the measurements described in this work did only show significant differences for homozygous knockouts compared to WT

mice for absolute brain weights, Thaxton et al. (2018) identified significant differences for brain and body weights in heterozygous knockouts in four different mouse models. Two of their mouse models utilize the same conditional *Tcf4* knockout used for this project, however, in combination with different promoters under which the Cre recombinase is expressed. The differences seen in the heterozygotes could thus arise from the fact that the *Actin* and *Nestin* promoters used by Thaxton et al. (2018) become active around E10.5 in the brain (Cheng et al., 2004; Bertola et al., 2008), compared to *hGFAP* which becomes active only at E13.5 (Zhuo et al., 2001). In addition, Thaxton et al. (2018) measured the weights in adult mice aged P70-90, which indicates that stronger effects regarding (brain) weights might also be expected in the *hGFAP-cre::Tcf4*$^{fl/fl}$ mouse at later stages.

For an even more detailed analysis, mice could be weighed and measured on a daily basis and not only the weights, but also the volumes of mice brains could be analysed. Getting more frequent measurements, additional to the three time points (P7, 14 and 21), will also provide a better estimate as to when exactly do brain weights start decreasing, i.e. when does the increased apoptosis and decreased proliferation start. Moreover, growth curves could then be calculated for a better statistical analysis.
Another interesting aspect to evaluate is the hippocampal volume as very recently performed by Jung et al. (2018). The group measured the hippocampal volume and cortical diameter following a *Tcf4* knockout using the *Tcf4*^{LacZ} mouse and identified a significantly reduced hippocampal volume in heterozygous mice.

The alterations observed in mouse brains on P14 and especially P21 correlate well with the MR images from PTHS patients and the findings made by other groups (see Section 3.5.3). Comparing the anatomical structure of mouse brains of *hGFAP-cre::Tcf4*$^{fl/fl}$ mice with those of Pitt-Hopkins patients, a lot of similarities were identified, giving validation to the idea that this mouse model can be used to investigate CNS changes in Pitt-Hopkins syndrome, e.g. microcephaly, cerebellar hypoplasia, alterations of the hippocampus (Fig. 14, 16, and 19). However, these distinct features can only be found in mice carrying a homozygous knockout, whereas Pitt-Hopkins syndrome is defined as the haploinsufficiency of *TCF4*, i.e. a heterozygous knockout. Furthermore, the knockout of *TCF4* occurs with the activation of *hGFAP* which is around day E13.5 in multi-potential neuronal stem cells and thus only affects a subset of cells (Zhuo et al., 2001); which stands in contrast to PTHS, a germline mutation of *TCF4*, where all cells are affected. To prove that the newly introduced transgenic mouse model is still suitable to function as a model for Pitt-Hopkins syndrome, further research involving some behavioural and learning

ability tests need to be carried out. This type of tests have already been performed in the *Tcf4*$^{+/-}$ mice by Kennedy et al. (2016) and just recently by Thaxton et al. (2018). It would therefore be of great interest to identify whether the *hGFAP-cre::Tcf4*$^{fl/fl}$ mouse exhibits similar features and can be used as an additional model alongside the already published ones.

4.1.2 Migratory deficits in the cerebellar cortex of *Tcf4*-deficient mice

Besides proposing an explanation for the known differences in body and brain weights in *Tcf4*-deficient mice, that have already been published by other groups, this project identified new structural alterations in the cerebellum that have not yet been addressed.

The results presented in this work provide evidence that (part of) the newly observed histological alterations in mice with a homozygous loss of *Tcf4* are based on deficits in migration of granule cells from the EGL to the IGL (Fig. 18). Under normal circumstances, granule cells migrate into the inner regions of the cerebellar cortex alongside the radial fibres of the Berman glia. Other processes, such as the degradation of cellular matrix, the formation of proliferative premigratory zones, and forms of chemotaxis, are also know to be involved in the migration (Edmondson and Hatten, 1987; Bénard et al., 2015). As the granule cells in *Tcf4*-deficient mice fail to migrate into the IGL, it is tempting to hypothesize that not only the granule cells themselves but also the glia and the processes involved in the migration are affected by a loss of *Tcf4* and contribute to the observed phenotype.

A tentative evidence for this hypothesis comes from the comparison of the effects of a *Tcf4* knockout under the *hGFAP* promoter and the *Math1* promoter (Fig. 16 and 29). *HGFAP-cre::Tcf4*$^{fl/fl}$ mice clearly exhibit more severe alterations in comparison to the *Math1-cre::Tcf4*$^{fl/fl}$ mice which can be explained by the fact that more cell types are affected by a knockout under the *hGFAP* promoter (see Section 1.4.5). A closer look into the functional changes of other affected cell lines and processes might then lead to a more comprehensive understanding of the impact of *Tcf4* on granule cell migration and the consequences that arise from its loss. The idea that the PTHS phenotype could be due to migratory deficits has already been proposed by Peippo and Ignatius (2011) as they write *"intellectual disability, breathing abnormalities and epilepsy could be due to aberrant migration of specific groups of cortical neurons..."*.

Also Flora et al. (2007) demonstrated that a homozygous loss of *Tcf4* can cause disruption and delay in migration by revealing that neuronal precursors "*were unable to reach the pontine nucleus region*". Moreover, Chen et al. (2016) have recently shown that *"in utero suppression of Tcf4 arrest[s] neuronal migration"* and that *Tcf4 "controls neuronal migration of the cerebral cortex through regulation of Bmp7"*. These results are in accordance with the findings of the present work and it would thus be of great interest to examine if an upregulation of *Bmp7* can also be observed in the neurons of the cerebella of the mice used for this project.

4.2 Comparison of the PTHS mouse models

This thesis introduces a new mouse model for Pitt-Hopkins syndrome. Contrary to the ones already published, it is the only one that shows a viable homozygous knockout (Kennedy et al., 2016; Jung et al., 2018; Thaxton et al., 2018). With its distinct phenotype, the *hGFAP-cre::Tcf4*$^{fl/fl}$ mouse can ideally be used to study CNS alterations following a homozygous loss of *Tcf4* in detail.

Currently, six different PTHS mouse models are published, comprising different kinds of knockouts such as permanent and inducible knockouts and whole gene deletions, deletions of exons and point mutations, with all of the published mice modelling a heterozygous knockout as seen in PTHS (Table 3).
The first mouse to be examined as a model for PTHS was the *Tcf4*$^{+/-}$ mouse. It models a germline mutation, a heterozygous loss of *Tcf4*, as generally found in patients suffering from Pitt-Hopkins syndrome (Zhuang et al., 1996; Kennedy et al., 2016). These mice harbour a behavioural phenotype and also the GI phenotype found in PTHS patients (Grubišić et al., 2015). Intriguingly, the CNS phenotype as well as microcephaly and postnatal growth retardation are not present; and as such, the mouse fails to model major characteristics of PTHS (Kennedy et al., 2016).
Jung et al. (2018), using the *Tcf4*^{LacZ} mouse originally generated by Skarnes et al. (2011), were able to show a microcephaly arising due to a heterozygous knockout of *Tcf4* and a CNS phenotype similar to but not as distinct as seen in the *hGFAP-cre::Tcf4*$^{fl/fl}$ mouse. The main focus during the examination of the *Tcf4*^{LacZ} mouse was on the cerebrum and less on the cerebellum. Interestingly, Jung et al. (2018) report that the Purkinje cell layer exhibits the highest TCF4 expression in the cerebellum, which stands in contrast to the *hGFAP-cre::Tcf4*$^{fl/fl}$ mouse, where expression of TCF4 in the Purkinje cell layer was not detectable and the highest expression was seen in the granule cells (Fig. 15). A behavioural phenotype was not examined in the *Tcf4*^{LacZ} mouse (Jung et al., 2018).

Table 3: Comparison of the PTHS mouse models. Essential features of published PTHS mouse models in comparison to the *Tcf4* model introduced in this work. Genotypes are given as stated in the respective publications. Description is given as CNS = central, het = heterozygous, hom = homozygous, KO = knockout, GI = gastrointestinal, N/A= not applicable, PGR = postnatal growth retardation. Features are given as 'present' and 'not present' if mentioned in the papers and as 'not examined' if not mentioned in the respective literature. The label 'not applicable' is given if the genotypes do not allow examination of the characteristic. CNS phenotype describes alterations to the structure and anatomy of the CNS as mentioned in some of the publications, whereas microcephaly describes the general finding of decreased volume of the brain.

Mouse Model	$\boldsymbol{Tcf4^{+/-}}$	$\boldsymbol{Tcf4^{lacZ/WT}}$	$\boldsymbol{Tcf4^{fl/+}}$***::Actin-cre***	$\boldsymbol{Tcf4^{fl/+}}$***::Nestin-cre***	$\boldsymbol{Tcf4^{R579W}}$	$\boldsymbol{Tcf4^{\Delta 574-579}}$	***hGFAP-cre::Tcf4***$\boldsymbol{^{fl/fl}}$
Reference	Zhuang et al., 1996 Kennedy et al., 2016	Skarnes et al., 2011 Jung et al., 2018	Bergqvist et al., 2000 Thaxton et al., 2018	Bergqvist et al., 2000 Thaxton et al., 2018	Thaxton et al., 2018	Thaxton et al., 2018	Bergqvist et al., 2000 Schüller laboratory (this work)
Knockout	het *Tcf4* KO	het *Tcf4* KO	conditional het *Tcf4* KO, pan-cellular	conditional het *Tcf4* KO, CNS specific	het *Tcf4* mutation, non-functional TCF4	het *Tcf4* mutation, non-functional TCF4	conditional hom *Tcf4* KO in cerebellar cell types
CNS phenotype	not present	present	not examined	not examined	not examined	not examined	present
Microcephaly	not present	present	not present	present	present	present	present
PGR	not present	not examined	present	present	present	not present	present
Behavioural phenotype	present	not examined	present	not examined	present	not examined	not examined
GI phenotype	present	not examined	not examined	N/A	not examined	not examined	N/A

Thaxton et al. (2018) generated a total of four different mouse models, with two of the models using the *Tcf4*$^{fl/fl}$ mouse from Bergqvist et al. (2000) that was also used for the *hGFAP-cre::Tcf4*$^{fl/fl}$ mouse in the present project. Thaxton et al. (2018) expressed the Cre recombinase under two different promoters, *Actin* to create a pan-cellular knockout and *Nestin* to create a CNS-specific knockout of *Tcf4*. With these two mouse models, *Tcf4* is knocked out in a different set of cells. Both models were solely investigated as heterozygous knockouts and as such showed a post-natal growth retardation. Additionally, the *Tcf4*$^{fl/+}$*::Actin-cre* mouse presented with a behavioural phenotype but no microcephaly, and the *Tcf4*$^{fl/+}$*::Nestin-cre* mouse presented with a microcephaly, the behavioural phenotype was not investigated (Thaxton et al., 2018). This suggests that the time of knockout and the cell types that are affected have different influences on the phenotype.
Thaxton et al. (2018) generated two more mice. The *Tcf4*^{R579W} mouse, modelling the most common PTHS mutation in humans (in humans it is R580W, Whalen et al., 2012) and the *Tcf4*$^{\Delta 574-579}$ mouse, an in-frame deletion which was generated accidentally. Both showed a microcephaly; the *Tcf4*^{R579W} furthermore presented with a post-natal growth retardation and a behavioural phenotype. All mutant mice were investigated as heterozygous knockouts only, since homozygous knockouts resulted in early mortality (Thaxton et al., 2018).

In comparison, the *hGFAP-cre::Tcf4*$^{fl/fl}$ mouse models a conditional homozygous knockout of *Tcf4* in the CNS, starting from about E13.5 (Zhuo et al., 2001). It was demonstrated that the *hGFAP-cre::Tcf4*$^{fl/fl}$ mouse mimics the specific anatomical alterations reported in the CNS of PTHS patients very well (Section 3.5.3). The model described in this work also exhibits a microcephaly and a post-natal growth retardation as seen in PTHS (Peippo and Ignatius, 2011). Nevertheless, *hGFAP-cre::Tcf4*$^{fl/fl}$ mice only model a loss of *Tcf4* in the CNS and can therefore not be used to examine other features of this disorder. A behavioural phenotype has not yet been investigated in the *hGFAP-cre::Tcf4*$^{fl/fl}$ mice.

To summarise, all present mouse models resemble Pitt-Hopkins syndrome in one way or another, with none of them featuring all characteristics of the syndrome. Especially the epilepsy and breathing abnormalities have not been described. The *hGFAP-cre::Tcf4*$^{fl/fl}$ mice is exceptional regarding the fact that it is the only model that produces viable offspring following a homozygous knockout and it clearly has the most distinct CNS phenotype, with anatomical alterations not seen or described in any of the other models. This mouse model can therefore be used to investigate a homozygous *Tc4*

knockout in the CNS in detail, giving not only rise to investigations of PTHS but the function and importance of *Tcf4* for CNS development in general. Further investigation of this model will clarify whether a behavioural phenotype is present. Moreover, it will be interesting to determine which cell types are responsible for the different features observed in PTHS and the respective mouse models. It is also of great interest to identify the cell line and the time of knockout that lead to the early mortality in homozygous *Tcf4* knockouts.

4.3 Role of *TCF4* in SHH medulloblastoma

Kool et al. (2014) reported that somatic *TCF4* mutations can be found in 14 % of adult SHH MB patients, sparking interest in the question what role does *TCF4* play in medulloblastoma growth and progression. The herein obtained results now strengthen the hypothesis that *TCF4* functions as a tumour suppressor in postnatal development (Fig. 7, 9, and 10). Herbst et al. (2009b) were the first to identify *TCF4* as a potential tumour suppressor, demonstrating that *TCF4 "induces cell cycle arrest via p21^{Cip1}"*. However, a definite 'label' for *TCF4* is yet to be determined as other findings suggest that *TCF4* shows oncogenic potential (Mologni et al., 2010; Appaiah et al., 2014). Even Kolligs et al. (2002) initially thought *TCF4* was exhibiting oncogenic potential before Herbst, one of the group's members, discovered *TCF4*'s tumour-suppressing nature (Herbst et al., 2009a).

The analysis of the data available on human MB revealed that high *TCF4* mRNA levels improve the overall survival of patients with SHH MB (Fig. 7). Similarly, Brandl et al. (2015) demonstrated that high protein levels of TCF4 are correlated with a better outcome for patients with colorectal carcinoma, providing evidence that *TCF4* exhibits characteristics of a tumour suppressor.

The hypothesis that *TCF4* functions as a tumour suppressor was further confirmed during the experimental analysis of TCF4 mutants in this project (Fig. 9). The findings showed that introducing WT TCF4 into a MB cell line (DAOY) significantly decreases cell proliferation. Unfortunately, the DAOY cell line was originally obtained from a young boy (Jacobsen et al., 1985) and is therefore not an adult SHH MB. Ideally, a MB cell line derived from an adult SHH MB should be used for this type of experiment. However, as the four currently established SHH MB lines were all obtained from children, there is no adult cell line available (Ivanov et al., 2016).

Besides, although *TCF4* mutations have solely been found in adults, the effects that the mRNA levels have on the survival of patients, and the raised mRNA levels in general, were seen in all three SHH MB age groups; i.e. infant, child, and adult MB (Fig. 6). In agreement with the described results, Kim et al. (2008) demonstrated that the expression of *TCF4* can decrease cell growth in a gastric cancer cell line and that silencing of *TCF4* plays a role in tumour formation.

Apart from the *in vitro* experiments performed in a tumourous environment, the *in vivo* effects of a *Tcf4* knockout seen in mice with SHH MB were very similar to those obtained in mice with a sole *Tcf4* knockout (Fig. 17 and 21), meaning that a prenatal *Tcf4* knockout increased the number of cells undergoing apoptosis. In what ways a postnatal knockout of *Tcf4* alters proliferation and apoptosis rates in the SHH MB mouse model, has yet to be determined. Nevertheless, an additional loss of *Tcf4* did not change survival rates of both SHH MB mouse models analysed (Fig. 20 and 22), regardless of a prenatal or postnatal loss of *Tcf4*. These findings suggest that the effects of a *Tcf4* knockout regarding cell growth are independent of the *Smo* mutation and the development of SHH MB. All experiments carried out in respect to SHH MB provide evidence for *TCF4* functioning as a tumour suppressor when knocked out postnatally.

4.4 Prenatal versus postnatal *TCF4* knockout

The results presented in this work suggest that the role of *TCF4* is time-sensitive, as the obtained findings point out that *Tcf4* influences granule cells in different ways depending on the time of the knockout. While a prenatal knockout of *Tcf4* increases apoptosis and decreases proliferation, a postnatal *Tcf4* loss leads to a significant increase in proliferation (Fig. 10, 17, and 23).

The observation that a gene can have opposing roles during development is not new; in fact, very similar results regarding another gene have just been published by Merk et al. (2018). Here, the role of the factor *CREBBP*, another gene identified to have somatic mutations in SHH MB and that is associated with the neurodevelopmental disorder Rubinstein-Taybi syndrome, was reported to have time-sensitive effects.

To get a better understanding of these different influences, knockouts at additional time points should be examined. As mentioned before, mice with a total *Tcf4* knockout ($Tcf4^{-/-}$ mice) are not viable and are mostly stillborn (Flora et al., 2007), providing evidence that *Tcf4* is essential for survival.

A study performed by de Pontual et al. (2009), examining the expression pattern of *Tcf4* during early development, could be used to determine suitable points to knock out *Tcf4* and investigate how cells and the whole organism react to its loss. This might solve the question as to when a *Tcf4* knockout leads to an upregulation in apotosis and when in cell proliferation.

The relevance of the different occurrences of a *TCF4* loss are also demonstrated by the fact that a germline mutation in *TCF4*, as seen in PTHS, does not increase the tumour incidence in those patients, since there is only one case reported so far in which a PTHS patient developed cancer (Zweier et al., 2007).
Having a closer look into the different functions of *TCF4* depending on the time of knockout will help shed more light onto its different roles in neurodevelopment and neuromaintenance, and identify whether PTHS is solely a neurodevelopmental disorder or if the lack of TCF4 throughout adult life contributes to the PTHS phenotype.

5 Conclusions

The *Tcf4* knockout mouse model *hGFAP-cre::Tcf4*$^{fl/fl}$ presented in this thesis is a suitable model to investigate a homozygous *Tcf4* knockout *in vivo*. With its similarity to PTHS, it can be used to examine this rare neurodevelopmental disorder. The *hGFAP-cre::Tcf4*$^{fl/fl}$ mouse is furthermore of special interest, as it is the only PTHS mouse model to date that is viable as a homozygous knockout and as such shows a very distinct phenotype not observed in any of the other published models.

The results obtained for this project point out that the function of *TCF4* is time-sensitive with its effects differing depending on whether the knockout occurs prenatally or postnatally. More precise, there is a difference in the effects between a germline and a somatic *TCF4* mutation. A prenatal knockout of *Tcf4* leads to microcephaly most likely caused by a decrease in proliferation and an increase in apoptosis in granule cells. It furthermore leads to migratory deficits in granule cells with its molecular cause still to be determined. It is tempting to propose that the glia plays an important part in this phenomenon. A postnatal knockout on the other hand causes an increase in proliferation *in vitro*.
The investigation of an acquired loss of *TCF4* provided evidence for the protein to function as a tumour suppressor in medulloblastoma, as overexpression of *TCF4* improves overall survival rates in SHH MB. Moreover, the expression of wild-type TCF4 is able to decrease proliferation in a medulloblastoma cell line.

6 Perspectives

The findings presented in this thesis contribute to the understanding of the function of *TCF4*. However, further work is required for a more comprehensive picture of *TCF4*, its role in CNS development, and its influence on SHH MB. Especially the different effects of prenatal and postnatal *TCF4* knockouts should be addressed in more detail. Sweatt (2013) already raised the question as to how different the effects of *TCF4* during development and adult stages are. The author explained that the PTHS symptoms are caused by the *TCF4* knockout during the developmental stages but what happens in the adult brain remains unclear: *"It is unclear whether PTHS is caused exclusively by disruption of TCF4 function during development or whether loss of TCF4 in the mature CNS might also contribute to neurobehavioral and cognitive dysfunction in PTHS patients"* (Sweatt, 2013).

Apart from the time-dependent effects of *TCF4*, other aspects mentioned in this thesis merit further investigation. For example, the development of the whole brain after loss of *TCF4* with special focus on the hippocampus should be observed more closely. This would also give a better estimate as to how well does the herein introduced mouse model mimic Pitt-Hopkins syndrome and in what ways can it be used to investigate this rare disorder. Moreover, behavioural studies and cognitive testing of this mouse model need to be carried out.

An even closer look into the cells and their behaviour itself, especially a better investigation of migration and formation of cells as well as the development of dendritic arbours, will give a more comprehensive understanding in respect to the alteration of the anatomical structure in the cerebellum and cerebrum. As described before, this research should also include the role of the extracellular matrix and other cell types involved in the migratory process, specifically the glia. The question of whether *"distinct cell populations may require different TCF4 dosages and whether there is cell type-/region-specific vulnerability to pathologically altered TCF4 expression levels"* (Jung et al., 2018) should also be addressed in future research into *TCF4*.

A next step in this context would then be to investigate the effects of reintroducing *TCF4* following its earlier knockout and to determine if there is the possibility of rescuing the phenotype. For example, by generating vectors using the foamy virus, which inserts its genome solely in a subset of proliferating cells in the brain such as hippocampal neurons (Counsell et al., 2018), the effect of reintroducing *TCF4* in separate cell lineages could be investigated.
Furthermore, the examination of effects of *TCF4* knockouts in the adult brain, i.e. at later time points than P5, would give more information about the function of *TCF4* in general and its role in the adult brain in specific. Sweatt (2013) already proposed that *"a new understanding of the role of TCF4 in the fully developed CNS might allow the development of new therapeutic approaches to PTHS treatment based on restoration or augmentation of TCF4 function after CNS development is largely finished"*. In particular, the inducible knockout system used in this project is ideally suited to investigate the postdevelopmental brain in respect to TCF4 function.

Another question that has yet to be answered, is why the other two E-proteins, E2A and HEB, are unable to compensate for the loss of function of TCF4 despite them being conserved (Murre, 2005). Looking closer into the heterodimerisation partners and identifying the partners that pair with the E-proteins across different cell types and tissues will help to understand the mechanism behind the potentially different behaviour of these E-proteins.

Regarding SHH MBs, further research into the impact of a postnatal *TCF4* knockout and the possibility of using TCF4 and its heterodimerisation partners for treatment of this tumour entity is of great interest. Specifically the impact of introducing or activating *TCF4*, as described in DAOY cells and seen in patients with high mRNA levels of *TCF4*, should be investigated.

7 Material and Methods

7.1 Material

7.1.1 Appliances

Appliances	Manufacturer	Type
CO_2 incubator	Heraeus	HercaCell 240
Fluorescence Microscope	Olympus	IX50 Mikroskop
Optical Microscope	Olympus	Olympus Bx50 Microscope
Spectrophotometer	NanoDrop Technologies	Nanodrop 1000
Sterile bench	Thermo	HERAsafe

7.1.2 Software

Software	Manufacturer	Type
Cell counts	ImageJ	ImageJ
Gel documentation	Synoptics Limited	Syngene Geldokumentationssystem
Microscope Software	Olympus	ColorView Soft imaging Systems
Statistical analysis	GraphPad	Prism 5.02 Software and Prism 7.01 Software

7.1.3 Chemicals

Substance	Manufacturer	Type
Blocking reagent	Invitrogen	I-Block blocking reagent
BrdU	Sigma-Aldrich	
DAPI	Roth	4´,6-Diamidin-2-phenylindol
DEPEC Water	Roth	
DMEM	PAN	
DMEM-F12	Invitrogen	
DNA Ladder	Promega	
DNAse	Invitrogen	
DPBS	Invitrogen	
FCS	Invitrogen	
Glucose	Sigma	D(+)-Glucose
Glutamax	Invitrogen	
HBSS	Gibco	
HEPES	Sigma	
Klenow Fragment	Thermo Scientific	
Leibovitz	Invitrogen	
Ligase	Thermo Scientific	T4 DNS Ligase
Loading Dye	Promega	6x Loading Dye
Lysozyme	Merck	
N2 supplement	Invitrogen	
NanoJuice	Novagen	NanoJuice^{TM} Tranfection Reagent and Kits
Opti-MEM	Gibco	
Pen/Strep	Invitrogen	Penicillin/Streptomycin 100x
PLO	Sigma	Poly-L-ornithine

Substance	Manufacturer	Type
Polymerase	Agilent	Herculase II Fusion DNA Polymerase
Tamoxifen	SigmaAldrich	
TransIT-2020	Mirus	TransIT®-2020 Tranfection Reagent
Trizol	Invitrogen	
Trypsin-EDTA	Sigma	
X-tremeGENE	Roche	X-tremeGENE HP

7.1.4 Kits

Kit	Manufacturer	Type
Gel extraction	Qiagen	QIAquick Gel Extraction Kit
Immunostaining	Dako	System-HRP DAB-Kit
MaxiPrep	Qiagen	QIAprep Spin Midi/MaxiPrep Kit
MiniPrep	Qiagen	QIAprep Spin MiniPrep Kit
Protein concentration	Sartorius	Vivaspin6
Protein purification	Macherey Nagel	Protino Ni TED 2000 NiDA 200 packed columns Kit

7.1.5 Antibodies

Antibody	Manufacturer	No.
Anti-BrdU	Sigma	11170376001
Anti-Caspase-3 (Asp175)	Cell Signaling Tech	9664
Anti-GFP (mouse)	Invitrogen	A11120
Anti-GFP (rabbit)	Santa Cruz	sc-8334
Anti-PAX6	DSHB	
Anti-phospho-Histone-H3	Cell Signaling Tech	9706S
Anti-TCF4	Sigma	HPA025958
Anti-Rabbit IgG H&L (Alexa Fluor® 488)	Invitrogen	A11034
Anti-Mouse IgG H&L (Alexa Fluor® 488)	Invitrogen	A11029
Anti-Rabbit IgG H&L (Alexa Fluor® 546)	Invitrogen	A11035
Anti-Mouse IgG H&L (Alexa Fluor® 546)	Invitrogen	A11003

7.1.6 Plasmids

Plasmid	Size	Charateristics	Use
pcDNA3	5.4 kb		site directed mutagenesis
pN8-gag-pol		Backbone: pN8-epsilon	packaging plasmid
pN8-VSV-G		Backbone: pN8-epsilon	envelope plasmid
MSCV-IRES-GFP	6.5 kb	expresses GFP	CGNP, site directed mutagenesis
MSCV-Cre-IRES-GFP	8.4 kb	expresses CRE and GFP	CGNP

Modified Plasmid	Size	Characteristics	Use
pcDNA3-ITF2B	7.4 kb	backbone: pcDNA3, WT TCF4	site directed mutagenesis
IRES-GFP-TCF4	8.5 kb	backbone: IRES-GFP, WT TCF4	DAOY transfection
IRES-GFP-TCF4_V613F	8.5 kb	backbone: IRES-GFP, mutation V613	DAOY transfection
IRES-GFP-TCF4_216del	8.5 kb	backbone: IRES-GFP, mutation 216_219del	DAOY transfection
IRES-GFP-TCF4_451del	8.5 kb	backbone: IRES-GFP, mutation 451_453del	DAOY transfection
IRES-GFP-TCF4_R157X	8.5 kb	backbone: IRES-GFP, mutation R157X	DAOY transfection
IRES-GFP-TCF4_R174X	8.5 kb	backbone: IRES-GFP, mutation R174X	DAOY transfection

7.1.7 Mouse strains

Strain	Characteristics	Publication
C57/Bl6	WT mouse	
FBV	WT mouse	
hGFAP-cre	expression of Cre recombinase under the *hGFAP* promoter	Zhuo et al., 2001
Math1-cre	expression of Cre recombinase under the *Math1* promoter	Matei et al., 2005; Schüller et al., 2007
Math1-creER^{T2}	inducible expression of Cre recombinase	Machold and Fishell, 2005
SmoM2-YFP$^{fl/fl}$	conditional mutation of *Smo*	Mao et al., 2006
Tcf4$^{fl/fl}$	conditional knockout of *Tcf4*	Bergqvist et al., 2000

Conditional knockouts	
hGFAP-cre::SmoM2-YFP$^{fl/+}$	activation of SHH signalling pathway
hGFAP-cre::Tcf4$^{fl/fl}$	knockout of *Tcf4* under the *hGFAP* promoter
hGFAP-cre::Tcf4$^{fl/fl}$SmoM2-YFP$^{fl/+}$	activation of SHH signalling pathway and loss of *Tcf4*
Math1-cre::Tcf4$^{fl/fl}$	conditional knockout of *Tcf4* under the *Math1* promoter

Inducible knockouts	
Math1-creER^{T2}::SmoM2-YFP$^{fl/+}$	inducible activation of SHH signalling pathway
Math1-creER^{T2}::Tcf4$^{fl/fl}$	knockout of *Tcf4* under the *Math1* promoter
Math1-creER^{T2}::Tcf4$^{fl/fl}$SmoM2-YFP$^{fl/+}$	inducible activation of SHH signalling pathway and loss of *Tcf4*

7.1.8 Self-made buffers and media

Cell culture medium Cell culture medium for permanent cell lines was DMEM with added 10 % FCS, 1 % glutamax, 1 % penicillin/streptomycin, and 1 % HEPES buffer.

SOC Medium (Super Optimal Broth with Catabolite repression) For the production of 100 ml of SOC medium, 0.5 g yeast extract, 2 g peptone, 1 ml 1M $MgSO_4$, 1 ml 1M $MgCl_2$, 0.05 g NaCl, and 0.25 ml 1M KCl were mixed in 100 ml of ddH_2O and the solution was autoclaved. Then, 2 ml of sterile filtered glucose was added (1.8015 g in 10 ml = 1 M). The medium was aliquoted in 15 ml falcon tubes and stored at - 20 °C.

2× HBS (HEPES buffered saline) For 200 ml of 2× HBS, 3.2 g NaCl, 40 mg Na_2HPO_4, 540 mg glucose, and 2 g HEPES were diluted in 200 ml ddH_2O. The pH was adjusted to 7.1 using HCl. The 2× HBS was sterile filtered with a 0.2 μm syringe filter and aliquots of 1.5 ml were stored at -20 °C.

2.5 M $CaCl_2$ For the 2.5 M $CaCl_2$ solution, 36.75 g of $CaCl_2 \times 2H_2O$ were diluted in 100 ml of ddH_2O, sterile filtered with a 0.2 μm syringe filter and aliqouts of 10 ml stored at -20 °C.

Laird's lysis buffer Lysis buffer consisted of 200 mM NaCl, 100 mT Tris-HCl adjusted to pH 8.3, 5 mM EDTA, 0.2 % SDS and 200 μg/ml proteinase K in ddH_2O.

TE buffer Tris-EDTA buffer solution consisted of 20 mM Tris-HCl adjusted to pH 8.3 and 1 mM EDTA in ddH_2O.

Sonic hedgehog protein Sonic hedgehog was produced by the laboratory technical assistants. SHH expressing bacteria (BL21/pEXP-DEST-LRC4) were thawed and transferred to agar for overnight incubation at 37 °C. One single colony was picked the next day for the production of SHH. Bacterial cells were then grown in LB (Luria Broth) medium until an optical density (OD, 600) of 0.4-0.6 was reached. Expression of SHH was subsequently induced using isopropyl β-D-1-thiogalactopyranoside (1 mM in LB medium). Cells were pelleted and SHH was purified using the Protino Ni TED 2000 or NiIDA 200 packed column Kits from Macherey Nagel. The purified protein was concentrated 30-fold using Vivaspin6 columns. SHH was stored in SHH storage buffer (5 mM Na_2HPO_4, 150 mM NaCl in ddH_2O) with 0.5 mM dithiothreitol at -80 °C. Protein concentration was determined via a BCA (bicinchoninic acid) assay.

Tamoxifen Tamoxifen was administered intraperitoneally at a concentration of 20 mg/ml. Mice were usually treated with 1 mg of tamoxifen (25 μg per gramm body weight, i.e. 50 μl of 20 mg/ml solution). For the production of the solution, 100 mg tamoxifen were dissolved in 100 μl of 100 % ethanol and shaken for 20 min at 55 °C. 900 μl corn oil were added and the mixture was shaken at 55 °C until almost dissolved. The solution was then transferred into a 15 ml falcon flask containing another 4 ml of corn oil, mixed and stored at 4 °C until usage.

7.2 Methods

7.2.1 General molecular biological methods

7.2.1.1 Cloning and site directed mutagenesis

To determine the effects of introducing *TCF4* to a TCF4 deficient medulloblastoma cell line, plasmids containing WT *TCF4* and several known *TCF4* mutants found in SHH-associated medulloblastoma were transferred separately into the DAOY cell line. Hereby, the effect of TCF4 on cell growth as well as the left-over function of the different mutants could be examined.

Preparation of *TCF4* plasmids A *pcDNA3* plasmid containing the human *TCF4* sequence (isoform *ITF-2B*$^-$) with an added HA-tag was received from the group of Professor Frank Kolligs (LMU Munich).
For further use, the *TCF4* sequence was cut out of the plasmid and cloned into the *MSCV-IRES-GFP* backbone which was also used for the production of viral particles (expression vector). The *MSCV-IRES-GFP* vector was kindly provided by Professor David Rowitch (Cambridge). To cut the *TCF4* insert, the plasmid had to be amplified first. Therefore, transformation of plasmids was carried out using XL2 blue chemically competent bacterial cells. The bacterial cells were thawed on ice, 100 ng of DNA was added and incubated for 30 min on ice. The bacteria were then heat-shocked for 42 s and subsequently incubated on ice for another 2 min. 500 μl of SOC medium was added and the solution was incubated for 60 min on a shaker (250 rpm) at 37 °C. Cells were plated onto an agar plate containing ampicillin as a selection marker and incubated at 37 °C overnight. Up to five single colonies were picked the next morning and incubated separately for another night in liquid media (5 ml LB medium with ampicillin 1:1000) for DNA preparation the next day. DNA preparation using mini columns was carried out according to the manufacturer's instruction (QIAprep Spin MiniPrep Kit, Qiagen) and the DNA yield was determined using a Nanodrop, a UV/VIS spectrophotometer measuring the concentration and quality of double stranded DNA.

The plasmid with its insert and the backbone (*MSCV-IRES-GFP*) were digested using restriction enzymes and the fragments were transferred to an agarose gel to separate the *pcDNA3* backbone and the *TCF4* insert. The DNA fragments could then be extracted and purified using the QIAquick Gel Extraction Kit (Qiagen). For ligation, a blunt-end ligation using the Klenow Fragment (ThermoScientific) was carried out, first

filling in the 5'-overhangs on the insert and the backbone and then ligating the two fragments with T4 ligase. The obtained plasmid was transformed into XL2 blue cells and the newly cloned plasmid amplified and purified as described above. The purified plasmid was then digested using restriction enzymes to verify ligation of backbone and insert. To check for correct ligation, i.e. the orientation of the insert, the plasmid was send off for sequencing (sequencing was done by Eurofins Scientific).

Site directed mutagenesis TCF4 mutants were generated through site-directed mutagenesis using overlap extension polymerase chain reaction (PCR). For the later transfection of the DAOY cell line, the plasmid *MSCV-IRES-GFP* was used as the backbone, however, due to difficulties during the PCR steps, the mutants were generated in the *pcDNA3* plasmid, cut out and inserted into the *MSCV-IRES-GFP* backbone.

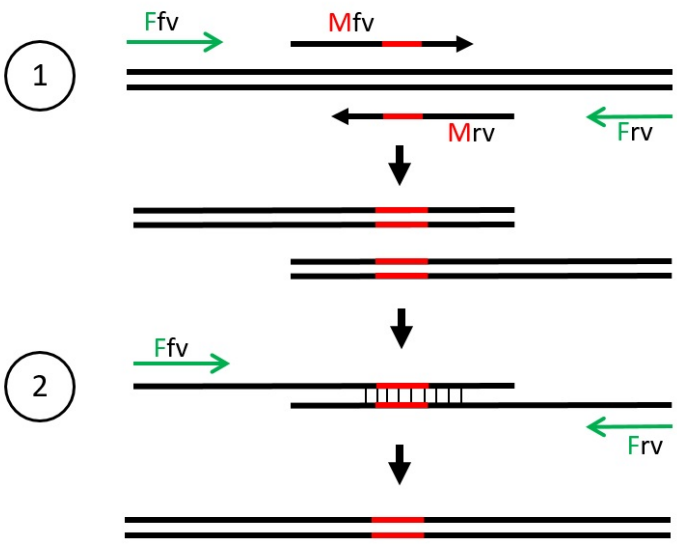

Figure 24: Principle for site directed mutagenesis. Modified after Heckman and Pease (2007). For site directed mutagenesis, a first PCR (marked with 1) was performed using Ffv (flanking primer forward) and Mrv (mutagenic primer reverse) and Mfv (mutagenic primer forward) and Frv (flanking primer reverse) respectively to receive overlapping DNA fragments. Mfv and Mrv carry the mutation shown in red. A second PCR (marked with 2) using only Ffv and Frv was used to create a continuous DNA fragment carrying the mutation.

Design of mutants was mainly performed according to the protocol of Heckman and Pease (2007) *"Gene splicing and mutagenesis by PCR-driven overlap extension"*, with small adjustments for the purposes of this experiment.

For each mutant, two pairs of primers were used, all listed in Table 4, with one pair introducing the mutation (mutagenic primers) and the second pair for amplifying the whole insert (flanking primers). The introduction of the mutation was then done in two steps.

Table 4: Primer sequences used for site directed mutagenesis. Primer name contains the respective mutation. Flanking primers were designed for the *pcDNA3* backbone carrying recognition sites for *Eco*RI and *Xho*I respectively.

Primer	Sequence in 5' - 3'
216_219del fw	CCTAGCTCCTTCGGCCATCACAGC
216_219del rv	GCTGTGATGGCCGAAGGAGCTAGG
451_453del fw	CATTCACTCATGCATCGTGAAGAT
451_453del rv	ATCTTCACGATGCATGAGTGAATG
V613F fw	CGGTGGCCTTCATCCTCAGTC
V613F rv	GACTGAGGATGAAGGCCACCG
R157X fw	CAATAATCCCTGAAGGAGGCC
R157X rv	GGCCTCCTTCAGGGATTATTG
R174X fw	CAAAGAAAGTTTGAAAAGTTCCTC
R174X rv	GAGGAACTTTTCAAACTTTCTTTG
flanking primer fw	GTACCGAGCTCGAATTCACC
flanking primer rv	ATGCATGCTCGAGTCAGGC

First, the forward flanking primer and the reverse mutagenic primer and vice versa were used in separate PCRs to create two DNA fragments carrying the mutation (Fig. 24). The primer sequences of the mutagenic primers were designed so that the PCR amplicons were overlapping. The products from the first PCR were purified and a second PCR was performed, using only the two flanking primers, to create a continuous insert.

Normally, this insert would then be purified and ligated into the original backbone. In this specific case however, the mutation had to be introduced into a different plasmid than the one of interest for the experiment. This was due to a repetitive sequence in the *MSCV-IRES-GFP* plasmid producing a hairpin structure that the DNA polymerase could not read. To solve this problem, the flanking primers had been designed in a way that they also carried the sequences of the recognition sites for the restriction enzymes *Eco*RI and *Xho*I, which are present in the multiple cloning site of the *MSCV-IRES-GFP* backbone. Therefore, the inserts could be produced using

the *pcDNA3* backbone. The synthesised inserts were then purified, digested (using a double-digest with the above mentioned enzymes), purified again, and ligated using a sticky-end ligation with the *MSCV-IRES-GFP* backbone that had also been digested with *Eco*RI and *Xho*I.

All plasmids were subsequently transformed into XL2 blue cells for DNA preparation. Yielded DNA was purified and location of insert was verified via restriction digest and gel electrophoresis of obtained fragments. Purified plasmid DNA was send off for sequencing (Eurofins) to check for correct mutations and insertion into the backbone. The plasmids were then used for transfection of DAOY cells.

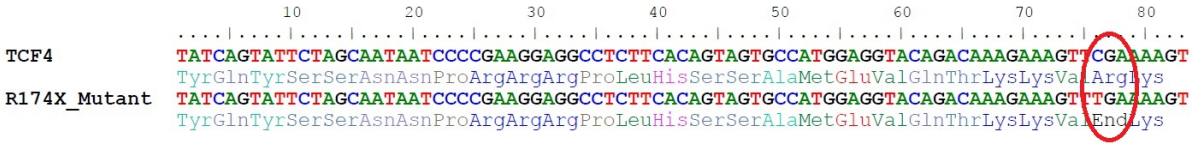

Figure 25: Example DNA and protein sequence of *TCF4* mutant. Excerpt of *TCF4* (top) sequence and sequence of the *TCF4* mutant R174X (bottom). Given are the DNA sequences and the corresponding protein sequence. The triplett CGA (marked in red) coding for the AA arginine (Arg) was changed to TGA, a stop codon (End).

7.2.1.2 Virus production

To compare the growth of *Tcf4* deficient and *Tcf4* sufficient cells, a knockout of *Tcf4* in CGNP cell cultures was generated by transducing the cells with retroviral particles. Two different viruses, containing either *IRES-GFP* or *Cre-IRES-GFP*, had therefore to be produced and tested.

Retroviral particles were produced in Human Embryonic Kidney (HEK) cells via a triple transfection with a packaging plasmid (*pN8-gag-pol*), an envelope plasmid (*pN8-VSV-G*), and the *MSCV-IRES-GFP* or *MSCV-Cre-IRES-GFP* vector. The *MSCV-IRES-GFP* and *MSCV-Cre-IRES-GFP* plasmid were kindly provided by Professor David Rowitch (Cambridge).
Transfection was performed using the calcium phosphate method. The day before transfection, HEK cells were plated onto 10 cm dishes at a confluency of 15-20 % in order to achieve a confluency of 50-70 % 24 h later. The next day, medium was changed 1 h prior to transfection. For the transfection itself, a total of 45 μg DNA, with 15 μg of each plasmid, were mixed with TE buffer in an overall volume of 50 μl. 400 μl nuclease free water and 50 μl of $CaCl_2$ were added and the mixture vortexed. This solution was added

dropwise to a new tube containing 500 μl of 2× HBS and incubated for 30 min at room temperature (RT). The transfection reagents were then added dropwise into the media of the cell culture dishes and incubated at 37 °C for a day. After 24 h and 48 h, the HEK cells were observed under the fluorescence microscope to examine viral production. Efficiency of transfection and viral production could easily be determined by estimating the fraction of green fluorescent cells, since GFP was produced. The media containing the viral particles was harvested 24 h and 48 h post transfection and subsequently filtered through a 0.45 μm syringe filter to remove cell debris and any contamination. The virus was then aliquoted and stored at -80 °C.
Before use on CGNP cultures, the virus was tested on HEK cells. Therefore, 24-well plates were seeded with HEK cells. The next day, media was taken off and replaced with 200 μl of media containing the virus and plates were incubated at 37 °C for 4 h. The virus was then discarded, 500 μl of fresh media added to the wells and the HEK cells again incubated at 37 °C. Efficiency of transduction was determined 24 h and 48 h later by estimating the fraction of GFP-positive cells in the wells through fluorescence microscopy.

7.2.1.3 Transfection of DAOY cells

The effects of WT TCF4 and TCF4 mutants on cell proliferation were tested on a medulloblastoma cell line. DAOY cells were transfected with seven different plasmids (the backbone alone, TCF4 WT, and five different TCF4 mutants, see Table 5) using the *MSCV-IRES-GFP* vector. The transfection of DAOY cells was found to be not very efficient, however, after testing several transfection reagents under different conditions, the transfection reagent TransIT-2020 (MiruBio) was the most promising. Transfection was first tested with calcium phosphate and later with the transfection reagents Fugene, NanoJuice, and X-tremeGENE, all of which showed a transduction efficiency of around 5 %. To optimse the efficiency, several reagents from Mirus were tested and the Trans-IT 2020 reagent was found to have an efficiency in DAOY cells of about 25 %, which was used for the following experiment.

The day before transfection, DAOY cells were plated in 24-well plates at a confluency of 40 %. 2 h prior to transfection, the medium was changed. For each well, the transfection mixture was prepared as follows: To a tube filled with 50 μl of Opti-MEM medium, 1.5 μg of the respective plasmid DNA and 1.5 μl of Trans-IT 2020 (vortexed just before use) were added and mixed. The transfection mixture was incubated for 15-30 min at RT and then added dropwise to the well.

The plates were incubated at 37 °C for two days. 48 h post transfection, the DAOY cells were pulsed with BrdU (final concentration of 25 μg/ml) for 2 h and then the media discarded. Cells were fixated with 4 % paraformaldehyde (PFA) and subsequently stained for either BrdU and TCF4 or BrdU and GFP (see Section 7.2.4.2 for exact protocols). The tranfected, fixated, and stained cells were observed under the fluorescence microscope. Transfected cells were identified by their expression of GFP and proliferation rates of BrdU-positive cells was compared between WT TCF4 and the different mutants. Statistical analysis was done using chi-squared tests.

Table 5: Plasmids used for transfection of DAOY cells. The table lists all conditions used for the transfection of DAOY cells. The WT TCF4 and mutant TCF4 were inserted into the *MSCV-IRES-GFP* backbone, also used as a control. The names of the respective plasmid are given and the mutation and functional domain are noted.

Plasmid	**Mutation and functional domain**
no plasmid	control
MSCV-IRES-GFP	backbone as control
MSCV-IRES-GFP-TCF4	WT TCF4
MSCV-IRES-GFP-TCF4-R157X	nonsense mutation in NLS
MSCV-IRES-GFP-TCF4-R174X	nonsense mutation in NLS
MSCV-IRES-GFP-TCF4-216del	deletion
MSCV-IRES-GFP-TCF4-451del	deletion
MSCV-IRES-GFP-TCF4-V613F	missense mutation in bHLH domain

7.2.2 Cell culture

Two types of cell cultures were used for this project. First of all, a primary cell culture established from cerebellar granule neuron precursors of mice was used for the examination of *Tcf4* knockouts *in vitro*. Two immortalised cell lines, HEK 293T and DAOY cells, were also used during the experiments. Whereas HEK cells were only used for purposes of producing and testing retroviral particels, DAOY cells were needed to investigate effects of TCF4 in an MB cell line *in vitro*. All cell lines were adherent, i.e. growing in monolayers.

7.2.2.1 Cerebellar Granule Neuron Precursor Culture

To investigate the influence of a *Tcf4* loss on cell growth in cerebella of mice *in vitro*, cell growth in *Tcf4*-deficient cerebellar granule neuron precursor cell cultures was examined. For preparation of CGNP cultures, a 24-well culture plate was first plated with poly-L-ornithine (PLO). Therefore, 12 ml phosphate buffered saline (PBS) were mixed with 100× stock of 1.5 mg/ml PLO in ddH_2O and 500 μl PLO were added to each well. Plates were stored at 4 °C overnight. Several media were needed for the CGNP cultures and were prepared as follows: Hanks buffered saline solution (HBSS) was adjusted to a pH of 7.4 and 6 mg/l glucose was added. The solution was sterile filtered with a 0.2 μM filter and aliquots of 50 ml were stored at 4 °C. A lysis buffer (papain/EDTA/Leibovitz) was prepared by adding 20 μl papain and 5 μl EDTA to 2 ml Leibovitz medium.
For the culture medium, 50 ml DMEM-F12 were mixed with 500 μl of N2 supplement (100× stock), 500 μl of 1x penicillin/streptomycin solution and 5 μl of 2.5 M KCl for a final concentration of 0.25 mM KCl. A volume of 20 ml of the medium were transferred to another flask and 2 ml of foetal calf serum (FCS), which had been heat inactivated at 56 °C for 30 min previously, was added (total of 10 % FCS).

Cerebella of $Tcf4^{fl/fl}$ mice aged P5 to P7 were dissected in HBSS and stored in 15 ml centrifuge tubes in HBSS on ice until further use. Cerebella were centrifuged at 800 rpm for 5 min at 4 °C, the HBSS discarded and 1 ml of lysis buffer added, and the cerebella incubated for 10 min at 37 °C in a water bath. The papain in the lysis buffer was subsequently inactivated with 1 ml of the prepared culture medium containing FCS. Cerebella were centrifuged at 1,500 rpm for 5 min. The solutions was aspirated and replaced with 5 ml of HBSS/glucose. The cerebellar fragments were gently pipetted up and down to break up the pellet and spun again at 1,500 rpm for 5 min. After aspiration of the HBSS/glucose, the pellet was re-suspended in 1 ml HBSS/glucose, broken down and spun as before. The HBSS/glucose was discarded and 2 ml of culture medium with FCS were added to the cells. Then, the cells were counted in a Neubauer cell count chamber and the volume of the medium was adjusted to a total of 1 million cells per ml. In the meantime, the PLO plated 24-well plates were washed twice with 500 μl of PBS per well and subsequently 500 μl of the cell culture medium containing the cerebellar precursors were added to each well (total of 500,000 cells/well). Cell culture plates were stored in a CO_2 incubator at 37 °C, 5 % CO_2, and 95 % air humidity for 6-12 h. The cell culture medium was carefully removed and fresh culture medium with added SHH protein at a final concentration of 3 μg/ml SHH was added. The cells were cultured in this medium for 24 h. Sonic hedgehog protein causes all cells, except granule cells, to

leave the cell cycle during the 24 hours cultivation in this media, hence solely granule precursors will proliferate under these circumstances.

In a next step, the media containing SHH was taken off and 200 μl of media containing the viral particles - either sole *IRES-GFP* or *Cre-IRES-GFP* - was added and cells incubated for 4 h. These retroviral particles only infect cells undergoing proliferation, other than lentiviral particles which are able to infect all cells, which ensures that only granule cells were transduced. The *Cre-IRES-GFP* virus expresses the Cre recombinase to cut out *Tcf4* using the *loxP sites* (see Section 7.2.3.1) generating the *Tcf4* KO. Medium was then removed and fresh medium with SHH protein was added for another 24 h. Finally, 1.25 μl of BrdU (10 mg/ml) for a final concentration of 25 μg/ml was added to the medium for 2 h. Subsequently cells were fixed with 4 % PFA and stained for BrdU and GFP (see Immunofluorescence).

7.2.2.2 Immortalised cell lines

All cell lines were cultivated in DMEM supplemented with 10 % FCS, 1 % glutamax, 1 % penicillin/streptomycin, and 1 % HEPES and grown in a CO_2 incubator at 37 °C, 5 % CO_2, and 95 % air humidity. The general handling of the cell lines was as follows: Cryovials containing the frozen cells were taken from the nitrogen tank, where they were stored, and thawed quickly in a water bath at 37 °C. Cells were then washed in 7 ml pre-warmed cell culture medium by resuspending and subsequent centrifugation to remove DMSO (dimethyl sulfoxide). The washed cells were transferred to a T-25 cell culture flask containing 5 ml of pre-warmed medium. The flask was gently shaken in order to mix the cells equally in the medium and incubated as described above.

HEK293T cells Human embryonic kidney 293T cells (herein referred to as HEK cells) were first established in 1973 in Alex van der Eb's laboratory by transforming normal human embryonic kidney cells with adenovirus 5 DNA (Graham et al., 1977). HEK293T cells were received from the American Type Culture Collection (ATCC). HEK cells were grown in the cell culture medium described above. The cells were cultivated in T-75 cell culture flasks and spilt 1:10 every 3-4 days. HEK cells were used to produce retroviral particles for transduction of primary cell cultures and for testing of produced viruses as well as antibodies for immuno staining.

DAOY cells DAOY (ATCC HTB-186™) cells are an adherent cell line isolated from a desmoplastic cerebellar medulloblastoma of a 4 year old Caucasian male established in 1985 by P. F. Jacobsen of the Royal Perth Hospital in Western Australia (Jacobsen et al., 1985). At the time of characterisation, a genetic profile of the DAOY cell line was not available. However, *"the Daoy MB cell line is derived from a desmoplastic MB [and has since been shown] to exhibit global activation of SHH-pathway genes and is statistically classified as SHH subgroup based on hierarchical clustering and PCA [pincipal component analysis] with patient samples"* (Liang et al., 2015). Cells were cultivated in the cell culture medium described above and split three times a week. DAOY cells were used for testing the effects of reintroducing WT TCF4 and different TCF4 mutants into a SHH-associated medulloblastoma cell line.

7.2.3 Mouse experiments

All animal experiments were carried out in accordance with the Protection of Animal Act and were approved by the Regierung von Oberbayern. Mice were housed in a SPF-animal facility (specific-pathogen-free) in individually venitaled cages. The animal facility kept a day and night rhythm of 12 to 12 hours. Water and food was available *ad libitum*. For preparation of mice brains, adult mice were sacrificed via cervical dislocation, mice younger than 14 days of age were sacrificed through decapitation.

7.2.3.1 Mouse strains

All mouse strains are listed in Section 7.1.7. For the mouse experiments, different transgenic mouse strains were used; these were *SmoM2-YFP*$^{Fl/Fl}$ (Mao et al., 2006), *hGFAP-cre* (Zhuo et al., 2001), *Math1-cre* (Matei et al., 2005; Schüller et al., 2007), *Math1-creER*^{T2} (Machold and Fishell, 2005), and *Tcf4*$^{Fl/Fl}$ (Bergqvist et al., 2000). Additionally, the wild type strains *C57/Bl6* and *FVB* were used.

Conditional knockout mice An often used site-specific recombinase technology to carry out deletions, translocations, inversions etc., is the Cre-Lox recombination. The Cre recombinase is able to recombine DNA between specific sites, known as *loxP sites*, where the Cre recombinase binds and catalyzes recombination (Sauer, 1987; Sauer and Henderson, 1988). Transgenic mouse strains carrying *loxP sites* can be mated with Cre-driverline strains to create these conditional *Cre-loxP-systems*. Hence, the Cre recombinase can be expressed under different promoters (here *hGFAP* and *Math1*) and initiate recombination between the *loxP sites* in the DNA to cut out DNA sequences that lie within these sites. Using different promoters, knockouts in specific tissues and cell lines can be created.

Inducible knockout mice The oestrogen analogue tamoxifen can be used to induce knockouts in mice by binding to a modified oestrogen receptor at any given point in time. Transgenic mice carrying the genetic information for a fusion protein of the Cre recombinase and the oestrogen receptor are available (*creER*^{T2}). Although the fusion protein is expressed continuously in these mice, it is only able to enter the nucleus, which is necessary for the Cre recombinase to initiate recombination, after treatment with tamoxifen. The time point of tamoxifen injection then defines the initiation of the respective knockout. This fusion protein can be expressed under different promoters, additionally creating tissue-specific knockouts, e.g. *Math1-creER*^{T2} (Feil et al., 1997; Helms et al., 2000; Machold and Fishell, 2005).

7.2.3.2 Genotyping

For genoytping, mice tails from mice aged 3 days or ear dies from mice aged 21 days and older were used. The tissue was digested in 500 μl of Laird's lysis buffer and incubated for at least 2 hours at 56 °C on a shaker. Afterwards, samples were centrifuged at 16,100 g for 5 min and the supernatant was transferred to a new tube containing 500 μl of isopropanol. The tube with the suspension was shaken, causing the extracted DNA to precipitate. The sample was centrifuged once more at 16,100 g for 5 min, the supernatant discarded and the pellet dissolved in TE buffer and stored at 4 °C. The genomic DNA could then be used for genotyping. PCR was used to amplify specific regions of the DNA, distinguishing mutant and wild-type alleles.

All primer sequences used for PCR were taken from the original publications. Primers were ordered from and synthesized by Eurofins. They were delivered as a lyophilisate and had to be dissolved in ddH_2O according to manufacturer's specifications prior to use. Primers were stored at -20 °C. For daily use, primers were diluted 1:10 (final concentration of 10 μM) and stored at 4 °C. Primers and PCR cycling conditions are listed in Tables 6 and 7.

The PCR mastermix was prepared as follows: For 10 samples, 2.5 μl of each, forward and reverse, primer (concentration 10 μM) were mixed with 1.5 μl of 10 mM dNTPs, 20 μl of 5× PCR buffer, 1 μl of Taq polymerase, and 62.5 μl of PCR water. The solution was mixed and $MgCl_2$ was added accordingly (see Table 6). For each sample, 9 μl of PCR mix and 1 μl of the respective DNA were mixed. PCR was carried out depending on the gene of interest.

Table 6: Primers used for genotyping and conditions for PCR. Primers are given as fw (forward) and rv (reverse) primer in 5' - 3' direction. Noted are annealing temperature and additional reagents for each PCR.

PCR	Primer in 5' - 3'	Conditions
TCF4	fw TGTGTATGTGCATATTTCCTTTATATTCC rv AGATACCATGCGCAGAAATCTTT	annealing 60 °C
CRE	fw TCCGGGCTGCCACGACCAA rv GGCGCGGCAACACCATTTT	2 μl 25 mM $MgCl_2$ in 100 μl sample, annealing 65 °C
hGFAP	fw ACTCCTTCATAAAGCCCTCG rv ATCACTCGTTGCATCGACCG	annealing 65 °C
SMO MUT	fw GAACGGCATCAAGGTGAA rv CGATGGGGGTGTTCTGCT	annealing 60 °C
SMO WT	fw GGAGCGGGAGAAATGGATATG rv CGTGATCTGCAACTCCAGTC	2 μl 25 mM $MgCl_2$ in 100 μl sample, annealing 65 °C

Table 7: PCR thermal cycler programmes used for genotyping. Given are the different steps of each PCR according to annealing temperature and number of cycles.

	Annealing 60 °C 35 cycles	**Annealing 65 °C 32 cycles**
Heating-up	92 °C, 2 min	94 °C, 3 min
Denaturisation	92 °C, 30 s	94 °C, 30 s
Annealing	60 °C, 30 s	65 °C, 60 s
Elongation	72 °C, 60 s	72 °C, 60 s
Stop	4°C	4 °C

To verify PCR products, a gel electrophoresis was carried out. Products were loaded onto a 1 % or 2 % agarose gel (150 ml TE buffer with 3 g agarose for a 2 % gel and 1.5 g agarose for a 1 % gel were mixed and heated up in the microwave until transparent. 3 μl of SybrGold were added). The chamber was set to 70 V for 90 min. A UV transilluminator was used to visualize PCR products.

7.2.3.3 Mouse weights

To examine whether a prenatal knockout of *Tcf4* has effects on the growth of mice, whole body weights, brain weights, and cerebrum and cerebellar weights separately of *hGFAPcre::Tcf4*$^{fl/fl}$, *hGFAPcre::Tcf4*$^{fl/+}$, *hGFAPcre::Tcf4*$^{+/+}$ mice were determined and statistically analysed using t-tests. For whole body masses, mice were weighed every other day until their death. Brain weights were determined on days P7, 14, and 21.

7.2.3.4 Tamoxifen treatment

Tamoxifen inducible mouse models were used to investigate the influence of a postnatal *Tcf4* knockout in a tumorous and non-tumorous environment. Through the injection of tamoxifen in these transgenic mice, it is possible to activate the Cre recombinase postnatally (see Section 7.2.3.1). In this project, the tamoxifen inducible mouse model *Math1-creER*^{T2} was used, which makes it possible to specifically activate the Cre recombinase postnatally at any chosen point in solely *Math1*-positive cells. Mice were induced with tamoxifen on day 5 through intra-peritoneal injection of 0.1 mg tamoxifen dissolved in corn oil (25 μg per gramm body weight, i.e. 50 μl of 2 mg/ml solution).

7.2.3.5 BrdU pulse

For the investigation of proliferation rates of cerebellar granule cells *in vivo*, the different mouse models were pulsed with BrdU and sacrificed two hours later. Mice received 25 μg BrdU/g total body weight via an intra-peritoneal injection. BrdU is an analogue of the nucleotide thymidine and is thus integrated into the DNA strand of proliferating cells. Cells that incorporated BrdU, i.e. were proliferating during time of injection, could later be visualised through the staining for BrdU. Therefore, mouse brains were embedded in paraffin, stained for BrdU, and proliferation rates of the different layers of the cerebellum were analyzed.

7.2.3.6 Tumour models in mice

Tumour models were used to determine the influence of *Tcf4* knockouts on cell growth and survival rates in SHH-associated medulloblastoma. Two different mouse models, *hGFAP-cre::Tcf4*$^{Fl/Fl}$*SmoM2-YFP*$^{Fl/+}$ and *Math1-creER*^{T2}*Tcf4*$^{Fl/Fl}$*SmoM2-YFP*$^{Fl/+}$, were investigated. Mice were examined daily by the staff of the animal facility to check for symptoms and illness of mice. Mice were then either killed at a defined age for investigation of cell proliferation and apoptosis or sacrificed when symptoms became severe. These data were used for analysis of survival rates.

7.2.4 Histological methods

7.2.4.1 Embedded tissues

Preparation of tissues Tissues for staining with haematoxylin and eosin (H&E) and other immunostaining were firstly stored in formaldehyde and later prepared and incubated in 4 % PFA and PBS overnight and embedded in paraffin thereafter. The embedded tissue was cut using a microtome, slices were of 5 μm, and the tissue was fixed to microscope slides. Paraffin was washed out using xylole and tissues were rehydrated with a descending alcohol row. Tissues could then be stained. All pictures of embedded tissues were taken with an Olympus Bx50 microscope using the ColorView Soft imaging system (Olympus).

Immunohistochemistry General morphology of mice brains, specifically cerebella, were observed using H&E stains of the paraffin embedded and cut tissue sections. H&E staining was performed using standard protocols. The embedded slices were deparaffinated and rehydrated (xylole > 100 % ethanol > 95 % ethanol > 70 % ethanol > ddH_2O).
The slices were then cooked in citrate buffer (pH 6.0), five times for 4 min each, and cooled down for antigen retrieval. For inactivation of endogenous peroxidase, slices were washed in tab water and subsequently incubated in 5 % H_2O_2 in methanol (10 ml 30 % peroxide in 50 ml methanol) for 20 min. The slices were again washed in tab water (5 min), ddH_2O (shortly) and PBS (5 min) before the blocking reagent I-Block (Invitrogen) was added for 30 min. The primary antibody was added (dilution in PBS, see Table 8) over night at 4 °C. The next day, slices were washed with PBS twice (5 min each) and the slices were treated according to the System-HRP DAB-Kit protocol (Dako). Tissues were incubated in the SE reagent for 20 min, washed twice with PBS, incubated in poly-HRP for 30 min, washed with PBS and DAB (1 drop DAB in 1 ml DAB buffer) was added for 30 min. The slices were then washed twice with ddH_2O. In all the embedded tissues, nuclei were counterstained using haemalum. Slices were incubated for 2 min in haemalum and then directly blued in warm tab water for 10 min. In a last step, the slices were washed using the alcohol row vice versa and the tissues were covered with cover slips.

Table 8: Antibodies for immunohistochemistry (IHC) of embedded tissues. Given are the antibodies for IHC, their dilution factor used and the manufacturer for each antibody.

Antibody	Dilution	Manufacturer
anti-BrdU	1:500	Sigma
anti-CASP3	1:100	Cell Signaling Tech
anti-PAX6	1:50	DSHB
anti-PHH3	1:200	Cell Signaling Tech
anti-TCF4	1:25	Sigma

Analysis The H&E stains of mouse brains at different ages and with different genotypes were compared. The different mouse brains were also stained for PAX6 to investigate the formation of granule cells in the cerebella. Furthermore, stainings for CASP3 to compare apoptosis rates and for pHH3 to compare mitosis rates were carried out. As described above, mice received a BrdU pulse and hence, cell proliferation rates using BrdU staining were determined as well. For the different stainings, cell numbers in the different layers (EGL and IGL) were counted using ImageJ, compared between different age groups and genotypes and tested for significance using chi-squared tests.

7.2.4.2 Cell cultures

Immunofluorescence For staining of cell cultures, cells had to be fixated first. Therefore, the culture medium was aspirated and replaced with 300 μl of 4 % PFA for 30 min at room temperature on the shaker. Then, cells were washed twice with PBS for 5 min each, and washed again twice with PBS + 0.3 % Triton X-100 for 5 min each. The PBS solution was discarded and 300 μl of 4N HCl was added for 10 min at RT on the shaker. HCl was replaced with 300 μl of 0.1 M sodium borate buffer with a pH of 8.5 for 10 min. Sodium borate was aspirated and 200 μl of blocking buffer (PBS + 0.3 % Triton X-100 + 10 % Normal Goat Serum) were added and the 24-well plates were shaken at RT for 30 min. The blocking buffer was discarded and 200 μl of primary antibodies, for example anti-GFP and anti-BrdU, in blocking buffer were added and incubated at 4 °C overnight (see Table 9 for dilution). In a next step, primary antibodies were washed off with PBS + 0.3 % Triton X-100 three times and 200 μl of secondary antibodies, fluorophore-linked antibodies (Alexa 488 and Alexa 546) targeting the primary antibodies, in blocking buffer were added for 1 h at RT. Plates containing the cells had to be kept in darkness starting with this step, i.e. plates were wrapped in aluminium foil. After incubation with the

secondary antibodies, cells were washed twice with PBS + 0.3 % Triton X-100 and 500 μl of 4',6-diamidino-2-phenylindole (DAPI, 1:1000 diluted in PBS) for staining of nuclei was added for 10 min at RT. Subsequently, cells were washed with PBS once and kept in 300 μl of PBS thereafter. Fixated and stained cells were stored at 4 °C until analysis under the fluorescence microscope (Olympus IX50) using the ColorView Soft imaging System.

Table 9: Antibodies for immunofluorescence (IF) of cell cultures and their respective dilutions. Noted are the antibodies and their dilutions for IF, including manufacturer's name. The antibodies are given as pairs as used in the IF of tissue cultures.

Antibody	Dilution	Manufacturer
anti-GFP (rabbit)	1:200	Santa Cruz
anti-BrdU (mouse)	1:500	Sigma
anti-TCF4 (rabbit)	1:500	Sigma
anti-GFP (mouse)	1:200	Invitrogen
anti-mouse (secondary)	1:500	Invitrogen
anti-rabbit (secondary)	1:500	Invitrogen

Analysis For the analysis of GCNP cultures, the fixated cells were stained for GFP to determine cells that contained the *Cre-IRES-GFP* and the *IRES-GFP* plasmids respectively; for BrdU, to see which cells were actively growing, and for DAPI to mark cells. Cells were analyzed under a fluorescence microscope. Several hundred cells from different fields of vision in five different experiments (n=5) were counted and the numbers of *IRES-GFP* and *Cre-IRES-GFP* positive cells from all $BrdU^+$ cells were compared.

Analysis of DAOY cell cultures was done similarly. Cells were either stained for GFP and TCF4 to determine if transduced cells were producing a functioning TCF4 protein. Additionally, cells were stained for GFP and BrdU to determine which of the transduced cells were actively proliferating. $GFP^+/BrdU^+$ double-positive cells were counted and the fraction of $BrdU^+$ cells of all transduced cells was calculated and compared to the growth rates of untreated cells.

7.2.5 Human data

For the mRNA expression profiles of human medulloblastoma, the open access database R2 (R2: microarray analysis and visualization platform, http://r2.amc.nl) was searched. A total of 464 samples of medulloblastoma, with 122 being SHH-associated medullo-

blastoma were available. For 103 of these patients, not only expression profiles but also survival data could be extracted. Since the data was made available by different research groups, having used different sequencing technology, the data had to be normalised before use. To unify gene expression measures, data from each batch were normalised (standardised) and summarised separately resulting in gene expression estimates for each sample and gene. Relative gene expression values were calculated using z-scores. Normalisation was done by Dr. Julia Neumann.

In collaboration with the German Cancer Research Centre, a group of 133 samples with secured pathological activation of the Sonic hedgehog signalling pathway was sequenced and somatic mutations in TCF4 could be found in 14 % of cases (7/50) with adult SHH-associated medulloblastoma (see Appendix Fig. 28, Kool et al., 2014).

7.2.6 Statistical analysis

All statistical analysis was carried out using the Prism 5.02 and Prism 7.01 software (GraphPad). For the comparison of different groups (e.g. weights), all samples were tested for Gaussian distribution first. In case of normal distribution, the groups were compared using unpaired, two-tailed (Student's) t-tests. If no Gaussian distribution was found, a Mann-Whitney-U test was performed. Furthermore, chi-squared tests, a qualitative test, were used to compare cell counts between different groups. For data of patient and animal survival, Kaplan-Meier plots were drawn. Significance was calculated using a logrank test. The level of significance for all statistical analysis was set to 5 % ($p<0.05$). Standard deviation and mean were calculated for all data and plotted where suitable. For all analysis, at least three samples/biological replicates (n=3) were used.

8 Bibliography

Amiel, J., M. Rio, L. de Pontual, R. Redon, V. Malan, N. Boddaert, P. Plouin, N. P. Carter, S. Lyonnet, A. Munnich, and L. Colleaux
2007. Mutations in TCF4, encoding a class I basic helix-loop-helix transcription factor, are responsible for Pitt-Hopkins syndrome, a severe epileptic encephalopathy associated with autonomic dysfunction. *American journal of human genetics*, 80(5):988–993.

Appaiah, H., P. Bhat-Nakshatri, R. Mehta, M. Thorat, S. Badve, and H. Nakshatri
2014. ITF2 is a target of CXCR4 in MDA-MB-231 breast cancer cells and is associated with reduced survival in estrogen receptor-negative breast cancer. *Cancer Biology & Therapy*, 10(6):600–614.

Aquino, A., M. Perini, S. Cosmai, S. Zanon, V. Pisa, C. Castagna, and S. Uberti
2017. Osteopathic Manipulative Treatment Limits Chronic Constipation in a Child with Pitt-Hopkins Syndrome. *Case reports in pediatrics*, 2017:5437830.

Aumüller, G. and L. J. Wurzinger
2010. *Anatomie: 208 Tabellen*, Duale Reihe, 2. überarb. aufl. edition. Stuttgart: Thieme.

Baratz, K. H., N. Tosakulwong, E. Ryu, W. L. Brown, K. Branham, W. Chen, K. D. Tran, K. E. Schmid-Kubista, J. R. Heckenlively, A. Swaroop, G. Abecasis, K. R. Bailey, and A. O. Edwards
2010. E2-2 protein and Fuchs's corneal dystrophy. *NEJM*, 363(11):1016–1024.

Beauchamp, E. M., L. Ringer, G. Bulut, K. P. Sajwan, M. D. Hall, Y.-C. Lee, D. Peaceman, M. Ozdemirli, O. Rodriguez, T. J. MacDonald, C. Albanese, J. A. Toretsky, and A. Uren
2011. Arsenic trioxide inhibits human cancer cell growth and tumor development in mice by blocking Hedgehog/GLI pathway. *The Journal of clinical investigation*, 121(1):148–160.

Behesti, H. and S. Marino
2009. Cerebellar granule cells: insights into proliferation, differentiation, and role in medulloblastoma pathogenesis. *The international journal of biochemistry & cell biology*, 41(3):435–445.

Bénard, M., A. Lebon, H. Komuro, D. Vaudry, and L. Galas
2015. Ex Vivo Imaging of Postnatal Cerebellar Granule Cell Migration Using Confocal Macroscopy. *JoVE*, (99):e52810–e52810.

Bergqvist, I., M. Eriksson, J. Saarikettu, B. Eriksson, B. Corneliussen, T. Grundström, and D. Holmberg
2000. The basic helix-loop-helix transcription factor E2-2 is involved in T lymphocyte development. *European Journal of Immunology*, 30(10):2857–2863.

Bertola, L. D., E. B. Ott, S. Griepsma, F. J. Vonk, and C. P. Bagowski
2008. Developmental expression of the alpha-skeletal actin gene. *BMC evolutionary biology*, 8:166.

Brandl, L., D. Horst, E. de Toni, T. Kirchner, A. Herbst, and F. T. Kolligs
2015. ITF-2B protein levels are correlated with favorable prognosis in patients with colorectal carcinomas. *American journal of cancer research*, 5(7):2241–2248.

Brockschmidt, A., A. Filippi, I. P. Charbel, M. Nelles, H. Urbach, N. Eter, W. Driever, and R. G. Weber
2011. Neurologic and ocular phenotype in Pitt-Hopkins syndrome and a zebrafish model. *Human genetics*, 130(5):645–655.

Brzozka, M. M., K. Radyushkin, S. P. Wichert, H. Ehrenreich, and M. J. Rossner
2010. Cognitive and sensorimotor gating impairments in transgenic mice overexpressing the schizophrenia susceptibility gene Tcf4 in the brain. *Biological psychiatry*, 68(1):33–40.

Butts, T., M. J. Green, and R. J. T. Wingate
2014. Development of the cerebellum: simple steps to make a 'little brain'. *Development*, 141(21):4031–4041.

Casey, A. F., V. Pickard, C. Ullrich, and Z. MacNeil
2017. An adapted walking intervention for a child with Pitt Hopkins syndrome. *Disability and rehabilitation. Assistive technology*, Pp. 1–9.

Chen, T., Q. Wu, Y. Zhang, T. Lu, W. Yue, and D. Zhang
2016. Tcf4 Controls Neuronal Migration of the Cerebral Cortex through Regulation of Bmp7. *Frontiers in molecular neuroscience*, 9:94.

Cheng, L., Z. Jin, L. Liu, Y. Yan, T. Li, X. Zhu, and N. Jing
2004. Characterization and promoter analysis of the mouse nestin gene. *FEBS Letters*, 565(1-3):195–202.

Choudhry, Z., A. A. Rikani, A. M. Choudhry, S. Tariq, F. Zakaria, M. W. Asghar, M. K. Sarfraz, K. Haider, A. A. Shafiq, and N. J. Mobassarah
2014. Sonic hedgehog signalling pathway: a complex network. *Annals of neurosciences*, 21(1):28–31.

Chung, S.-H., C.-T. Kim, Y.-H. Jung, N.-S. Lee, and Y.-G. Jeong
2010. Early cerebellar granule cell migration in the mouse embryonic development. *Anatomy & cell biology*, 43(1):86–95.

Cisse, B., M. L. Caton, M. Lehner, T. Maeda, S. Scheu, R. Locksley, D. Holmberg, C. Zweier, H. N. S. den, S. G. Kant, W. Holter, A. Rauch, Y. Zhuang, and B. Reizis
2008. Transcription factor E2-2 is an essential and specific regulator of plasmacytoid dendritic cell development. *Cell*, 135(1):37–48.

Counsell, J. R., R. Karda, J. A. Diaz, L. Carey, T. Wiktorowicz, S. M. Buckley, S. Ameri, J. Ng, J. Baruteau, F. Almeida, R. d. Silva, R. Simone, E. Lugarà, G. Lignani, D. Lindemann, A. Rethwilm, A. A. Rahim, S. N. Waddington, and S. J. Howe
2018. Foamy Virus Vectors Transduce Visceral Organs and Hippocampal Structures following In Vivo Delivery to Neonatal Mice. *Molecular Therapy - Nucleic Acids*, 12:626–634.

de Garibay, G. R., F. Mateo, A. Stradella, R. Valdés-Mas, L. Palomero, J. Serra-Musach, D. A. Puente, A. Díaz-Navarro, G. Vargas-Parra, E. Tornero, I. Morilla, L. Farré, M. Martinez-Iniesta, C. Herranz, E. McCormack, A. Vidal, A. Petit, T. Soler, C. Lázaro, X. S. Puente, A. Villanueva, and M. A. Pujana
2018. Tumor xenograft modeling identifies TCF4/ITF2 loss associated with breast cancer chemoresistance. *Disease models & mechanisms*.

de Pontual, L., Y. Mathieu, C. Golzio, M. Rio, V. Malan, N. Boddaert, C. Soufflet, C. Picard, A. Durandy, A. Dobbie, D. Heron, B. Isidor, J. Motte, R. Newburry-Ecob, L. Pasquier, M. Tardieu, G. Viot, F. Jaubert, A. Munnich, L. Colleaux, M. Vekemans,

H. Etchevers, S. Lyonnet, and J. Amiel
2009. Mutational, functional, and expression studies of the TCF4 gene in Pitt-Hopkins syndrome. *Human mutation*, 30(4):669–676.

de Winter, C. F., M. Baas, E. K. Bijlsma, J. van Heukelingen, S. Routledge, and R. C. M. Hennekam
2016. Phenotype and natural history in 101 individuals with pitt-hopkins syndrome through an internet questionnaire system. *Orphanet journal of rare diseases*, 11:37.

Dufour, C., A. Beaugrand, B. Pizer, J. Micheli, M.-S. Aubelle, A. Fourcade, D. Couanet, A. Laplanche, C. Kalifa, and J. Grill
2012. Metastatic Medulloblastoma in Childhood: Chang's Classification Revisited. *International journal of surgical oncology*, 2012:245385.

Dutta, S. and P. Sengupta
2016. Men and mice: Relating their ages. *Life sciences*, 152:244–248.

Echelard, Y., D. J. Epstein, B. St-Jacques, L. Shen, J. Mohler, J. A. McMahon, and A. P. McMahon
1993. Sonic hedgehog, a member of a family of putative signaling molecules, is implicated in the regulation of CNS polarity. *Cell*, 75(7):1417–1430.

Edmondson, J. C. and M. E. Hatten
1987. Glial-guided granule neuron migration in vitro: a high-resolution time-lapse video microscopic study. *The Journal of neuroscience*, 7(6):1928–1934.

Ellison, D. W., M. Kocak, J. Dalton, H. Megahed, M. E. Lusher, S. L. Ryan, W. Zhao, S. L. Nicholson, R. E. Taylor, S. Bailey, and S. C. Clifford
2011. Definition of disease-risk stratification groups in childhood medulloblastoma using combined clinical, pathologic, and molecular variables. *Journal of clinical oncology*, 29(11):1400–1407.

Ericson, J., J. Briscoe, P. Rashbass, V. van Heyningen, and T. M. Jessell
1997. Graded sonic hedgehog signaling and the specification of cell fate in the ventral neural tube. *Cold Spring Harbor symposia on quantitative biology*, 62:451–466.

Feil, R., J. Wagner, D. Metzger, and P. Chambon
1997. Regulation of Cre recombinase activity by mutated estrogen receptor ligand-binding domains. *Biochemical and biophysical research communications*, 237(3):752–757.

Flora, A., J. J. Garcia, C. Thaller, and H. Y. Zoghbi
2007. The E-protein Tcf4 interacts with Math1 to regulate differentiation of a specific subset of neuronal progenitors. *PNAS*, 104(39):15382–15387.

Forrest, M., R. M. Chapman, Am Doyle, C. L. Tinsley, A. Waite, and D. J. Blake
2012. Functional analysis of TCF4 missense mutations that cause Pitt-Hopkins syndrome. *Human mutation*, 33(12):1676–1686.

Forrest, M. P., M. J. Hill, D. H. Kavanagh, K. E. Tansey, A. J. Waite, and D. J. Blake
2017. The Psychiatric Risk Gene Transcription Factor 4 (TCF4) Regulates Neurodevelopmental Pathways Associated With Schizophrenia, Autism, and Intellectual Disability. *Schizophrenia bulletin*.

Forrest, M. P., M. J. Hill, A. J. Quantock, E. Martin-Rendon, and D. J. Blake
2014. The emerging roles of TCF4 in disease and development. *Trends in molecular medicine*, 20(6):322–331.

Furumura, M., S. B. Potterf, K. Toyofuku, J. Matsunaga, J. Muller, and V. J. Hearing
2001. Involvement of ITF2 in the transcriptional regulation of melanogenic genes. *The Journal of biological chemistry*, 276(30):28147–28154.

Gaffney, C. and P. McNally
2015. Successful use of acetazolamide for central apnea in a child with Pitt-Hopkins syndrome. *American journal of medical genetics. Part A*, 167(6):1423.

Gajjar, A., M. Chintagumpala, D. Ashley, S. Kellie, L. E. Kun, T. E. Merchant, S. Woo, G. Wheeler, V. Ahern, M. J. Krasin, M. Fouladi, A. Broniscer, R. Krance, G. A. Hale, C. F. Stewart, R. Dauser, R. A. Sanford, C. Fuller, C. Lau, J. M. Boyett, D. Wallace, and R. J. Gilbertson
2006. Risk-adapted craniospinal radiotherapy followed by high-dose chemotherapy and stem-cell rescue in children with newly diagnosed medulloblastoma (St Jude Medulloblastoma-96): Long-term results from a prospective, multicentre trial. *The Lancet Oncology*, 7(10):813–820.

Galas, L., M. Bénard, A. Lebon, Y. Komuro, D. Schapman, H. Vaudry, D. Vaudry, and H. Komuro
2017. Postnatal Migration of Cerebellar Interneurons. *Brain sciences*, 7(6).

Gibson, P., Y. Tong, G. Robinson, M. C. Thompson, D. S. Currle, C. Eden, T. A. Kranenburg, T. Hogg, H. Poppleton, J. Martin, D. Finkelstein, S. Pounds, A. Weiss, Z. Patay, M. Scoggins, R. Ogg, Y. Pei, Z.-J. Yang, S. Brun, Y. Lee, F. Zindy, J. C. Lindsey,

M. M. Taketo, F. A. Boop, R. A. Sanford, A. Gajjar, S. C. Clifford, M. F. Roussel, P. J. McKinnon, D. H. Gutmann, D. W. Ellison, R. Wechsler-Reya, and R. J. Gilbertson
2010. Subtypes of medulloblastoma have distinct developmental origins. *Nature*, 468(7327):1095–1099.

Gilbertson, R. J. and D. W. Ellison
2008. The origins of medulloblastoma subtypes. *Annual review of pathology*, 3:341–365.

Gilthorpe, J. D., E.-K. Papantoniou, A. Chédotal, A. Lumsden, and R. J. T. Wingate
2002. The migration of cerebellar rhombic lip derivatives. *Development*, 129(20):4719–4728.

Giordana, M. T., P. Schiffer, M. Lanotte, P. Girardi, and A. Chio
1999. Epidemiology of adult medulloblastoma. *International journal of cancer*, 80(5):689–692.

Graham, F. L., J. Smiley, W. C. Russell, and R. Nairn
1977. Characteristics of a human cell line transformed by DNA from human adenovirus type 5. *The Journal of general virology*, 36(1):59–74.

Grammel, D., M. Warmuth-Metz, A. O. von Bueren, M. Kool, T. Pietsch, H. A. Kretzschmar, D. H. Rowitch, S. Rutkowski, S. M. Pfister, and U. Schüller
2012. Sonic hedgehog-associated medulloblastoma arising from the cochlear nuclei of the brainstem. *Acta neuropathologica*, 123(4):601–614.

Grubišić, V., A. J. Kennedy, J. D. Sweatt, and V. Parpura
2015. Pitt-Hopkins Mouse Model has Altered Particular Gastrointestinal Transits In Vivo. *Autism research*, 8(5):629–633.

Harrington, H. A., K. L. Ho, S. Ghosh, and K. C. Tung
2008. Construction and analysis of a modular model of caspase activation in apoptosis. *Theoretical biology & medical modelling*, 5:26.

Hasi, M., B. Soileau, C. Sebold, A. Hill, D. E. Hale, L. O'Donnell, and J. D. Cody
2011. The role of the TCF4 gene in the phenotype of individuals with 18q segmental deletions. *Human genetics*, 130(6):777–787.

Hatten, M. E. and N. Heintz
1995. Mechanisms of neural patterning and specification in the developing cerebellum. *Annual review of neuroscience*, 18:385–408.

Hatten, M. E. and M. F. Roussel
2011. Development and cancer of the cerebellum. *Trends in neurosciences*, 34(3):134–142.

Heckman, K. L. and L. R. Pease
2007. Gene splicing and mutagenesis by PCR-driven overlap extension. *Nature protocols*, 2(4):924–932.

Helms, A. W., A. L. Abney, N. Ben-Arie, H. Y. Zoghbi, and J. E. Johnson
2000. Autoregulation and multiple enhancers control Math1 expression in the developing nervous system. *Development (Cambridge, England)*, 127(6):1185–1196.

Herbst, A., G. T. Bommer, L. Kriegl, A. Jung, A. Behrens, E. Csanadi, M. Gerhard, C. Bolz, R. Riesenberg, W. Zimmermann, W. Dietmaier, I. Wolf, T. Brabletz, B. Goke, and F. T. Kolligs
2009a. ITF-2 is disrupted via allelic loss of chromosome 18q21, and ITF-2B expression is lost at the adenoma-carcinoma transition. *Gastroenterology*, 137(2):639–48, 648.e1–9.

Herbst, A., S. Helferich, A. Behrens, B. Goke, and F. T. Kolligs
2009b. The transcription factor ITF-2A induces cell cycle arrest via p21(Cip1). *Biochemical and biophysical research communications*, 387(4):736–740.

HGNC
2018. HGNC database of human gene names — HUGO Gene Nomenclature Committee. http://www.genenames.org/. Last accessed: 04/08/2018.

Ingham, P. W., Y. Nakano, and C. Seger
2011. Mechanisms and functions of Hedgehog signalling across the metazoa. *Nature reviews. Genetics*, 12(6):393–406.

Ivanov, D. P., B. Coyle, D. A. Walker, and A. M. Grabowska
2016. In vitro models of medulloblastoma: Choosing the right tool for the job. *Journal of biotechnology*, 236:10–25.

Jacobsen, P. F., D. J. Jenkyn, and J. M. Papadimitriou
1985. Establishment of a human medulloblastoma cell line and its heterotransplantation into nude mice. *Journal of neuropathology and experimental neurology*, 44(5):472–485.

Jessell, T. M.
2000. Neuronal specification in the spinal cord: inductive signals and transcriptional codes. *Nature reviews. Genetics*, 1(1):20–29.

Jia, J., A. Kolterud, H. Zeng, A. Hoover, S. Teglund, R. Toftgård, and A. Liu
2009. Suppressor of Fused inhibits mammalian Hedgehog signaling in the absence of cilia. *Developmental biology*, 330(2):452–460.

Jung, M., B. M. Häberle, T. Tschaikowsky, M.-T. Wittmann, E.-A. Balta, V.-C. Stadler, C. Zweier, A. Dörfler, C. J. Gloeckner, and D. C. Lie
2018. Analysis of the expression pattern of the schizophrenia-risk and intellectual disability gene TCF4 in the developing and adult brain suggests a role in development and plasticity of cortical and hippocampal neurons. *Molecular autism*, 9:20.

Kalscheuer, V. M., I. Feenstra, C. M. A. van Ravenswaaij-Arts, D. F. C. M. Smeets, C. Menzel, R. Ullmann, L. Musante, and H.-H. Ropers
2008. Disruption of the TCF4 gene in a girl with mental retardation but without the classical Pitt-Hopkins syndrome. *American journal of medical genetics. Part A*, 146A(16):2053–2059.

Kennedy, A. J., E. J. Rahn, B. S. Paulukaitis, K. E. Savell, H. B. Kordasiewicz, J. Wang, J. W. Lewis, J. Posey, S. K. Strange, M. C. Guzman-Karlsson, S. E. Phillips, K. Decker, S. T. Motley, E. E. Swayze, D. J. Ecker, T. P. Michael, J. J. Day, and J. D. Sweatt
2016. Tcf4 Regulates Synaptic Plasticity, DNA Methylation, and Memory Function. *Cell reports*, 16(10):2666–2685.

Kharbanda, M., K. Kannike, A. Lampe, J. Berg, T. Timmusk, and M. Sepp
2016. Partial deletion of TCF4 in three generation family with non-syndromic intellectual disability, without features of Pitt-Hopkins syndrome. *European journal of medical genetics*, 59(6-7):310–314.

Kim, S. K., H. R. Jang, J. H. Kim, M. Kim, S. M. Noh, K. S. Song, G. H. Kang, H. J. Kim, S. Y. Kim, H. S. Yoo, and Y. S. Kim
2008. CpG methylation in exon 1 of transcription factor 4 increases with age in normal gastric mucosa and is associated with gene silencing in intestinal-type gastric cancers. *Carcinogenesis*, 29(8):1623–1631.

Kolligs, F. T., M. T. Nieman, I. Winer, G. Hu, D. van Mater, Y. Feng, Im Smith, R. Wu, Y. Zhai, K. R. Cho, and E. R. Fearon
2002. ITF-2, a downstream target of the Wnt/TCF pathway, is activated in human cancers with beta-catenin defects and promotes neoplastic transformation. *Cancer cell*, 1(2):145–155.

Komuro, Y., J. K. Fahrion, K. D. Foote, K. B. Fenner, T. Kumada, N. Ohno, and H. Komuro
2013. Granule Cell Migration and Differentiation. In *Handbook of the cerebellum and cerebellar disorders*, M.-U. Manto, D. L. Gruol, J. D. Schmahmann, N. Koibuchi, and F. Rossi, eds., Springer reference, Pp. 107–125. New York: Springer.

Kool, M., D. T. W. Jones, N. Jäger, P. A. Northcott, T. J. Pugh, V. Hovestadt, R. M. Piro, L. A. Esparza, S. L. Markant, M. Remke, T. Milde, F. Bourdeaut, M. Ryzhova, D. Sturm, E. Pfaff, S. Stark, S. Hutter, H. Seker-Cin, P. Johann, S. Bender, C. Schmidt, T. Rausch, D. Shih, J. Reimand, L. Sieber, A. Wittmann, L. Linke, H. Witt, U. D. Weber, M. Zapatka, R. König, R. Beroukhim, G. Bergthold, P. van Sluis, R. Volckmann, J. Koster, R. Versteeg, S. Schmidt, S. Wolf, C. Lawerenz, C. C. Bartholomae, C. von Kalle, A. Unterberg, C. Herold-Mende, S. Hofer, A. E. Kulozik, A. von Deimling, W. Scheurlen, J. Felsberg, G. Reifenberger, M. Hasselblatt, J. R. Crawford, G. A. Grant, N. Jabado, A. Perry, C. Cowdrey, S. Croul, G. Zadeh, J. O. Korbel, F. Doz, O. Delattre, G. D. Bader, M. G. McCabe, V. P. Collins, M. W. Kieran, Y.-J. Cho, S. L. Pomeroy, O. Witt, B. Brors, M. D. Taylor, U. Schüller, A. Korshunov, R. Eils, R. J. Wechsler-Reya, P. Lichter, and S. M. Pfister
2014. Genome sequencing of SHH medulloblastoma predicts genotype-related response to smoothened inhibition. *Cancer cell*, 25(3):393–405.

Kool, M., A. Korshunov, M. Remke, D. T. W. Jones, M. Schlanstein, P. A. Northcott, Y.-J. Cho, J. Koster, A. Schouten-van Meeteren, D. van Vuurden, S. C. Clifford, T. Pietsch, A. O. von Bueren, S. Rutkowski, M. McCabe, V. P. Collins, M. L. Bäcklund, C. Haberler, F. Bourdeaut, O. Delattre, F. Doz, D. W. Ellison, R. J. Gilbertson, S. L. Pomeroy, M. D. Taylor, P. Lichter, and S. M. Pfister
2012. Molecular subgroups of medulloblastoma: an international meta-analysis of transcriptome, genetic aberrations, and clinical data of WNT, SHH, Group 3, and Group 4 medulloblastomas. *Acta neuropathologica*, 123(4):473–484.

Kool, M., J. Koster, J. Bunt, N. E. Hasselt, A. Lakeman, P. van Sluis, D. Troost, N. S.-v. Meeteren, H. N. Caron, J. Cloos, A. Mrsić, B. Ylstra, W. Grajkowska, W. Hartmann, T. Pietsch, D. Ellison, S. C. Clifford, and R. Versteeg
2008. Integrated genomics identifies five medulloblastoma subtypes with distinct genetic profiles, pathway signatures and clinicopathological features. *PloS one*, 3(8):e3088.

Kousoulidou, L., G. Tanteles, M. Moutafi, C. Sismani, P. C. Patsalis, and V. Anastasiadou
2013. 263.4 kb deletion within the TCF4 gene consistent with Pitt-Hopkins syndrome,

inherited from a mosaic parent with normal phenotype. *European journal of medical genetics*, 56(6):314–318.

Landsberg, R. L., R. B. Awatramani, N. L. Hunter, A. F. Farago, H. J. DiPietrantonio, C. I. Rodriguez, and S. M. Dymecki
2005. Hindbrain rhombic lip is comprised of discrete progenitor cell populations allocated by Pax6. *Neuron*, 48(6):933–947.

Lee, M. J., B. A. Hatton, E. H. Villavicencio, P. C. Khanna, S. D. Friedman, S. Ditzler, B. Pullar, K. Robison, K. F. White, C. Tunkey, M. LeBlanc, J. Randolph-Habecker, S. E. Knoblaugh, S. Hansen, A. Richards, B. J. Wainwright, K. McGovern, and J. M. Olson
2012. Hedgehog pathway inhibitor saridegib (IPI-926) increases lifespan in a mouse medulloblastoma model. *PNAS*, 109(20):7859–7864.

Li, Y.-J., M. A. Minear, J. Rimmler, B. Zhao, E. Balajonda, M. A. Hauser, R. R. Allingham, A. O. Eghrari, S. A. Riazuddin, N. Katsanis, J. D. Gottsch, S. G. Gregory, G. K. Klintworth, and N. A. Afshari
2011. Replication of TCF4 through association and linkage studies in late-onset Fuchs endothelial corneal dystrophy. *PloS one*, 6(4):e18044.

Liang, L., C. Aiken, R. McClelland, L. C. Morrison, N. Tatari, M. Remke, V. Ramaswamy, M. Issaivanan, T. Ryken, M. R. Del Bigio, M. D. Taylor, and T. E. Werbowetski-Ogilvie
2015. Characterization of novel biomarkers in selecting for subtype specific medulloblastoma phenotypes. *Oncotarget*, 6(36):38881–38900.

Louis, D. N., H. Ohgaki, O. D. Wiestler, and W. K. Cavenee, eds.
2016a. *WHO classification of tumours of the central nervous system*, World Health Organization classification of tumours, revised 4th edition edition. Lyon: International Agency for Research on Cancer.

Louis, D. N., A. Perry, G. Reifenberger, A. von Deimling, D. Figarella-Branger, W. K. Cavenee, H. Ohgaki, O. D. Wiestler, P. Kleihues, and D. W. Ellison
2016b. The 2016 World Health Organization Classification of Tumors of the Central Nervous System: a summary. *Acta neuropathologica*, 131(6):803–820.

MacDonald, T. J.
2008. Aggressive infantile embryonal tumors. *Journal of child neurology*, 23(10):1195–1204.

Machold, R. and G. Fishell
2005. Math1 is expressed in temporally discrete pools of cerebellar rhombic-lip neural progenitors. *Neuron*, 48(1):17–24.

Mao, J., K. L. Ligon, E. Y. Rakhlin, S. P. Thayer, R. T. Bronson, D. Rowitch, and A. P. McMahon
2006. A novel somatic mouse model to survey tumorigenic potential applied to the Hedgehog pathway. *Cancer research*, 66(20):10171–10178.

Marangi, G., S. Ricciardi, D. Orteschi, S. Lattante, M. Murdolo, B. Dallapiccola, C. Biscione, R. Lecce, P. Chiurazzi, C. Romano, D. Greco, R. Pettinato, G. Sorge, C. Pantaleoni, E. Alfei, I. Toldo, C. Magnani, P. Bonanni, F. Martinez, G. Serra, D. Battaglia, D. Lettori, G. Vasco, A. Baroncini, C. Daolio, and M. Zollino
2011. The Pitt-Hopkins syndrome: report of 16 new patients and clinical diagnostic criteria. *American journal of medical genetics. Part A*, 155A(7):1536–1545.

Marangi, G. and M. Zollino
2015. Pitt-Hopkins Syndrome and Differential Diagnosis: A Molecular and Clinical Challenge. *Journal of pediatric genetics*, 4(3):168–176.

Marigo, V., D. J. Roberts, S. M. Lee, O. Tsukurov, T. Levi, J. M. Gastier, D. J. Epstein, D. J. Gilbert, N. G. Copeland, C. E. Seidman, N. A. Jenkins, J. G. Seidman, A. P. McMahon, and C. Tabin
1995. Cloning, Expression, and Chromosomal Location of SHH and IHH: Two Human Homologues of the Drosophila Segment Polarity Gene Hedgehog. *Genomics*, 28(1):44–51.

Mary, L., A. Piton, E. Schaefer, F. Mattioli, E. Nourisson, C. Feger, C. Redin, M. Barth, S. El Chehadeh, E. Colin, C. Coubes, L. Faivre, E. Flori, D. Geneviève, Y. Capri, L. Perrin, J. Fabre-Teste, D. Timbolschi, A. Verloes, R. Olaso, A. Boland, J.-F. Deleuze, J.-L. Mandel, B. Gerard, and I. Giurgea
2018. Disease-causing variants in TCF4 are a frequent cause of intellectual disability: Lessons from large-scale sequencing approaches in diagnosis. *EJHG*.

Massari, M. E., P. A. Grant, M. G. Pray-Grant, S. L. Berger, J. L. Workman, and C. Murre
1999. A Conserved Motif Present in a Class of Helix-Loop-Helix Proteins Activates Transcription by Direct Recruitment of the SAGA Complex. *Molecular Cell*, 4(1):63–73.

Matei, V., S. Pauley, S. Kaing, D. Rowitch, K. W. Beisel, K. Morris, F. Feng, K. Jones, J. Lee, and B. Fritzsch
2005. Smaller inner ear sensory epithelia in Neurog 1 null mice are related to earlier hair cell cycle exit. *Developmental dynamics*, 234(3):633–650.

Merk, D. J., J. Ohli, N. D. Merk, V. Thatikonda, S. Morrissy, M. Schoof, S. N. Schmid, L. Harrison, S. Filser, J. Ahlfeld, S. Erkek, K. Raithatha, T. Andreska, M. Weißhaar, M. Launspach, J. E. Neumann, M. Shakarami, D. Plenker, M. A. Marra, Y. Li, A. J. Mungall, R. A. Moore, Y. Ma, S. J. M. Jones, B. Lutz, B. Ertl-Wagner, A. Rossi, R. Wagener, R. Siebert, A. Jung, C. G. Eberhart, B. Lach, M. Sendtner, S. M. Pfister, M. D. Taylor, L. Chavez, M. Kool, and U. Schüller
2018. Opposing Effects of CREBBP Mutations Govern the Phenotype of Rubinstein-Taybi Syndrome and Adult SHH Medulloblastoma. *Developmental cell*, 44(6):709–724.e6.

MGI-Guidelines
2018. MGI-Guidelines for Nomenclature of Genes, Genetic Markers, Alleles, & Mutations in Mouse & Rat. http://www.informatics.jax.org/mgihome/nomen/gene.shtml. Last accessed: 04/08/2018.

Moen, M. J., H. H. H. Adams, J. H. Brandsma, D. H. W. Dekkers, U. Akinci, S. Karkampouna, M. Quevedo, C. E. M. Kockx, Z. Ozgür, W. F. J. van IJcken, J. Demmers, and R. A. Poot
2017. An interaction network of mental disorder proteins in neural stem cells. *Translational psychiatry*, 7(4):e1082.

Mologni, L., H. Dekhil, M. Ceccon, S. Purgante, C. Lan, L. Cleris, V. Magistroni, F. Formelli, and C. B. Gambacorti-Passerini
2010. Colorectal tumors are effectively eradicated by combined inhibition of beta-catenin, KRAS, and the oncogenic transcription factor ITF2. *Cancer research*, 70(18):7253–7263.

Morales, D. and M. E. Hatten
2006. Molecular markers of neuronal progenitors in the embryonic cerebellar anlage. *The Journal of neuroscience*, 26(47):12226–12236.

Müller, F. and R. O'Rahilly
1990. The human brain at stages 21–23, with particular reference to the cerebral cortical plate and to the development of the cerebellum. *Anatomy and Embryology*, 182(4):375–400.

Murre, C.
2005. Helix-loop-helix proteins and lymphocyte development. *Nature immunology*, 6(11):1079–1086.

Neumann, J. E., F. J. Swartling, and U. Schüller
2017. Medulloblastoma: experimental models and reality. *Acta neuropathologica*, 134(5):679–689.

Northcott, P. A., A. Korshunov, H. Witt, T. Hielscher, C. G. Eberhart, S. Mack, E. Bouffet, S. C. Clifford, C. E. Hawkins, P. French, J. T. Rutka, S. Pfister, and M. D. Taylor
2011. Medulloblastoma comprises four distinct molecular variants. *Journal of clinical oncology*, 29(11):1408–1414.

O'Donnell, L., B. Soileau, P. Heard, E. Carter, C. Sebold, J. Gelfond, D. E. Hale, and J. D. Cody
2010. Genetic determinants of autism in individuals with deletions of 18q. *Human genetics*, 128(2):155–164.

Ohli, J., J. E. Neumann, D. Grammel, and U. Schüller
2015. Localization of SHH medulloblastoma in mice depends on the age at its initiation. *Acta neuropathologica*, 130(2):307–309.

Peippo, M. and J. Ignatius
2011. Pitt-Hopkins Syndrome. *Molecular Syndromology*, (2):171–180.

Pitt, D. and I. Hopkins
1978. A syndrome of mental retardation, wide mouth and intermittent overbreathing. *Australian paediatric journal*, 14(3):182–184.

Polkinghorn, W. R. and N. J. Tarbell
2007. Medulloblastoma: tumorigenesis, current clinical paradigm, and efforts to improve risk stratification. *Nature clinical practice. Oncology*, 4(5):295–304.

Pöschl, J., S. Stark, P. Neumann, S. Gröbner, D. Kawauchi, D. T. W. Jones, P. A. Northcott, P. Lichter, S. M. Pfister, M. Kool, and U. Schüller
2014. Genomic and transcriptomic analyses match medulloblastoma mouse models to their human counterparts. *Acta neuropathologica*, 128(1):123–136.

Rannals, M. D., G. R. Hamersky, S. C. Page, M. N. Campbell, A. Briley, R. A. Gallo, B. N. Phan, T. M. Hyde, J. E. Kleinman, J. H. Shin, A. E. Jaffe, D. R. Weinberger,

and B. J. Maher
2016a. Psychiatric risk gene transcription factor 4 regulates intrinsic excitability of prefrontal neurons via repression of scn10a and kcnq1. *Neuron*, 90(1):43–55.

Rannals, M. D., S. C. Page, M. N. Campbell, R. A. Gallo, B. Mayfield, and B. J. Maher
2016b. Neurodevelopmental models of transcription factor 4 deficiency converge on a common ion channel as a potential therapeutic target for Pitt Hopkins syndrome. *Rare diseases*, 4(1):e1220468.

Rimkus, T. K., R. L. Carpenter, S. Qasem, M. Chan, and H.-W. Lo
2016. Targeting the Sonic Hedgehog Signaling Pathway: Review of Smoothened and GLI Inhibitors. *Cancers*, 8(2).

Romer, J. and T. Curran
2005. Targeting medulloblastoma: small-molecule inhibitors of the Sonic Hedgehog pathway as potential cancer therapeutics. *Cancer research*, 65(12):4975–4978.

Rosenfeld, J. A., K. Leppig, B. C. Ballif, H. Thiese, C. Erdie-Lalena, E. Bawle, S. Sastry, J. E. Spence, A. Bandholz, U. Surti, J. Zonana, K. Keller, W. Meschino, B. A. Bejjani, B. S. Torchia, and L. G. Shaffer
2009. Genotype-phenotype analysis of TCF4 mutations causing Pitt-Hopkins syndrome shows increased seizure activity with missense mutations. *Genetics in medicine*, 11(11):797–805.

Roussel, M. F. and M. E. Hatten
2011. Cerebellum development and medulloblastoma. *Current topics in developmental biology*, 94:235–282.

Rubin, L. L. and F. J. de Sauvage
2006. Targeting the Hedgehog pathway in cancer. *Nature reviews. Drug discovery*, 5(12):1026–1033.

Rutkowski, S., U. Bode, F. Deinlein, H. Ottensmeier, M. Warmuth-Metz, N. Soerensen, N. Graf, A. Emser, T. Pietsch, J. E. A. Wolff, R. D. Kortmann, and J. Kuehl
2005. Treatment of early childhood medulloblastoma by postoperative chemotherapy alone. *NEJM*, 352(10):978–986.

Sauer, B.
1987. Functional expression of the cre-lox site-specific recombination system in the yeast Saccharomyces cerevisiae. *Molecular and cellular biology*, 7(6):2087–2096.

Sauer, B. and N. Henderson

1988. Site-specific DNA recombination in mammalian cells by the Cre recombinase of bacteriophage P1. *PNAS*, 85(14):5166–5170.

Schmahmann, J. D. and D. Caplan

2006. Cognition, emotion and the cerebellum. *Brain*, 129(Pt 2):290–292.

Schnütgen, F., S. De-Zolt, P. van Sloun, M. Hollatz, T. Floss, J. Hansen, J. Altschmied, C. Seisenberger, N. B. Ghyselinck, P. Ruiz, P. Chambon, W. Wurst, and H. von Melchner

2005. Genomewide production of multipurpose alleles for the functional analysis of the mouse genome. *PNAS*, 102(20):7221–7226.

Schüller, U., V. M. Heine, J. Mao, A. T. Kho, A. K. Dillon, Y.-G. Han, E. Huillard, T. Sun, A. H. Ligon, Y. Qian, Q. Ma, A. Alvarez-Buylla, A. P. McMahon, D. H. Rowitch, and K. L. Ligon

2008. Acquisition of granule neuron precursor identity is a critical determinant of progenitor cell competence to form Shh-induced medulloblastoma. *Cancer cell*, 14(2):123–134.

Schüller, U., Q. Zhao, S. A. Godinho, V. M. Heine, R. H. Medema, D. Pellman, and D. H. Rowitch

2007. Forkhead transcription factor FoxM1 regulates mitotic entry and prevents spindle defects in cerebellar granule neuron precursors. *Molecular and cellular biology*, 27(23):8259–8270.

Sepp, M., K. Kannike, A. Eesmaa, M. Urb, and T. Timmusk

2011. Functional diversity of human basic helix-loop-helix transcription factor TCF4 isoforms generated by alternative 5' exon usage and splicing. *PloS one*, 6(7):e22138.

Sepp, M., P. Pruunsild, and T. Timmusk

2012. Pitt-Hopkins syndrome-associated mutations in TCF4 lead to variable impairment of the transcription factor function ranging from hypomorphic to dominant-negative effects. *Human Molecular Genetics*, 21(13):2873–2888.

Shepherd, G. M., ed.

2004. *The synaptic organization of the brain*, 5th ed. edition. Oxford and New York: Oxford University Press.

Skarnes, W. C., B. Rosen, A. P. West, M. Koutsourakis, W. Bushell, V. Iyer, A. O. Mujica, M. Thomas, J. Harrow, T. Cox, D. Jackson, J. Severin, P. Biggs, J. Fu, M. Nefedov,

P. J. de Jong, A. F. Stewart, and A. Bradley
2011. A conditional knockout resource for the genome-wide study of mouse gene function. *Nature*, 474(7351):337–342.

Skerjanc, I. S., J. Truong, P. Filion, and M. W. McBurney
1996. A splice variant of the ITF-2 transcript encodes a transcription factor that inhibits MyoD activity. *The Journal of biological chemistry*, 271(7):3555–3561.

Slade, I., A. Murray, S. Hanks, A. Kumar, L. Walker, D. Hargrave, J. Douglas, C. Stiller, L. Izatt, and N. Rahman
2011. Heterogeneity of familial medulloblastoma and contribution of germline PTCH1 and SUFU mutations to sporadic medulloblastoma. *Familial cancer*, 10(2):337–342.

Smeyne, R. J. and D. Goldowitz
1989. Development and death of external granular layer cells in the weaver mouse cerebellum: a quantitative study. *The Journal of neuroscience*, 9(5):1608–1620.

Sobrado, V. R., G. Moreno-Bueno, E. Cubillo, L. J. Holt, M. A. Nieto, F. Portillo, and A. Cano
2009. The class I bHLH factors E2-2A and E2-2B regulate EMT. *Journal of cell science*, 122(Pt 7):1014–1024.

Soileau, B., M. Hasi, C. Sebold, A. Hill, L. O'Donnell, D. E. Hale, and J. D. Cody
2015. Adults with Chromosome 18 Abnormalities. *Journal of genetic counseling*, 24(4):663–674.

Soosaar, A., A. Chiaramello, M. X. Zuber, and T. Neuman
1994. Expression of basic-helix-loop-helix transcription factor ME2 during brain development and in the regions of neuronal plasticity in the adult brain. *Molecular Brain Research*, 25(1-2):176–180.

Spassky, N., Y.-G. Han, A. Aguilar, L. Strehl, L. Besse, C. Laclef, M. R. Ros, J. M. Garcia-Verdugo, and A. Alvarez-Buylla
2008. Primary cilia are required for cerebellar development and Shh-dependent expansion of progenitor pool. *Developmental biology*, 317(1):246–259.

Sweatt, J. D.
2013. Pitt-Hopkins Syndrome: intellectual disability due to loss of TCF4-regulated gene transcription. *Experimental & molecular medicine*, 45:e21.

Taddeucci, G., A. Bonuccelli, I. Mantellassi, A. Orsini, and E. Tarantino
2010. Pitt-Hopkins syndrome: report of a case with a TCF4 gene mutation. *Italian journal of pediatrics*, 36:12.

Tamberg, L., M. Sepp, T. Timmusk, and M. Palgi
2015. Introducing Pitt-Hopkins syndrome-associated mutations of TCF4 to Drosophila daughterless. *Biology open*, 4(12):1762–1771.

Taylor, M. D., L. Liu, C. Raffel, C.-c. Hui, T. G. Mainprize, X. Zhang, R. Agatep, S. Chiappa, L. Gao, A. Lowrance, A. Hao, A. M. Goldstein, T. Stavrou, S. W. Scherer, W. T. Dura, B. Wainwright, J. A. Squire, J. T. Rutka, and D. Hogg
2002. Mutations in SUFU predispose to medulloblastoma. *Nature genetics*, 31(3):306–310.

Taylor, M. D., P. A. Northcott, A. Korshunov, M. Remke, Y.-J. Cho, S. C. Clifford, C. G. Eberhart, D. W. Parsons, S. Rutkowski, A. Gajjar, D. W. Ellison, P. Lichter, R. J. Gilbertson, S. L. Pomeroy, M. Kool, and S. M. Pfister
2012. Molecular subgroups of medulloblastoma: the current consensus. *Acta neuropathologica*, 123(4):465–472.

Thaxton, C., A. D. Kloth, E. P. Clark, S. S. Moy, R. A. Chitwood, and B. D. Philpot
2018. Common Pathophysiology in Multiple Mouse Models of Pitt-Hopkins Syndrome. *The Journal of neuroscience*, 38(4):918–936.

Trepel, M.
2009. *Neuroanatomie: Struktur und Funktion*, 4., neu bearb. aufl. edition. München: Elsevier Urban & Fischer.

Vogel, C., R. d. S. Abreu, D. Ko, S.-Y. Le, B. A. Shapiro, S. C. Burns, D. Sandhu, D. R. Boutz, E. M. Marcotte, and L. O. Penalva
2010. Sequence signatures and mRNA concentration can explain two-thirds of protein abundance variation in a human cell line. *Molecular systems biology*, 6:400.

Wefers, A. K., M. Warmuth-Metz, J. Pöschl, A. O. von Bueren, C.-M. Monoranu, K. Seelos, A. Peraud, J.-C. Tonn, A. Koch, T. Pietsch, C. Herold-Mende, C. Mawrin, A. Schouten-van Meeteren, D. van Vuurden, K. von Hoff, S. Rutkowski, S. M. Pfister, M. Kool, and U. Schüller
2014. Subgroup-specific localization of human medulloblastoma based on pre-operative MRI. *Acta neuropathologica*, 127(6):931–933.

Whalen, S., D. Héron, T. Gaillon, O. Moldovan, M. Rossi, F. Devillard, F. Giuliano, G. Soares, M. Mathieu-Dramard, A. Afenjar, P. Charles, C. Mignot, L. Burglen, L. van Maldergem, J. Piard, S. Aftimos, G. Mancini, P. Dias, N. Philip, A. Goldenberg, M. Le Merrer, M. Rio, D. Josifova, J. M. van Hagen, D. Lacombe, P. Edery, S. Dupuis-Girod, A. Putoux, D. Sanlaville, R. Fischer, L. Drévillon, A. Briand-Suleau, C. Metay, M. Goossens, J. Amiel, A. Jacquette, and I. Giurgea
2012. Novel comprehensive diagnostic strategy in Pitt-Hopkins syndrome: Clinical score and further delineation of the TCF4 mutational spectrum. *Human mutation*, 33(1):64–72.

Wingate, R. J. and M. E. Hatten
1999. The role of the rhombic lip in avian cerebellum development. *Development*, 126(20):4395–4404.

Wu, X., P. A. Northcott, S. Croul, and M. D. Taylor
2011. Mouse models of medulloblastoma. *Chinese journal of cancer*, 30(7):442–449.

Zakrzewska, M., S. M. Gresner, K. Zakrzewski, B. Zalewska-Szewczyk, and P. P. Liberski
2013. Novel gene expression model for outcome prediction in paediatric medulloblastoma. *Journal of molecular neuroscience*, 51(2):371–379.

Zhang, J., M. Kalkum, S. Yamamura, B. T. Chait, and R. G. Roeder
2004. E protein silencing by the leukemogenic AML1-ETO fusion protein. *Science*, 305(5688):1286–1289.

Zhuang, Y., P. Cheng, and H. Weintraub
1996. B-lymphocyte development is regulated by the combined dosage of three basic helix-loop-helix genes, E2A, E2-2, and HEB. *Molecular and cellular biology*, 16(6):2898–2905.

Zhuo, L., M. Theis, I. Alvarez-Maya, M. Brenner, K. Willecke, and A. Messing
2001. hGFAP-cre transgenic mice for manipulation of glial and neuronal function in vivo. *Genesis*, 31(2):85–94.

Zweier, C., M. M. Peippo, J. Hoyer, S. Sousa, A. Bottani, J. Clayton-Smith, W. Reardon, J. Saraiva, A. Cabral, I. Gohring, K. Devriendt, T. de Ravel, E. K. Bijlsma, R. C. Hennekam, A. Orrico, M. Cohen, A. Dreweke, A. Reis, P. Nurnberg, and A. Rauch
2007. Haploinsufficiency of TCF4 causes syndromal mental retardation with intermittent hyperventilation (Pitt-Hopkins syndrome). *American journal of human genetics*, 80(5):994–1001.

9 Appendix

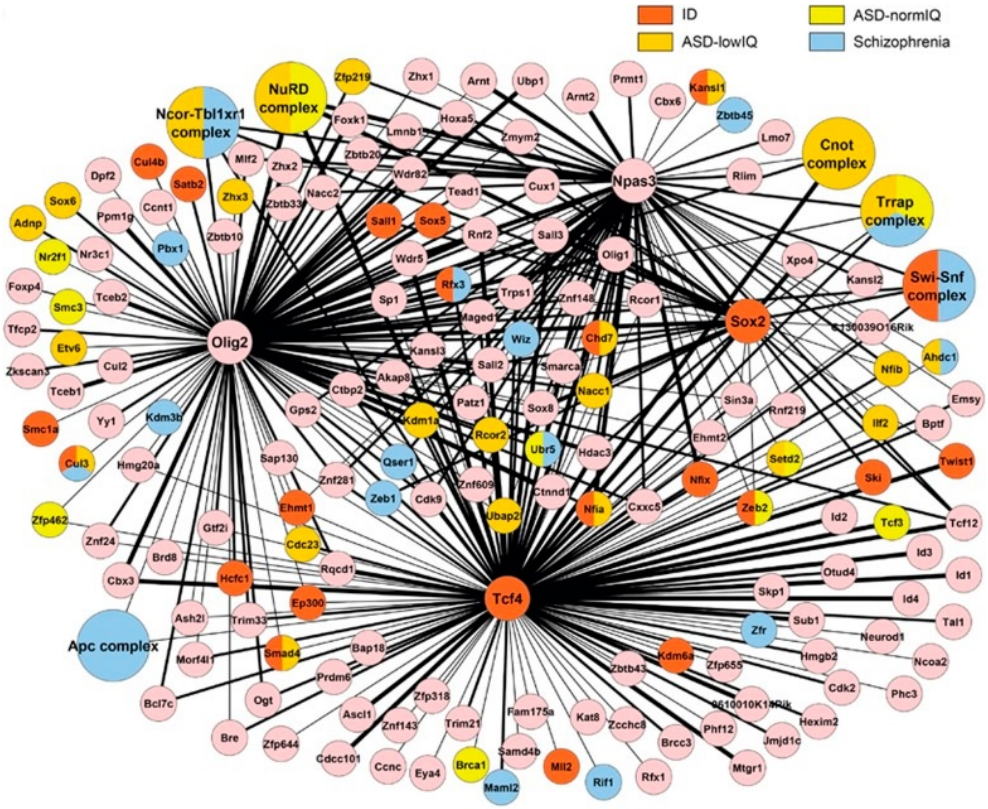

Figure 26: TCF4 interaction network from Moen et al. (2017).[6] Overview of the protein interaction network in neural stem cells. FLAG-tagged transcriptional regulators were purified and their interaction partners identified by mass spectrometry. TCF4 was one of the tagged proteins. The interaction network illustrates the various proteins TCF4 interacts with, many are associated with ID, schizophrenia, and autism-spectrum disorders. *"Red color indicates network protein or protein complex subunit(s) encoded by a known ID gene. Orange, yellow and blue color indicate de novo mutation(s) in patients with ASD-lowIQ, ASD-normIQ and schizophrenia, respectively."* (Moen et al., 2017).

[6] "An interaction network of mental disorder proteins in neural stem cells" original from Moen et al. (2017), *Translational Psychiatry* (Nature Publishing Group), part A from Fig. 1. Licensed under CC BY 4.0 (https://creativecommons.org/licenses/by/4.0/).

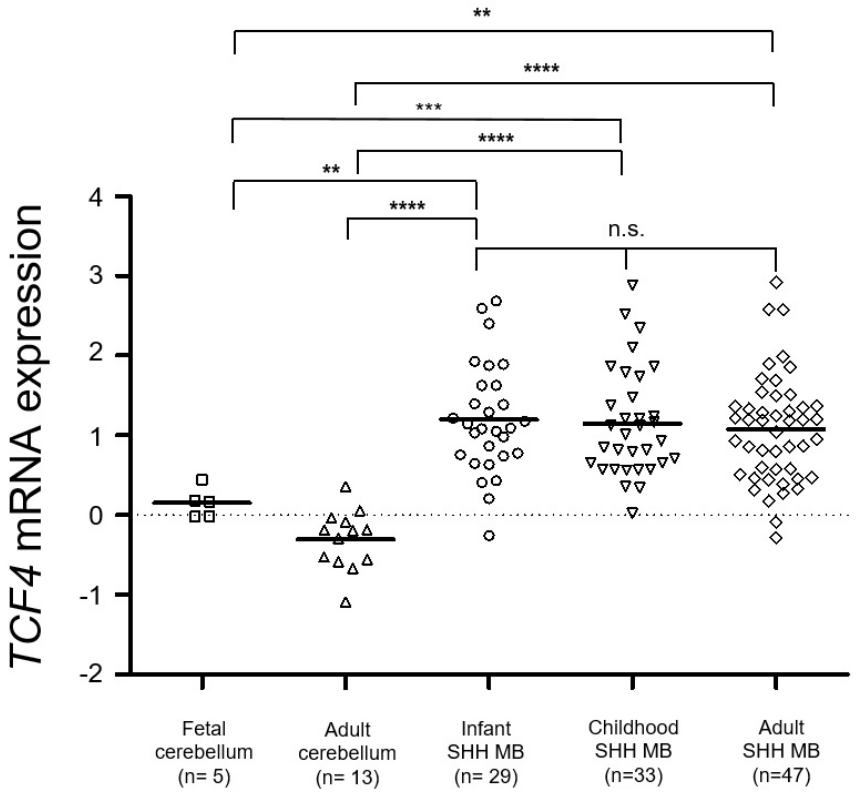

Figure 27: *TCF4* mRNA levels in SHH MB and normal brain tissue in different age groups. All SHH MB age groups showed a significant difference in *TCF4* mRNA expression compared to fetal and adult cerebellum. Comparison within the SHH subgroups were not significantly different. Relative gene expression values were calculated using z-scores. Values on y-axis indicate number of standard deviation by which the value of the expression level is different from the mean. Mean is shown as a bar for each group. Groups were compared with each other using two-tailed t-tests and Mann-Whitney-U tests, respectively. n.s. = $p > 0.05$, ** = $p < 0.01$, *** = $p < 0.001$, **** = $p < 0.0001$.

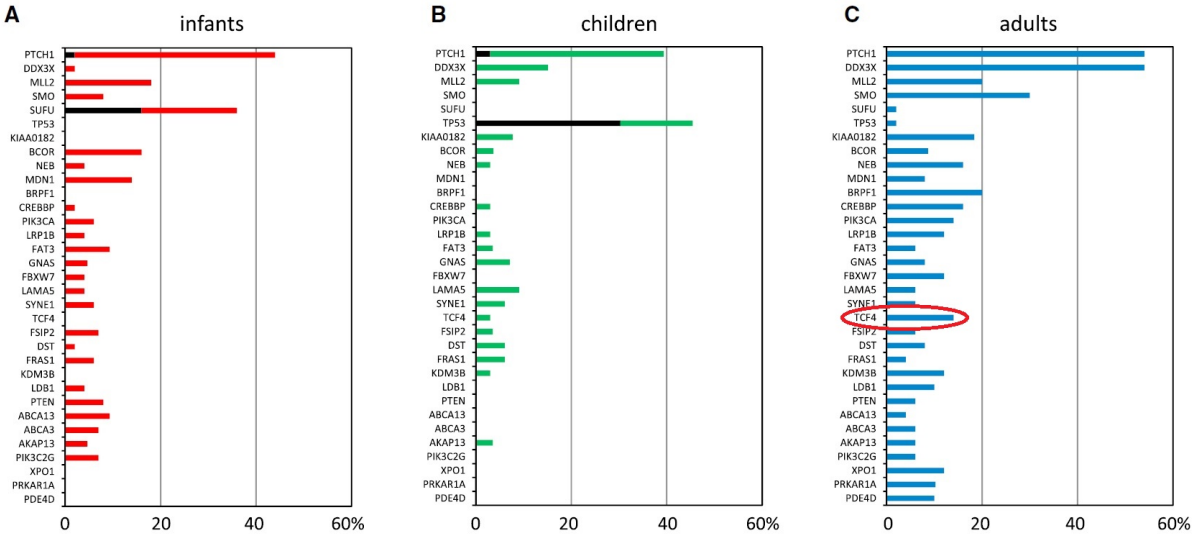

Figure 28: Summary of sequencing data from Kool et al. (2014).[7] Graphs **(A-C)** summarize the mutations found in different genes for the three age groups separately. *TCF4* is encircled in red in the adult SHH MB group, showing that 14 % of tumours were found to have a mutation.

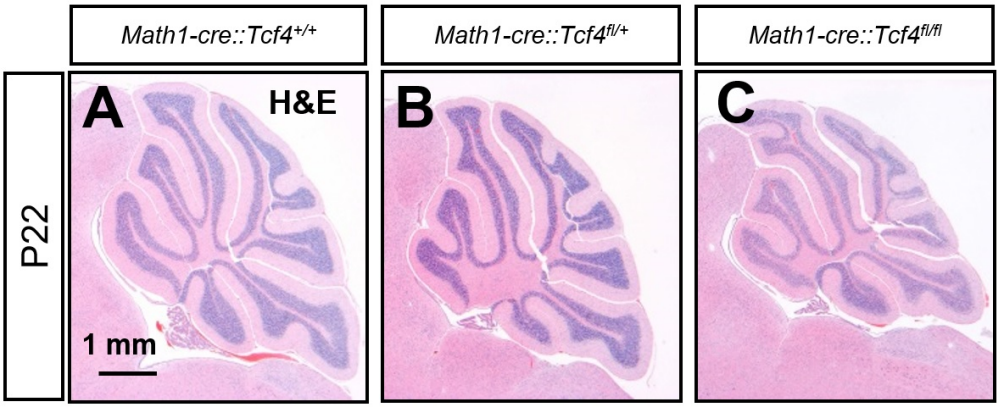

Figure 29: Overview H&E stain of *Math1-cre::Tcf4*$^{fl/fl}$ mice at P22. Comparison of cerebellar size shows that a homozygous knockout of *Tcf4* causes cerebellar hypoplasia.

[7]Reprinted from Cancer Cell, 25(3), Marcel Kool, David T.W. Jones, Natalie Jäger, Paul A. Northcott, Trevor J. Pugh, Volker Hovestadt, Rosario M. Piro, L. Adriana Esparza, Shirley L. Markant, Marc Remke, Till Milde, Franck Bourdeaut, Marina Ryzhova, Dominik Sturm, Elke Pfaff, Sebastian Stark et al., Genome Sequencing of SHH Medulloblastoma Predicts Genotype-Related Response to Smoothened Inhibition, 393-405, Copyright (2014), with permission from Elsevier.

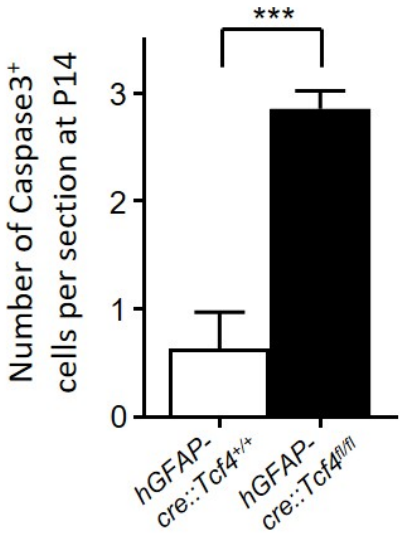

Figure 30: Apoptosis rates in *hGFAP-cre::Tcf4*$^{fl/fl}$ mice on P14. Cell counts of CASP3^{+} cells in *hGFAP-cre::Tcf4*$^{fl/fl}$ mice and WT mice at P14 in lobulus V. A significant higher number of CASP3^{+} cells occured after a homozygous knockout of *Tcf4*. Analysis was done using an unpaired t-test. Error bars show mean + SD, *** = p<0.001.

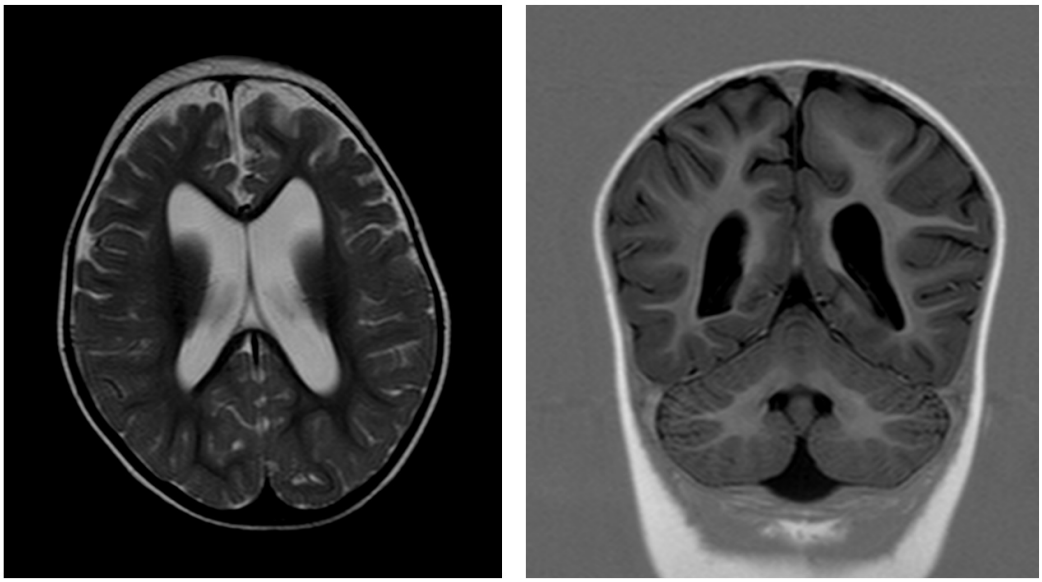

Figure 31: MRI of a 19-months old girl with PTHS. T2 weighted image (left) and T1 inversio recovery sequence (right) show a widening of the outer and inner CSF spaces, a reduced volume of the subtentorial brain and a hypoplasia of the cerebellar hemispheres and vermis. Furthermore, a slight disorganisation of the cerebellar folia can be seen. Pictures were received with kind permission from Prof. Dr. Ertl-Wagner.

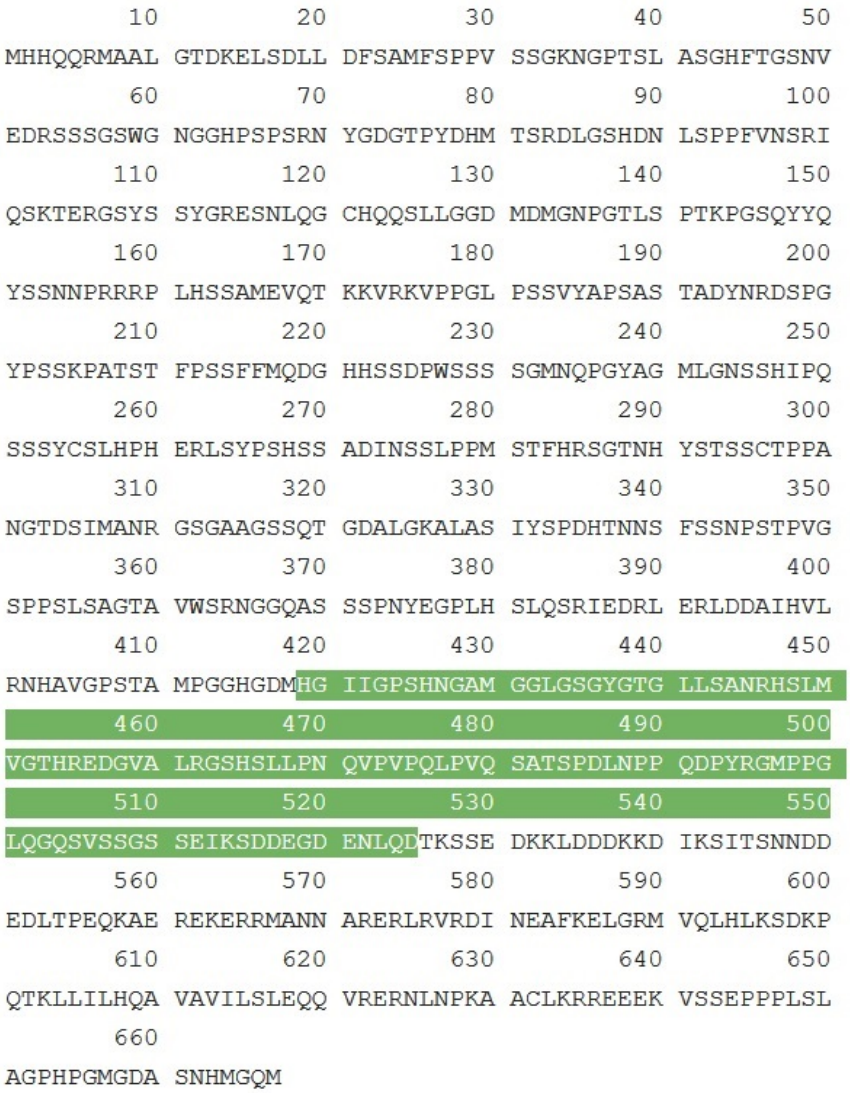

Figure 32: Human TCF4 protein sequence. Protein sequence of isoform SEF-1B, also known as TCF4-B^{-} with a length of 667 amino acids. Sequence from UniProt (UniProtKB - P15884 (ITF2_HUMAN), www.uniprot.org/uniprot/P15884). Antibody-binding domain of anti-TCF4 (Sigma, HPA025958) is marked in green.

Table 10: P-values for brain weights. Detailed list of all p-values calculated for comparison of brain weights on days P7, 14, and 21. P-values were calculated using two-tailed t-tests.

Genotypes	Brain weight			Cerebrum weight			Cerebellar weight		
	P7	**P14**	**P21**	**P7**	**P14**	**P21**	**P7**	**P14**	**P21**
hGFAP-cre::Tcf4$^{+/+}$ ***hGFAP-cre::Tcf4***$^{fl/+}$	0.9675	0.1989	0.0458	0.8439	0.3624	0.2995	0.2594	0.8788	0.42
hGFAP-cre::Tcf4$^{+/+}$ ***hGFAP-cre::Tcf4***$^{fl/fl}$	0.1853	<0.0001	<0.0001	0.0112	<0.0001	0.0029	0.0023	0.0015	0.0075
hGFAPcre::Tcf4$^{fl/+}$ ***hGFAP-cre::Tcf4***$^{fl/fl}$	0.1239	<0.0001	<0.0001	0.0109	0.0005	0.0015	0.0135	0.0016	0.0038